UNIVERSITÉ DU QUÉBEC

MÉMOIRE
PRÉSENTÉ À
L'UNIVERSITÉ DU QUÉBEC À CHICOUTIMI
COMME EXIGENCE PARTIELLE
DE LA MAÎTRISE EN SCIENCES DE LA TERRE

PAR

ARLENE BEISSWENGER

THE ORIGIN OF THE CANTON SAINT-ONGE WOLLASTONITE DEPOSIT,

LAC-SAINT-JEAN, QUÉBEC

1996

Mise en garde/Advice

ABSTRACT

Wollastonite is a naturally occurring anhydrous, fibrous calc-silicate mineral. As an industrial mineral it is particularly valuable for use in ceramic applications and its acicularity makes it an attractive and safe replacement for asbestos.

Wollastonite is formed by the reaction of calcite with silica which gives off CO_2; heat is needed to drive the reaction to completion. The heat can be provided by regional or contact metamorphism, the silica can be provided by quartz mixed with a limestone protolith or from a magmatic fluid of an intruding pluton.

The Canton Saint-Onge wollastonite deposit is situated near the centre of the Lac-Saint-Jean Anorthosite Complex. A major NE-SW trending lineament, the Lacs-Saint-Jean-Pipmuacan lineament, cuts the anorthosite. It stretches for over 200 km and is marked by solid state deformation and plutons of various composition and age. A lens of metasediments is preserved adjacent to this lineament. The metasediments include: hornfelsic gneiss, marbles, quartzite and the calc-silicate rocks which host the wollastonite.

The wollastonite occurs in a band of calc-silicate rocks trending N040° that are in contact with marble to the south-east which is in turn in contact with the Du Bras Pluton bordering a gabbroic facies of the anorthosite. The contact to the south-west is with the Astra syenite, a late undeformed pluton. The north-eastern contact is hidden by a valley without outcrop but on its other side there are wollastonite-free calc-silicate rocks followed by anorthosite. The wollastonite is interlayered with diopside on the millimetre to centimetre scale and strongly folded. Electron microprobe analyses of the layering shows that it is chemically abrupt, with no gradation in chemical composition between layers.

Whole-rock oxygen isotope ratios were measured to determine the origin of the fluids involved in the formation of the deposit. Both granitoids and the Lac-Saint-Jean Anorthosite have $\delta^{18}O$ values from 8 to 10 ‰, consistent with values in similar intrusions elsewhere in the Grenville Province. The marbles have much higher $\delta^{18}O$ values from 23 to 28 ‰, similar to sedimentary limestones, suggesting isochemical metamorphism. The calc-silicate rocks have values ranging from 8 to 22 ‰, with the lowest values similar to those of the plutons and the highest similar to those of the marbles. The wollastonite-bearing calc-silicate rocks generally have lower values than those of the barren calc-silicate rocks.

If the marbles are the protolith to the calc-silicate rocks some fluid must have been involved in order to lower the isotopic ratios of the latter. The data indicates that pristine meteoric water was not involved in the formation of the calc-silicate rocks, which would have resulted in lower, near zero isotopic values for the calc-silicate rocks. The fluid may

have been derived from one or more of the intrusions, or it may have been meteoric water that re-equilibrated with one of the intrusions. The generally lower values of the wollastonite-bearing calc-silicate rocks suggests that more fluid was involved in their formation as compared to the wollastonite-free rocks, if both came from a protolith with similar $\delta^{18}O$ values.

The stable isotope work suggests that the fluid concerned is in isotopic equilibrium with the plutons and possibly emanated from one of them. The fluid must have been rich in H_2O to lower the partial pressure of the CO_2 and in silica in order to complete the reaction from calcite to wollastonite. The whole rock geochemistry suggests the fluid also contained Ti, Al, Fe, Na, K, Co, Ba, Sr, Zr, La, and Lu and removed magnesium.

Isotopic cross-sections of the calc-silicate rocks show that the values tend to decrease towards the Astra Pluton. This could suggest that fluids in equilibrium with this pluton emanated from it and were channelled along the fault passing through the deposit oriented NW-SE parallel to the Lacs-Saint-Jean-Pipmuacan lineament.

RÉSUMÉ

La wollastonite est un minéral anhydre et aciculaire, que l'on retrouve à l'état naturel. Utilisé comme minéral industriel, elle est particulièrement utile dans la fabrication de la céramique et son acicularité la rend utile pour le remplacement de l'amiante.

La wollastonite est formée par la réaction de la calcite avec la silice ce qui libère du CO_2; la chaleur est requise pour initier cette réaction. La silice peut être fourni par le quartz présent dans les calcaires ou par un fluide magmatique issue d'une intrusion tandis que la chaleur peut être produite par un métamorphisme de contact ou régional.

Le gisement de wollastonite du Canton Saint-Onge est situé approximativement au centre du complexe anorthositique du Lac-Saint-Jean . Un linéament majeur orienté NE-SW qui coupe l'anorthosite, s'étant sur plus que 200 km et est marqué par du cisaillement et par la présence de plutons d'âges et compositions différents. On retrouve un lambeau de métasédiments adjacents à ce linéament. Ce lambeau est constitué de paragneiss hornfelsique, de marbres, de quartzite et de roches calco-silicatées qui sont hôtes à la wollasonite.

La wollastonite est contenue dans un lambeaux de roches calco-silicatées orientées N040°. En bordures des roches calco-silicatées et en se dirigeant vers le sud-est, on observe la séquence suivante: marbre, granite lenticulaire de Du Bras, et anorthosite gabbroïque. La bordure sud-ouest est caractérisée par une vallée sans affleurement, mais de l'autre côté de la vallée se trouvent des roches calco-silicatées sans wollastonite, et plus loin l'anorthosite. La bordure sud-ouest est caractérisée par la présence d'un pluton tardif, la syénite d'Astra. La wollastonite est interlitée avec de la diopside sur une échelle millimétrique à centimétrique et les lits sont fortement plissées. Les analyses à la microsonde montrent des changements de composition abrupts entre les lits des roches calco-silicatées mais peu de changements à l'intérieur des lits.

Des rapports isotopiques d'oxygène ont été mesurés pour déterminer l'origine des fluides impliqués dans la formation du gisement. Les trois plutons ont des valeurs de $\delta^{18}O$ se situant entre 8 et 10 ‰, qui sont consistant tant avec les valeurs des intrusions retrouvées dans la Province de Grenville. Les marbres ont des valeurs beaucoup plus élevées, $\delta^{18}O$ de 23 à 28 ‰, similaires aux calcaires non-métamorphisés indiquant aucun échange d'oxygène durant un métamorphisme isochimique. Par contre, les roches calco-silicatées stérile ont des valeurs $\delta^{18}O$ situées entre 14 et 18 ‰ avec un échantillon à 8, et les roches calco-silicatées contenant de la wollastonite ont des valeurs $\delta^{18}O$ comprises entre 8 à 13 ‰, mais deux échantillons sont à 22 et 23 ‰. En supposant que le marbre est le protolithe à ces roches, ces valeurs suggèrent un échange d'oxygène avec un fluide de faible $\delta^{18}O$.

Ces résultats indiquent clairement que l'eau météorique n'a pas été impliquée dans la formation des roches calco-silicatées, sinon les valeurs seraient encore plus basses, même devenant négatives. Le fluide peut être dérivé d'une ou de plusieurs intrusions, ou il peut être de l'eau météorique rééquilibrée avec les intrusions impliquées. Les bases valeurs des roches calco-silicatées contenant de la wollastonite suggèrent qu'une plus grande quantité de fluide a été impliqué dans leur formation par rapport aux roches calco-silicatées stériles, si les deux unités proviennent d'un protolithe avec des valeurs similaires de $\delta^{18}O$. La distribution géographique des valeurs des $\delta^{18}O$ des métasédiments est indistincte, mais ces valeurs ont l'apparence de baisser en s'approchant du pluton tardif d'Astra.

ACKNOWLEDGEMENTS

TABLE OF CONTENTS

LIST OF FIGURES

LIST OF TABLES

LIST OF PLATES

Chapter 1

INTRODUCTION

1.1 WOLLASTONITE CHARACTERISTICS

Wollastonite is a naturally occurring anhydrous calc-silicate, $CaSiO_3$, with a theoretical composition of 48.3% CaO and 51.7 SiO_2 % (Deer *et al.*, 1966). Although wollastonite has a single chain of silica tetrahedra as its basic structural unit, the tetrahedra are twisted in such a way that wollastonite is not a true pyroxene, but considered a pyroxinoid (Deer *et al.*, 1966). The common habit of wollastonite is as masses of silky-looking fibres; more rarely it occurs as tabular crystals. Wollastonite is a common constituent of metamorphosed impure limestones but also occurs in contact altered calcareous sediments where silica has been metasomatically introduced (Deer *et al.*, 1966). Used as an industrial mineral it is particulary valuable for ceramic applications, as well as a whitener for paint, a filler for plastics, and as a flux (Andrews, 1970; LaSalle 1988).

Its three distinct cleavages enhance its acicularity, making wollastonite an attractive replacement fibre for asbestos. Its most valuable characteristic is the ability to separate into long fibres upon grinding. The aspect ratio refers to the ratio of width to fibre length. High aspect ratio wollastonite, 1:15 - 1:20, finds uses as reinforcement in plastics and as an

asbestos replacement in insulating boards. Low aspect ratio wollastonite, typically 1:3 - 1:5, is confined to ceramics and metallurgical fluxes. Two of its other commercially important characteristics are the low loss-on-ignition values, for use as a flux, and the whiteness of the mineral, for use a whitening agent (Fournier and St. Seymour, 1992; LaSalle, 1988; Andrews, 1970).

1.2 MARKET

The principal producer of wollastonite presently is the Adirondack region of the United States with 66% of the world market, followed by Finland, Mexico, India and China (LaSalle, 1988). However, reserves in the United States are limited by geological and socio-political criteria, hence there is considerable interest in new deposits as demand increases with the discovery of new applications. Other deposits need to be found and searches have increasingly been focused on other Grenville metasediments. As with many industrial minerals there has been little research in the past on wollastonite genesis. Hence, a petrogenetic model is needed to understand these deposits and as an aid to exploration.

1.3 THE CANTON ST-ONGE PROPERTY

Recently, a new deposit of wollastonite was found in the Grenville structural province, in a band of northwest-trending metasediments situated near the centre of the Lac St-Jean Anorthosite Complex (LSJAC) in Canton Saint-Onge (figure 1.1). It is this deposit
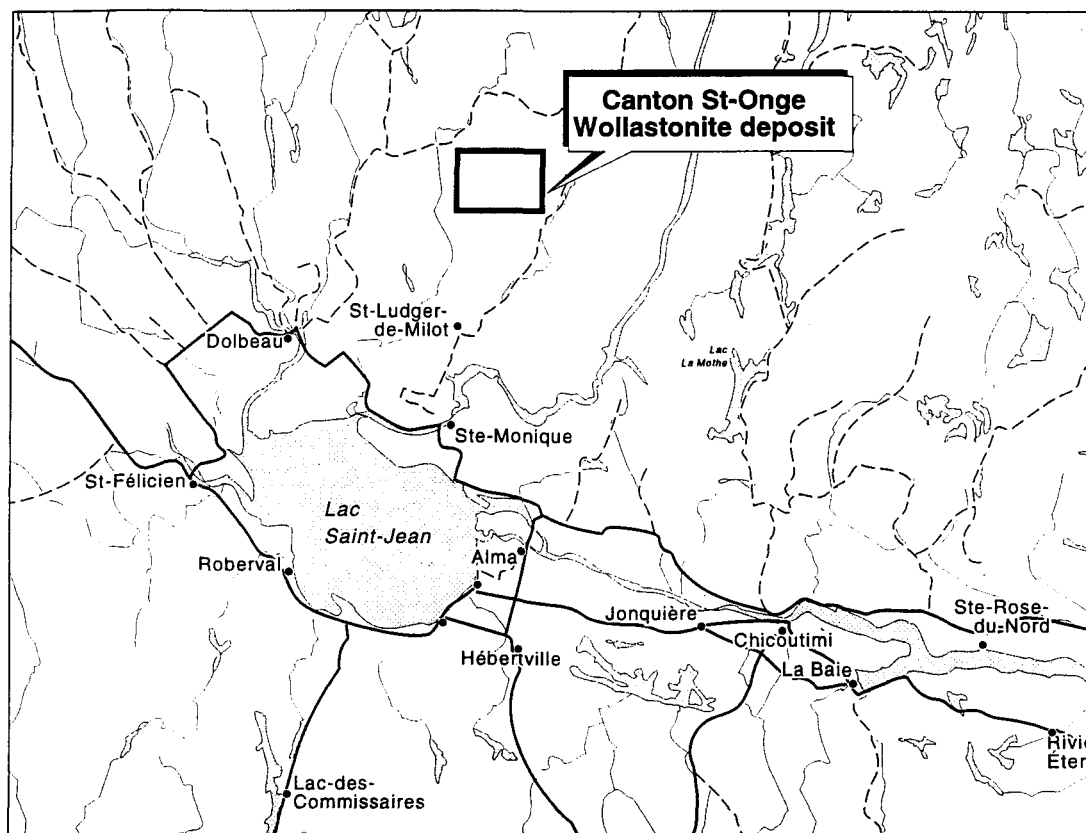
Figure 1.1: Location of the Canton St-Onge wollastonite deposit

that is the focus of this study. The deposit is located in the eastern half of the St-Onge

township, Lac St-Jean, Quebec, about 80 km north of the city of Alma and 40 km north of

the village of Saint-Ludger-de-Milot, following the Chutes-des-Passes road (figure 1.1).

The wollastonite deposit was discovered by local prospector Lionel Lefebvre in 1989, but is

now owned by Ressources Orléans, a junior exploration firm based in Montreal. Data from

sixty three drill holes, totalling 6,290 metres, have been used to estimate probable and

possible open-pit reserves totalling 25.6 million tonnes grading 37% wollastonite (Christie,

1994). The reserves are contained in a block 2.3 km long by 100 meters deep with a true

width that averages 60 meters (Christie,1993).

1.4 WOLLASTONITE GENESIS

Although normally fairly pure $CaSiO_3$, wollastonite can accept considerable

amounts of Fe and Mn, which replace the calcium (Deer *et al.*, 1966). Wollastonite is a

common constituent of thermally metamorphosed impure limestones, and is the product of

metasomatism where silica is added to calcareous sediments (Deer *et al.,*1966).

Wollastonite is usually formed by the isochemical reaction:

$$CaCO_3 + SiO_2 = CaSiO_3 + CO_2 \qquad\qquad 1$$
calcite   quartz   wollastonite
         or   silica$_{aq}$
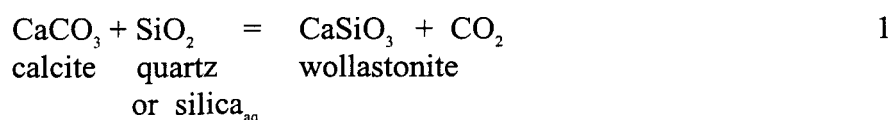
The presence of significant quantities of other elements in the system such as Mg, Al, OH, will complicate the reaction and result in the formation of diopside, grossular-andradite garnet, vesuvianite, tremolite and other calc-silicates (Simandl, 1990). Although the carbonates dolomite and magnesite react with quartz whenever it is present under low-grade metamorphic conditions, this is not true for calcite as will be shown later (Winkler, 1974).

The thin curves on figure 1.2 show the formation of wollastonite from silica and calcite for different fluid compositions (X_{CO_2}). These curves are based on experimental data to 3 kbars of Greenwood (1967) and Harker and Tuttle (1956) extended to 10 kbars using Thermocalc and the thermodynamic data of Holland and Powell (1990). They show the strong dependence of the reaction on the composition on the fluid phase.

Curve A (fig. 1.2) shows an equilibrium geotherm (from Fowler and Nisbet, 1982) representing a path a rock would take during slow burial regional metamorphism. This curve would only intersect the stability curve for wollastonite where the partial pressure of CO_2 is extremely low, lower than 0.01, and this only at high temperature and pressure conditions. Such a scenario of wollastonite formation from calcite and quartz during high grade regional metamorphism is unlikely since the formation of wollastonite will generate CO_2 thus increasing the X_{CO_2} which, in turn, will inhibit wollastonite formation. Therefore, under conditions of high grade
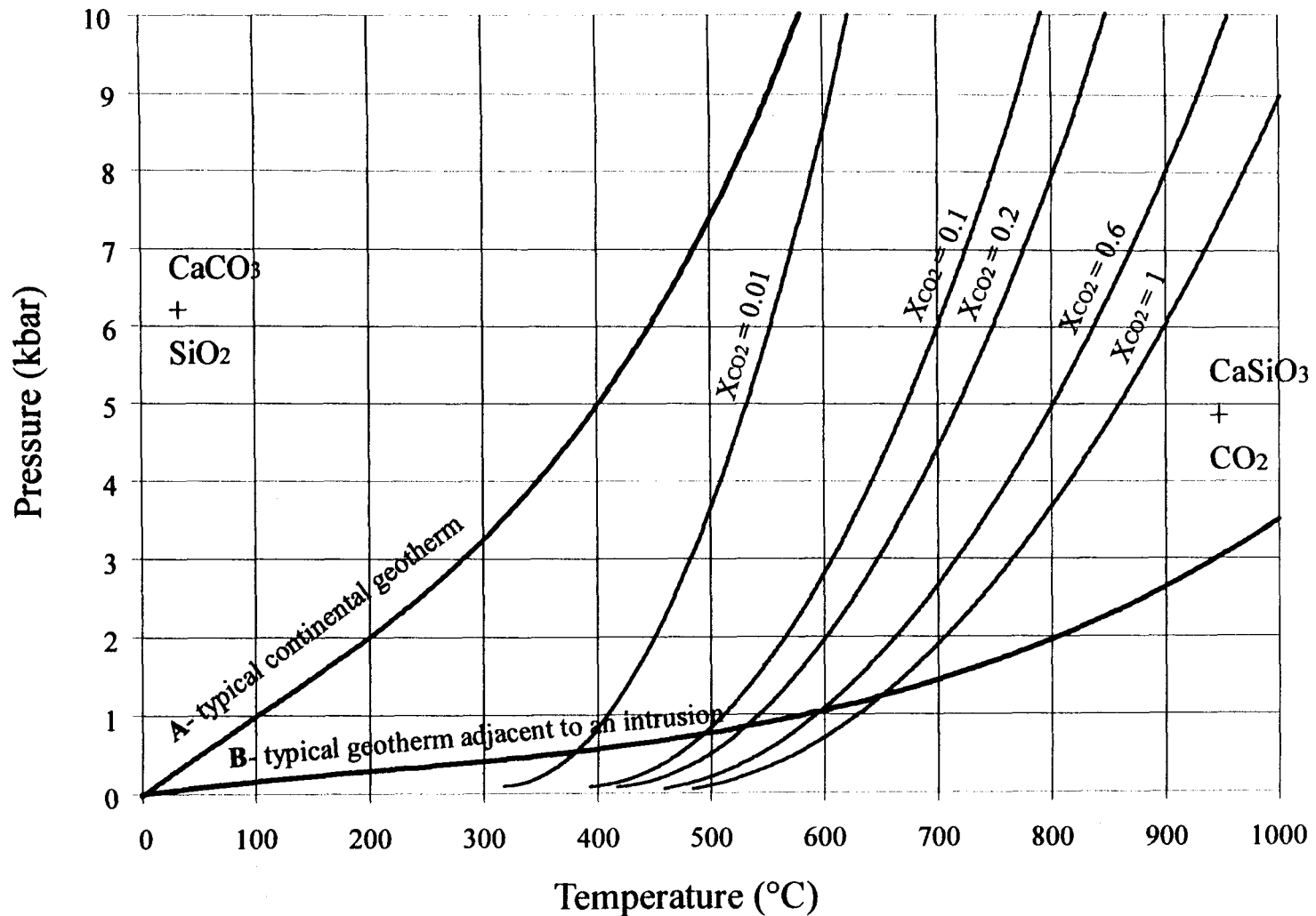
Figure 1.2. Formation of wollastonite. The thinner lines represent reaction equilibrium for various constant fluid pressure compositions. Curve A represents a typical continental geotherm (from Fowler and Nisbet, 1982). Curve B represents a typical geotherm adjacent to an intrusion (from Winkler, 1974).

regional metamorphism wollastonite may form only under special circumstances. One situation is where the carbon dioxide formed can be continually driven off, for example through a system of faults, which is unlikely in high grade regional metamorphism. Another situation in which wollastonite can be formed is if the CO_2 is diluted by very large quantities of H_2O, for example by the dehydration of H_2O-rich pelites (MacKinnon, 1990).

Curve B (fig. 1.2) shows a typical thermal gradient of contact metamorphism of rocks adjacent to a cooling pluton (taken from Winkler, 1974). Here the temperature increases without significantly increasing the pressure, resulting in the formation of wollastonite at temperatures around $600^{\circ}C$ for intrusions at a depth of 3 km (1 kbar) (Winkler, 1974). This scenario of contact metamorphism will form wollastonite from impure limestones containing calcite and quartz, resulting in a wollastonite-bearing marble or hornfels. The pluton only provides heat and only very local metasomatic chemical exchange takes place. The resulting rock is generally referred to as a skarnoid, or recrystallised skarn (Einaudi et al., 1981). As with the case of regional metamorphism the CO_2 must be continually driven off, or the fluid phase must be diluted with H_2O to maintain constant P_{CO2} (MacKinnon, 1990), i.e. externally buffered vs internally buffered.

Wollastonite can also be formed from relatively pure calcite where the silica is added by the infiltration and diffusion of silica-bearing metasomatic fluids outside the marble. This fluid interacts with the limestone and yields skarn rocks restricted to well-

defined zones at the contact of marbles and granitoids. The width of the wollastonite zone

is dependant on the depth of penetration of fluids migrating from the igneous body

(MacKinnon, 1990). This process is referred to as replacement skarn or skarn (Einaudi,

1981) where exoskarn and endoskarn are the transformed sedimentary and igneous

protoliths respectively (Meinert, 1992).

One of the problems to be resolved in this thesis is to determine by which of the

three above mentioned processes the wollastonite at the Canton-St-Onge was formed. The

first process requires the introduction of large quantities of H_2O during regional

metamorphism and is hence considered unlikely at this deposit because of the lack of large

quantities of metapelites or other hydrous rocks in the surrounding area to provide the

necessary quantities of H_2O. The second process would likely generate wollastonite-

bearing marbles of varying concentration due to uneven distribution of silica in the protolith

marbles: this was not observed in the field, the calc-silicates and marble form separate units

with little calcite or dolomite in the calc-silicate rocks and vice-versa.

The third possibility of metasomatism is considered to be the most likely because

the wollastonite bearing calc-siliate rocks of the Caton-Saint-Onge wollastonite deposit has

neighbouring plutons and is distributed in lenses alongside the marble (fig 1.3), similar to

skarn facies. However, if it did form by such a process we need to find out which pluton is
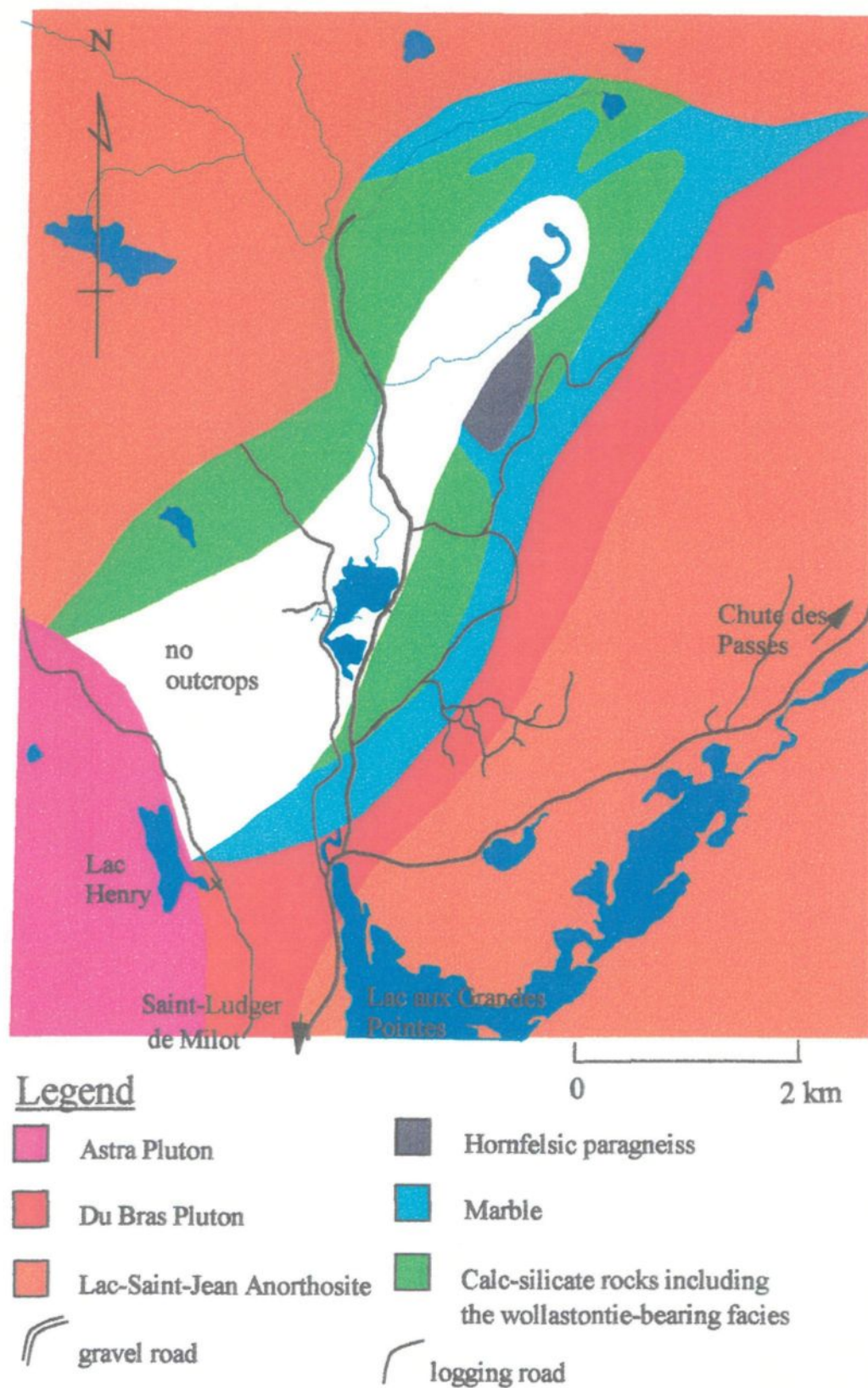
Figure 1.3. Geology of the Canton Saint-Onge wollastonite deposit

responsible for providing the siliceous fluids, since there are three intrusive bodies close to the wollastonite-bearing calc-silicate rocks.

1.5 OBJECTIVES AND METHODOLOGY

Based on the preceding discussion on the genesis of wollastonite the objectives of the study are as follows:

1) To develop a petrogenetic model for the Canton-Saint-Onge wollastonite deposit, Lac-Saint-Jean, Quebec. This includes:

    (a) identifying the protolith to the wollastonite-bearing rocks and other calc-silicates

    (b) determining how it was formed i.e. skarn or skarnoid

    and, if it is a skarn, finding the source of the magmatic fluids

    (c) determining the role and type of fluids involved

    (d) identifying the timing of wollastonite formation relative to that of the anorthosite

    and other plutons and other metasediments

2) To determine if the model is applicable to other deposits

3) To develop exploration criteria for other wollastonite deposits

In order to accomplish these goals three weeks of detailed field mapping and sampling of the wollastonite deposit and its surrounding were undertaken in the summer of 1992. I produced a 1:20 000 map of the area, showing sample collection sites, as well as

detailed section maps along the trenches made by various exploration companies. Sixty seven samples were collected from all rock units in the area. This includes the anorthosite, the gabbro, the Du Bras Pluton, the marble, the calc-silicate rocks, the Astra Pluton and the hornfelsic paragneiss.

Techniques used to determine the petrogenesis include: mapping, petrography, whole-rock geochemistry for major and minor elements, and oxygen isotopes.

Chapter 2

GEOLOGICAL SETTING

2.1 REGIONAL GEOLOGY

The Grenville Province is the youngest structural part of the Canadian Shield, cratonised around 1 Ga, and exposed mostly in Labrador, Quebec, Ontario and New York state over a an area of one million square kilometres (fig 2.1) (see review by Moore, 1986). This province is comprised of rocks of many origins (sedimentary, igneous, and metamorphic) and different ages (pre 2.7 Ga to 1.0 Ga) that were deformed and metamorphosed during the Grenville Orogeny (~1.2-1.0 Ga). The rocks now exposed on surface were reequilibrated under deep crustal conditions (typical depths were around 20 km and temperatures in the order of 600-700°C) during this orogeny (Moore, 1986).

The Saguenay-Lac-Saint-Jean area (SLSJ) is located within the central part of the Grenville Province, which has been termed the 'allochthonous polycyclic belt' (Rivers *et al.*, 1989) or the 'core zone' (Woussen *et al.*, 1986) or the 'Central Granulite Terrane' (Wynne-Edwards,1972) (fig 2.2). This area is dominated by granulite facies gneissic rocks and large anorthositic and mangeritic plutons (Roy et al., 1986). The rocks in the SLSJ area can
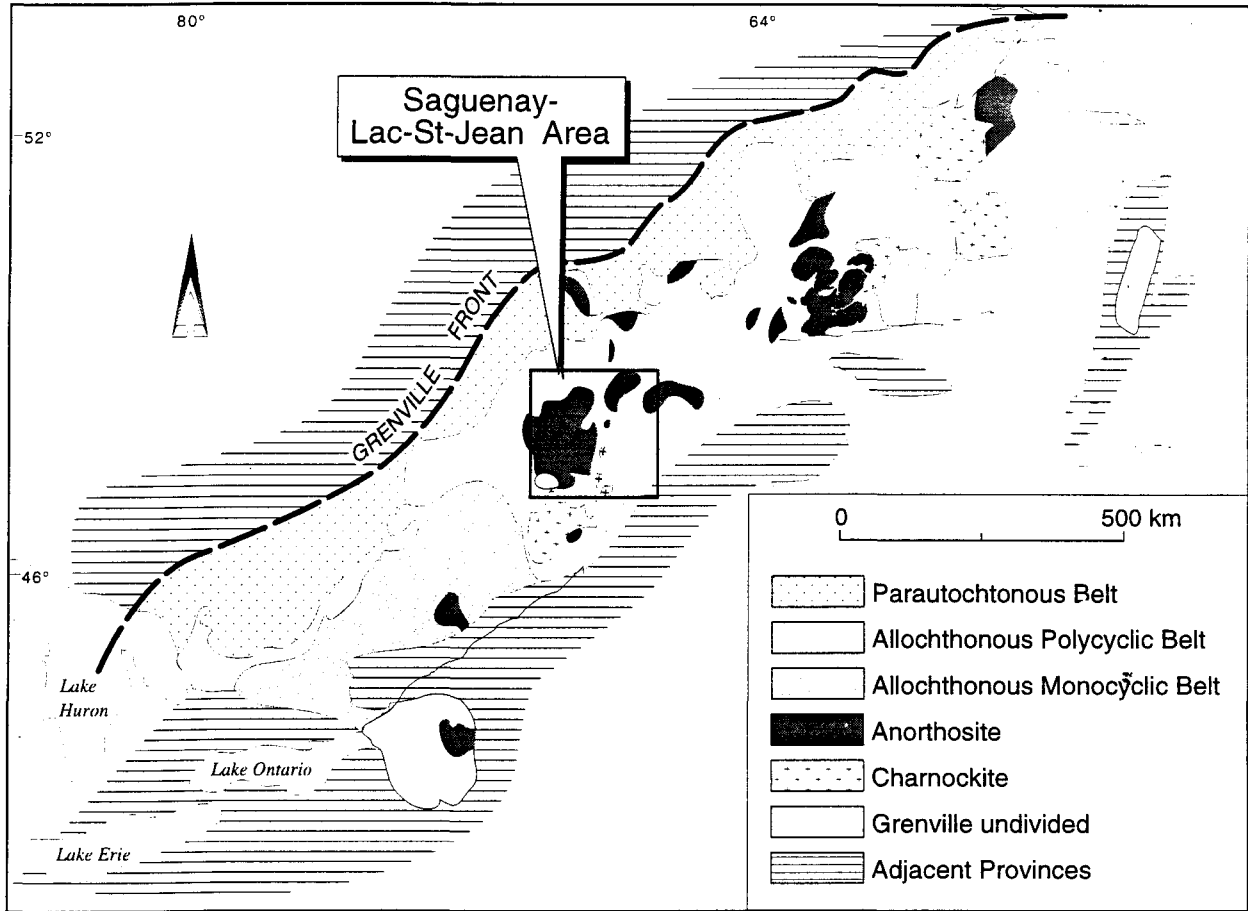
Figure 2.1. Geology of the Grenville Province. Divisions after Rivers *et al.* (1989)
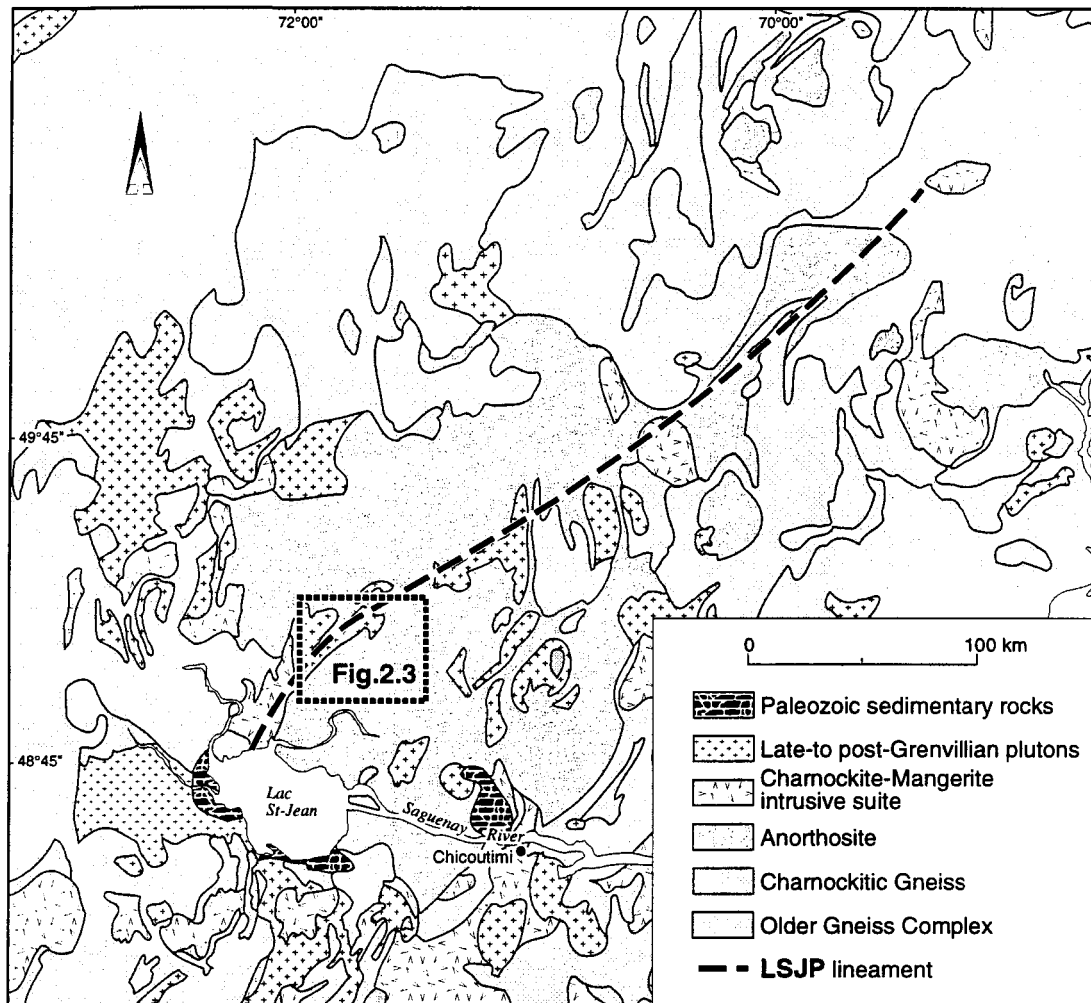
Figure 2.2. Geology of the Saguenay Lac-Saint-Jean area. Detail from Avramtchev and Piché (1981).

can be subdivided into three lithostructural units: the gneiss complex, the intrusive masses

of anorthositic and mangeritic rocks, and the late to post-tectonic plutons (Roy *et al.*, 1986).

The basement gneiss complex in this region includes rocks of three age groups

characterised by a decreasing extent of deformation and migmatization, 1) rafts of

Aphebian paragneiss that are enclosed by 2) multiply deformed and migmatised

quartzofeldspathic gneisses of unknown age, and 3) deformed and migmatised late to post-

Hudsonian granites (Firth and Doig, 1973, 1975). All these units are cut by

metamorphosed mafic dykes which are chronological stratigraphic markers permitting

correlation by age (Dimroth *et al.*, 1981).

The wollastonite deposit itself is located entirely within the Lac-Saint-Jean

anorthosite complex (LSJAC) (fig 2.2). The anorthosite complex covers an area of 20, 000

km^2 and is variable in composition, from true anorthosite to leucogabbro and leucotrocto-

lite, but almost all of the rocks are plagioclase cumulates (Dimroth *et al.*, 1981; Woussen *et

al.*,1981 and Roy *et al.*, 1986). The anorthosite consists mostly of plagioclase ($An_{45}-An_{60}$),

which is black when fresh, but paler in the more deformed facies. It ranges in grain size

from millimetric granoblastic grains in deformed rocks to megacrysts up to 70 cm long in

less deformed rocks. The mafic minerals vary in abundance (0-25%) and include

orthopyroxene, clinopyroxene and olivine. Solid-state deformation of the LSJAC was

extremely heterogeneous and has not been studied in detail: some areas retain almost

pristine igneous textures, whereas elsewhere the anorthosite has been transformed into a

grey plagioclase-rich gneiss. The foliation plane resulting from emplacement is commonly

sub-vertical, although shallow angles have been observed locally (Higgins and Van

Breeman, 1992). Where orthopyroxene -amphibole coronas developed between olivine and

plagioclase they post-date the deformation i.e. the minerals in the coronas show no sign of

crystal plastic deformation features.

The south-central and south-eastern parts of the anorthosite complex were emplaced

at 1157±3 Ma (U-Pb, Higgins and Van Breeman, 1992). Similar ages were obtained from

crosscutting deformed and undeformed dykes (Higgins and Van Breeman, 1992) and

indicate that the emplacement and cooling were synchronous with deformation. An age of

1142+/-3 Ma (U-Pb, Higgins and Van Breeman, 1992) from the south-western part of the

LSJAC is interpreted to represent igneous crystallisation, supporting the hypothesis that the

anorthosite represents a multiple intrusion (Roy *et al.*, 1986).

2.2 Local Geology

The Canton Saint-Onge wollastonite deposit is located entirely within the LSJAC

along a major NE-SW trending shear zone, termed the Lacs Saint-Jean - Pipmuacan

lineament (LSJP)(fig 2.2) (Hébert, 1991). It can be traced from the NE extremity of the

Pipmuacan reservoir to Dolbeau, near Lac-Saint-Jean and possibly projects further south

(Claude Hébert, pers.com.) for a distance of at least 200 km. It is marked by solid-state

deformation with many shear zones and mylonitic structures oriented N 050 to 060°, as

well as numerous intrusions of diverse composition: granite, syenite, gabbro, charnockite

etc. of probable different ages as suggested by the presence or lack of solid state

deformation (Hébert, 1991).

Numerous lenses of metasedimentary rocks, comprising paragneiss, calc-silicates

and marbles are found along the lineament, or within, the zone of deformation associated

with it, one such lens hosts the Canton Saint-Onge wollastonite deposit (fig. 2.3). The

geographical distribution of the metasedimentary rocks suggested to Gervais (1991) that

they represent roof pendants metamorphosed by the intruding anorthosite mass (fig. 2.4a).

However, their close association with the lineament suggests they could also represent

blocks dropped down by late renewed movement along the shear zone, hence preserving

them from subsequent erosion (figure 2.4b).

2.3 Deposit Geology

The deposit is located in the Canton Saint-Onge in the ZEC des Passes north of

Saint-Ludger-de-Milot (fig. 1.1). Access is from the Chemin des Passes road, turning off at

km 34 then following logging trails for easy access to the outcrops. There is little natural

outcropping, most having been exposed during the construction of the logging trails and

trenches dug during exploration work in the area. Previous exploration has focused on

Legend

- Granite
- Charnockite
- Mangerite
- Gabbro
- Anorthosite
- Paragneisses including calc-silicates rocks
- Marble
- ····· Major faults
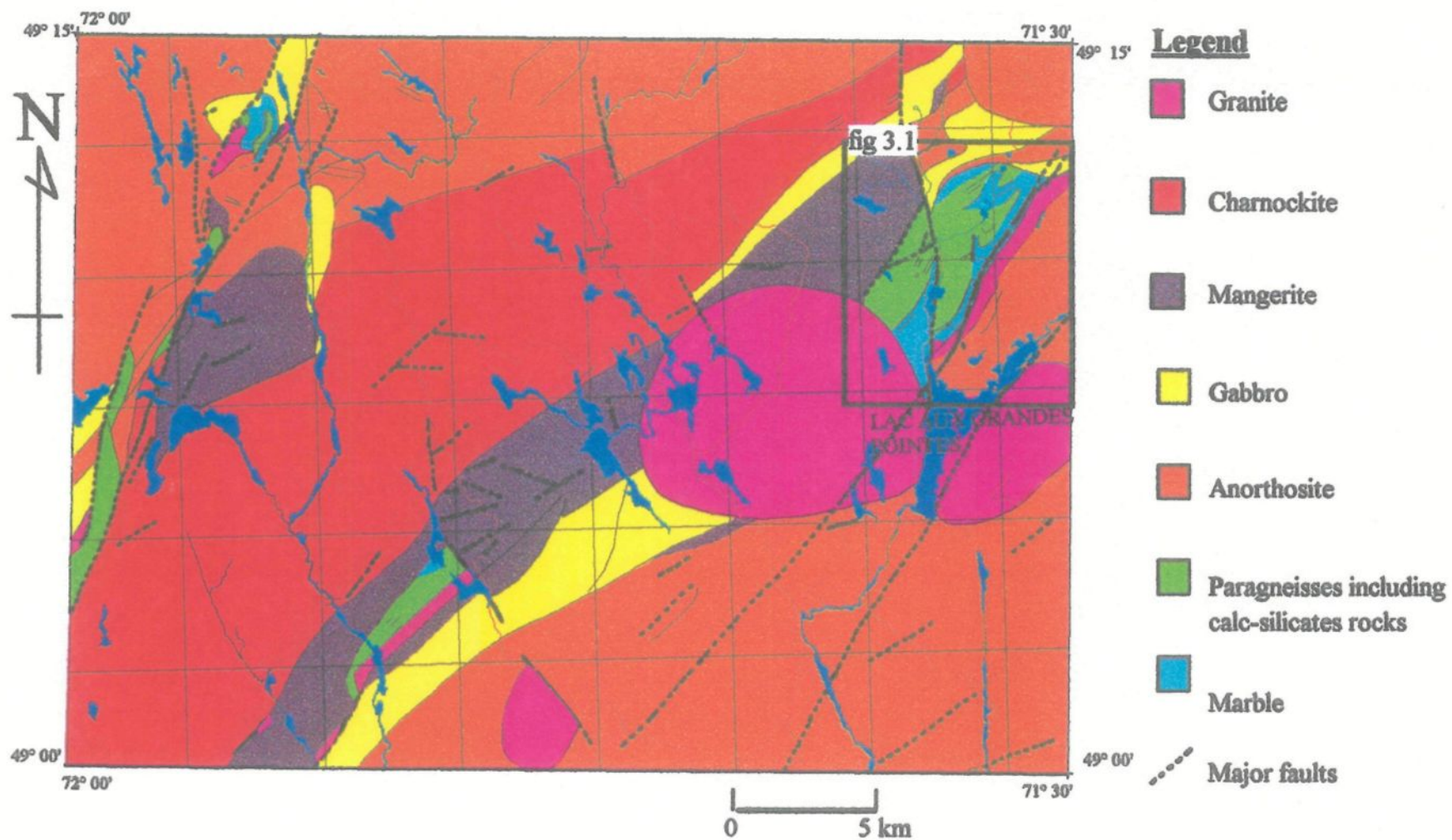
Figure 2.3. Regional geology of the Canton Saint-Onge wollastonite deposit (map sheet 22E/04) after Gervais (1990)..
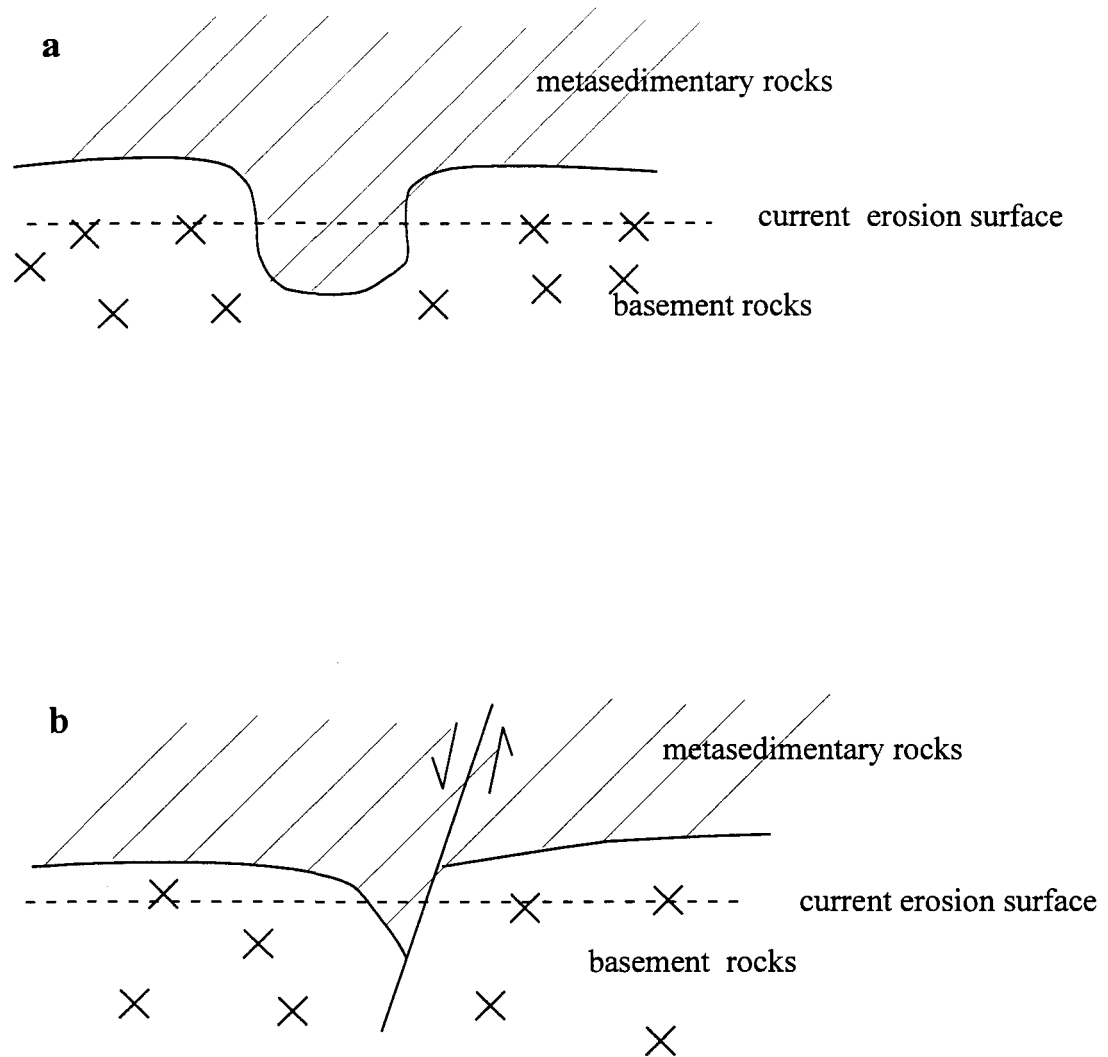
Figure 2.4. Possible mechanisms for the preservation of a lens of metasedimentary rocks; **a**) roof pendants, **b**) fault block

aggregate from the marbles, Balmat-Edwards type zinc and skarn type copper-nickel deposits.

The study area includes the region east of de la Rivières du Nord and du Bras lakes, extending into the anorthosite 4.2 km to the east. The wollastonite deposit is part of a band of metasedimentary rocks preserved along NNE trending faults (fig 1.3), that cuts the LSJP, which is itself in a gabbroic facies of the LSJAC. The southeast border of the metasedimentary rocks is defined by the lenticular Du Bras Pluton which has a width of around 500 m and was emplaced and deformed along these NNE trending faults (Gervais, 1991). The Astra Pluton lies to the south. A screen of marble around 300 m thick separates the calc-silicate skarn from the du Bras granite. These units are described in more detail in chapter 3.

Chapter 3

PETROGRAPHY AND MINERALOGY

3.0 INTRODUCTION

The laboratory part of the study was started with a petrographic analysis of samples collected in the field. Sampling was concentrated on the south-east side of the deposit, and their locations are shown on figure 3.1. The mineral assemblages and textures were identified using transmitted and reflected light optical microscopy. Samples then were selected for electron microprobe and geochemical studies.

3.1 LAC-SAINT-JEAN-ANORTHOSITE

The part of the Lac-Saint-Jean Anorthosite Complex bordering the Canton St-Onge metasediments is a more mafic phase of the anorthosite complex. A horizon of anorthositic gabbro, containing <25% mafics, borders the Du Bras pluton to the south-east, and grades in a south-easterly direction, away from the metasediments, into an anorthosite. Typical assemblages are summarised in table 3.1. The classification of the Lac-Saint-Jean anorthosite used is that of Laurin and Sharma (1975) developed for the Grenville mapping
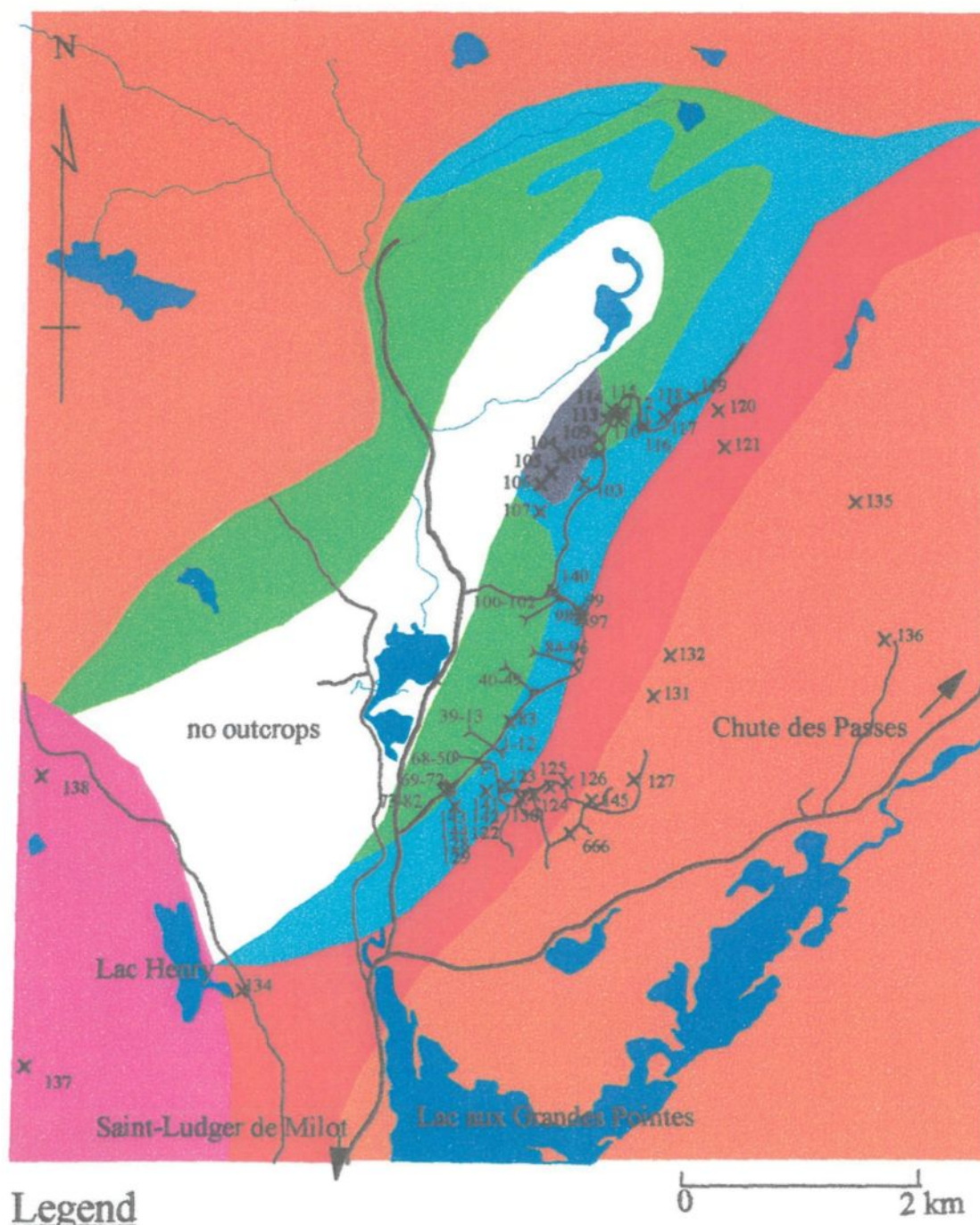
Figure 3.1. Geology of the Canton Saint-Onge wollastonite deposit with sample locations.

rock type	Anorthosite				Anorthositic gabbro
sample no.	ABM-132	ABM-135	ABM-136	ABM-666	ABM-131
plagioclase	82	87	92	93	67
olivine	10				
clinopyroxene	3	8		2	20
orthopyroxene	2		3	2	
hornblende			2		5
amphibole		2			
magnetite	3	2	tr	2	4
iddingsite					2
pyrite					1
quartz					1
biotite		1	2		
chlorite				1	

Table 3.1. Lac-Saint-Jean Anorthosite assemblages. Percentages based on visual estimate

project whereby an anorthosite contains 0 to 10% of mafic minerals, gabbroic anorthosite 11 to 20 % mafics and anorthositic gabbro 21 to 35% mafics. The latter is also distinguished by its high percentage of magnetite and ilmenite. The horizon of anorthositic gabbro consists of white, strained plagioclase (5 mm in size) comprising around 75% of the rock (plate 3.1). Mafic minerals include clinopyroxene, iddingsite, magnetite and pyrite. The anorthositic gabbro shows well-developed cumulus textures with the plagioclase as the euhedral cumulus phase surrounded by the mafic minerals making up the intercumulus phases.

The anorthosite to the south-east is composed mainly of plagioclase 5 mm in diameter. Iron-magnesium bearing minerals make up around 5% of the rock and include primary clinopyroxene with well-developed retrograde hornblende coronas which in turn are surrounded by chlorite-biotite coronas. The plagioclase is white in outcrop (plate 3.2a) and shows some sericitization and exhibits undulose extinction indicating strain (plate 3.2b) indicating partial recrystalisation or an episode of strain after recrystalisation. The unit probably formed as an adcumulate with additional growth on the plagioclase giving rise to large anhedral grains exhibiting triple junctions between grains.

3.2 DU BRAS PLUTON

The Du Bras Pluton is an igneous rock of granitic composition about 500 m wide and 10 km long, extending NE-SW, parallel to the lens of metasediments and the LSJP

25

Plate 3.1a. Anorthositic gabbro outcrop with white recrystalised cumulate plagioclase with intercumulate mafic minerals including clinopyroxene, iddingsite and magnetite.

Plate 3.1b. Anorthosite gabbro in thin section under cross-nicols showing plagioclase (white-grey) with clinopyroxene (blue-pink) and magnetite (black).
Field of view = 5 mm

26
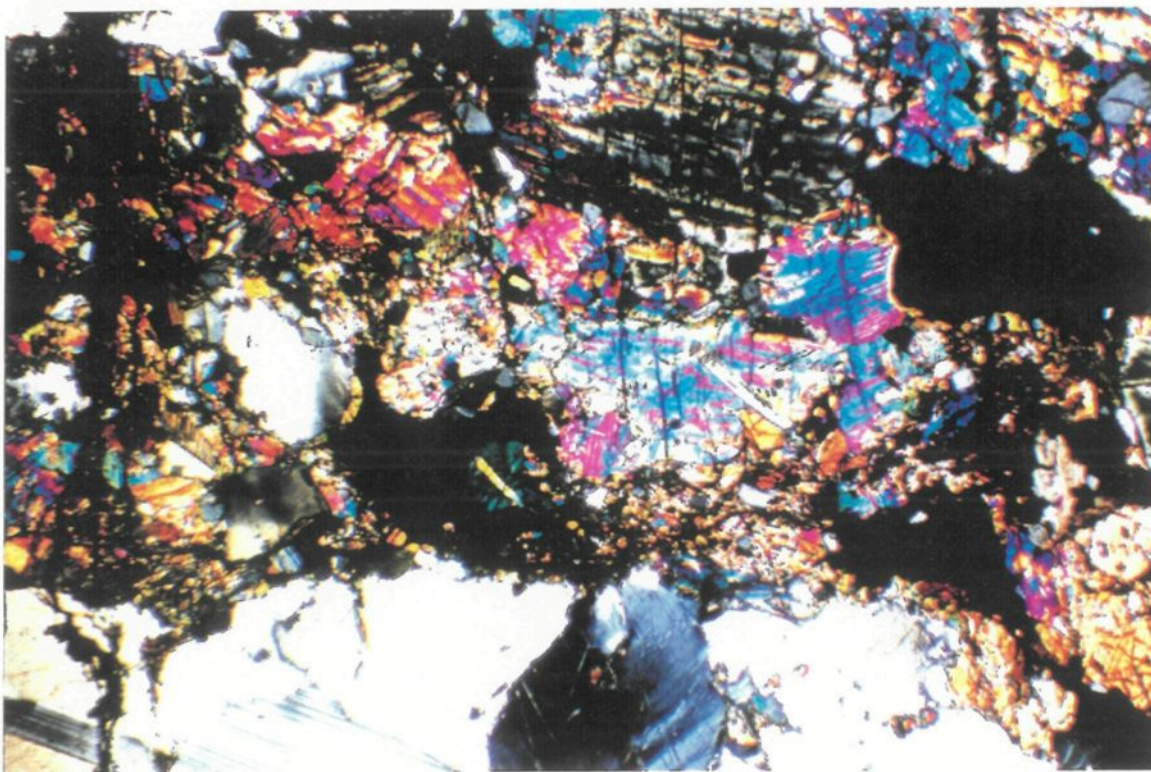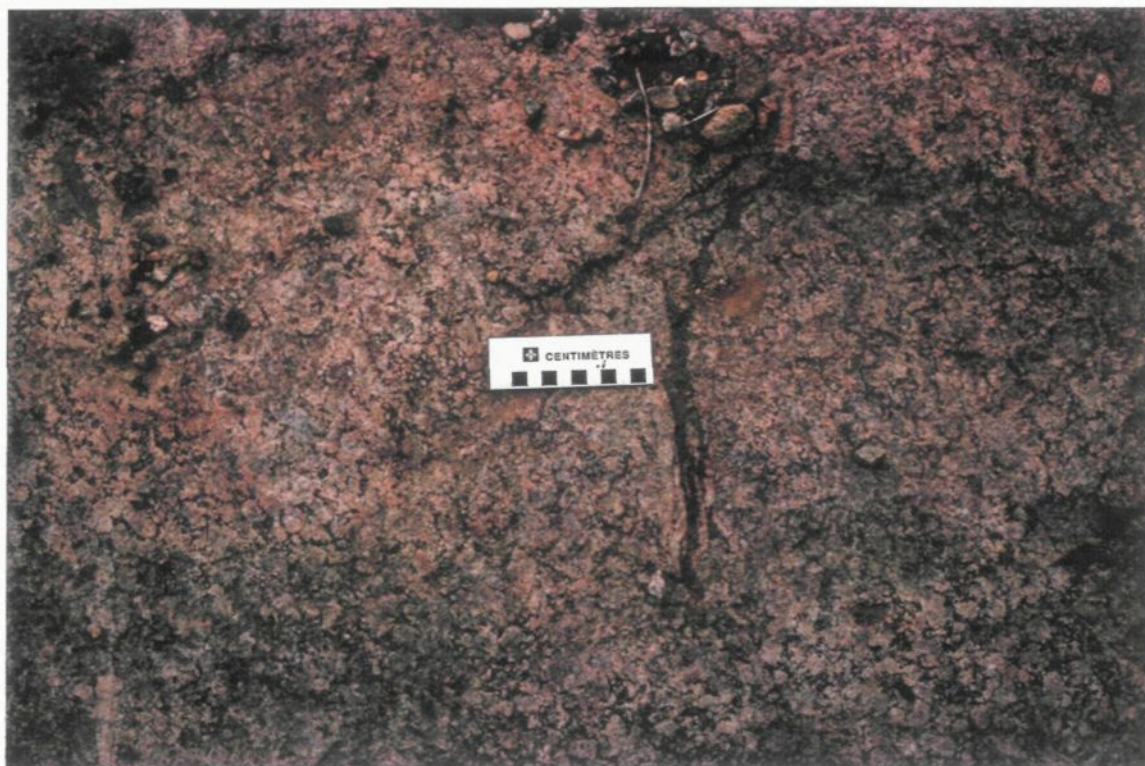
Plate 3.2a. Anorthosite outcrop composed mainly of recrystalised plagioclase.

Plate 3.2b. Anorthosite in thin section under crossed-nicols showing adcumulate recrystalised plagioclase with undulose extinction.
Field of view = 5 mm
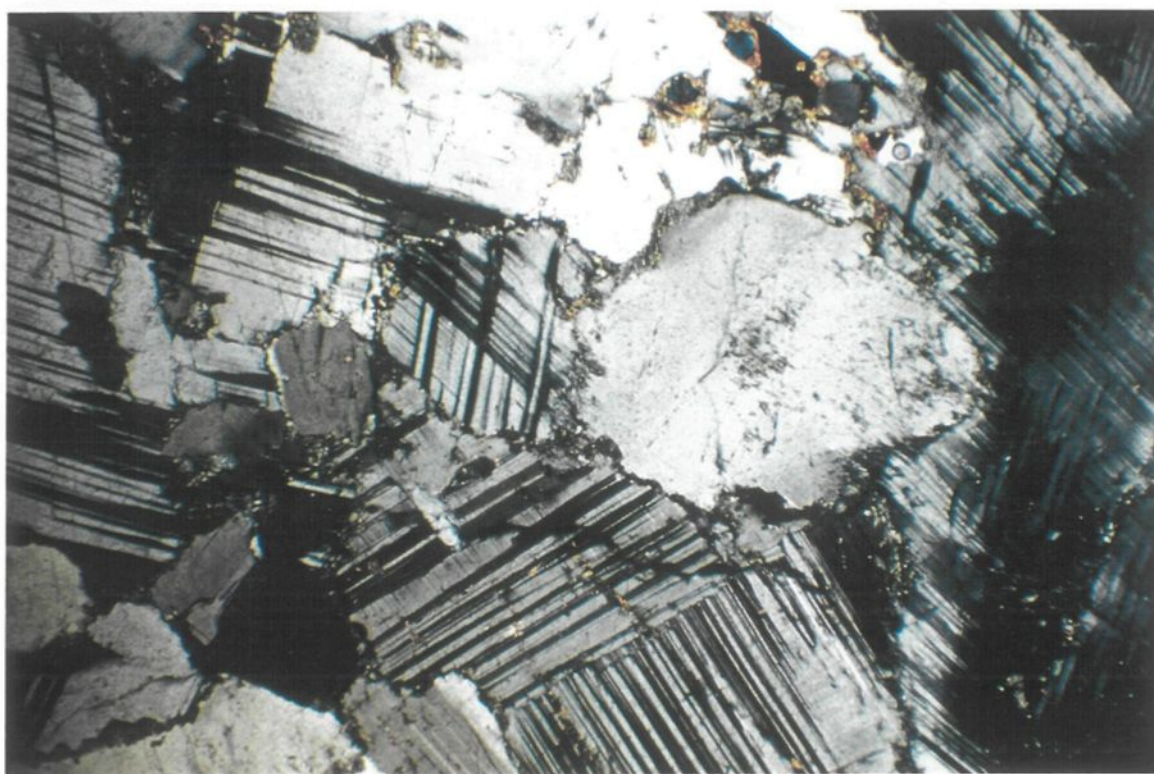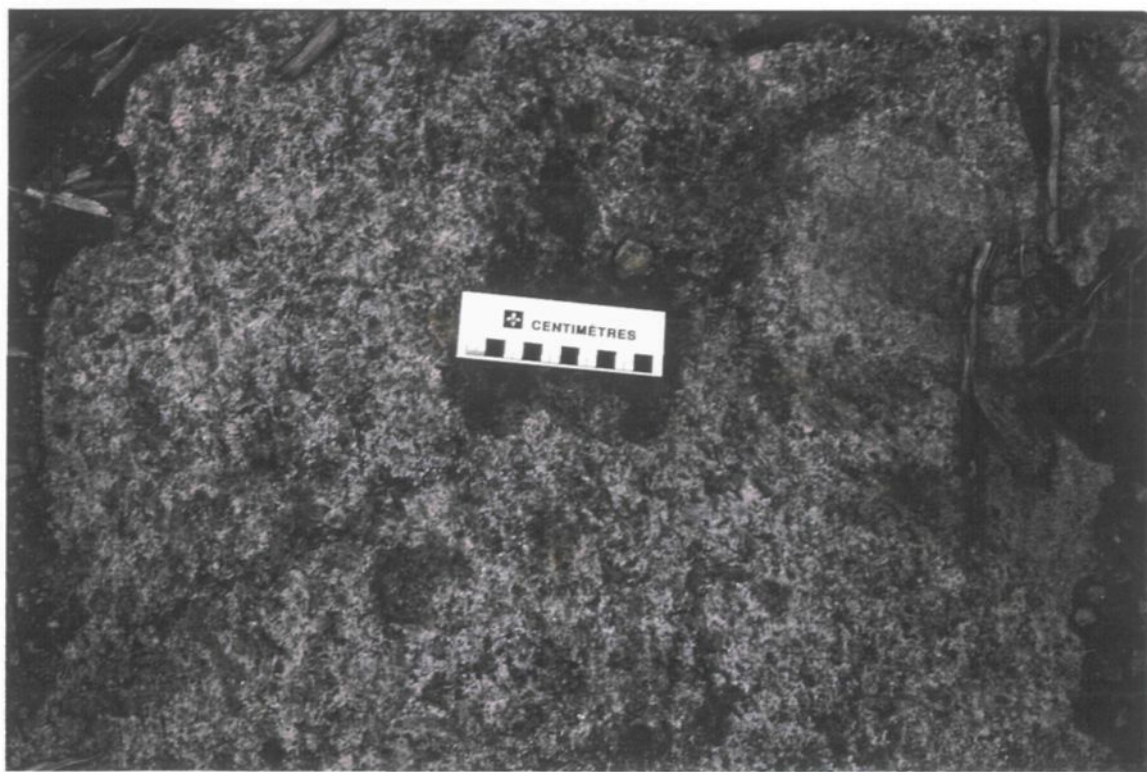
lineament. It borders the anorthosite to the north-west, and separates the marbles (to the north-east) from the anorthosite. The position of this intrusion has suggested to Gervais (1991) that the unit is a granophyre, produced by melting of the neighbouring metasediments upon the emplacement of the Lac-Saint-Jean Anorthosite. However, this hypothesis seems unlikely given the geochemical data to be presented later. The Du Bras Pluton has not yet been dated.

Typical assemblages of the Du Bras Pluton are summarised in table 3.2. The granite is comprised of quartz, that is commonly blue, perthitic orthoclase, plagioclase with minor biotite, hornblende, titanite, epidote, apatite, pyrite, and zircon (plate 3.3a). It has some rounded potassium-feldspar phenocrysts with mantles of plagioclase (plate 3.3b). Deformation is of variable extent, but mortar texture is fairly common. The grain size is bimodal with a groundmass average grain size of 1 mm and the K-feldspar phenocrysts averaging 1 cm; some of the plagioclase shows myrmekite texture. The pluton is most deformed in the south-west, as demonstrated by the development of a strong foliation, rotated phenocrysts and shear bands there. To the north-east the unit is undeformed.

3.3 ASTRA PLUTON

The Astra Pluton is a large (10 km diameter) syenitic intrusion emplaced into the Lac-Saint-Jean anorthosite to the south of the Canton Saint-Onge metasediments. The

sample no.	ABM-120	ABM-121	ABM-124	ABM-126	ABM-134	ABM-145
K-feldspar	50	40	35	35	30	30
plagioclase	10	15	7	7	20	15
quartz	31	40	52	50	37	45
hornblende	3	3		5		
biotite	3	2	5	3	10	2
augite						5
magnetite	2	tr				
apatite	1					
spinel						1
epidote					1	2
muscovite					2	

Table 3.2. Du Bras Pluton assemblages. Percentages determined by visual estimate

sample no.	ABM-137	ABM-138
microcline	60	50
myrmekite	5	10
quartz	30	30
plagioclase	5	3
biotite	5	5
epidote	2	2
magnetite		1

Table 3.3. Astra Pluton mineral assemblages. Percentages determined by visual estimate

29

Plate 3.3a. Outcrop of undeformed facies of the Du Bras Pluton of granitic composition.

Plate 3.3b. Du Bras Pluton in thin section under crossed-nicols showing phenocrysts of alkali-feldspar and plagioclase in a matrix of finer grained quartz and biotite.
Field of view = 5 mm
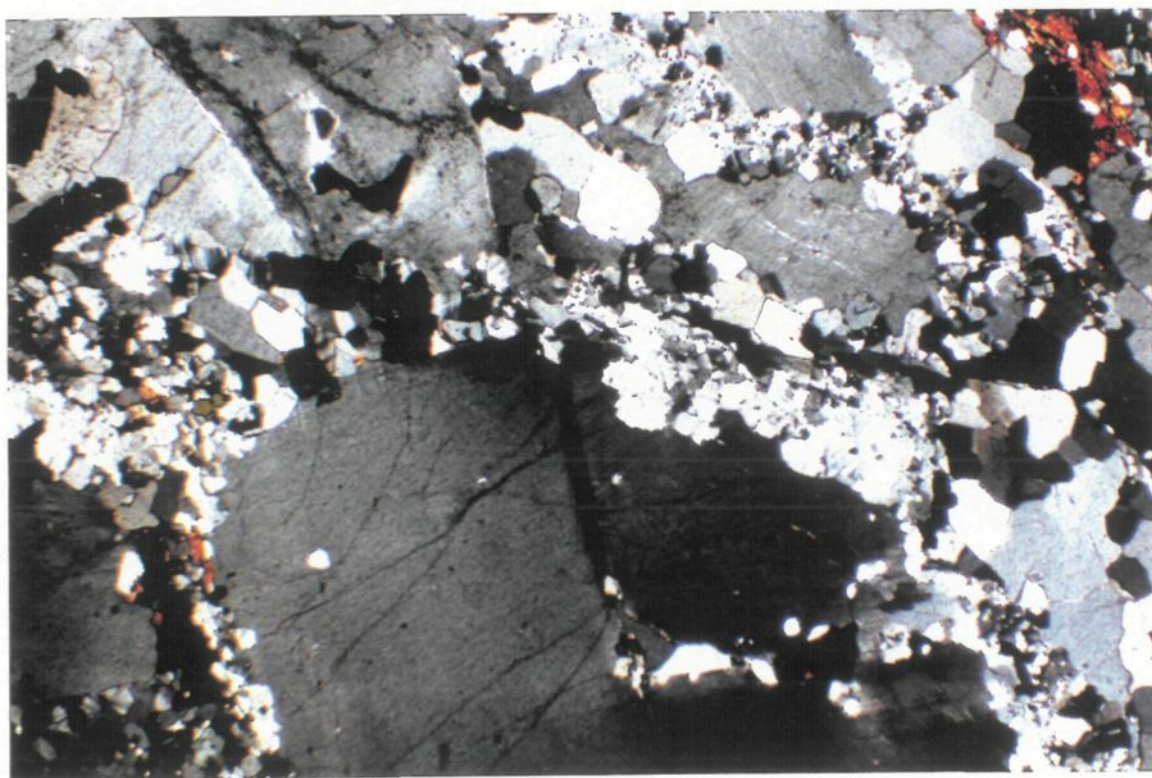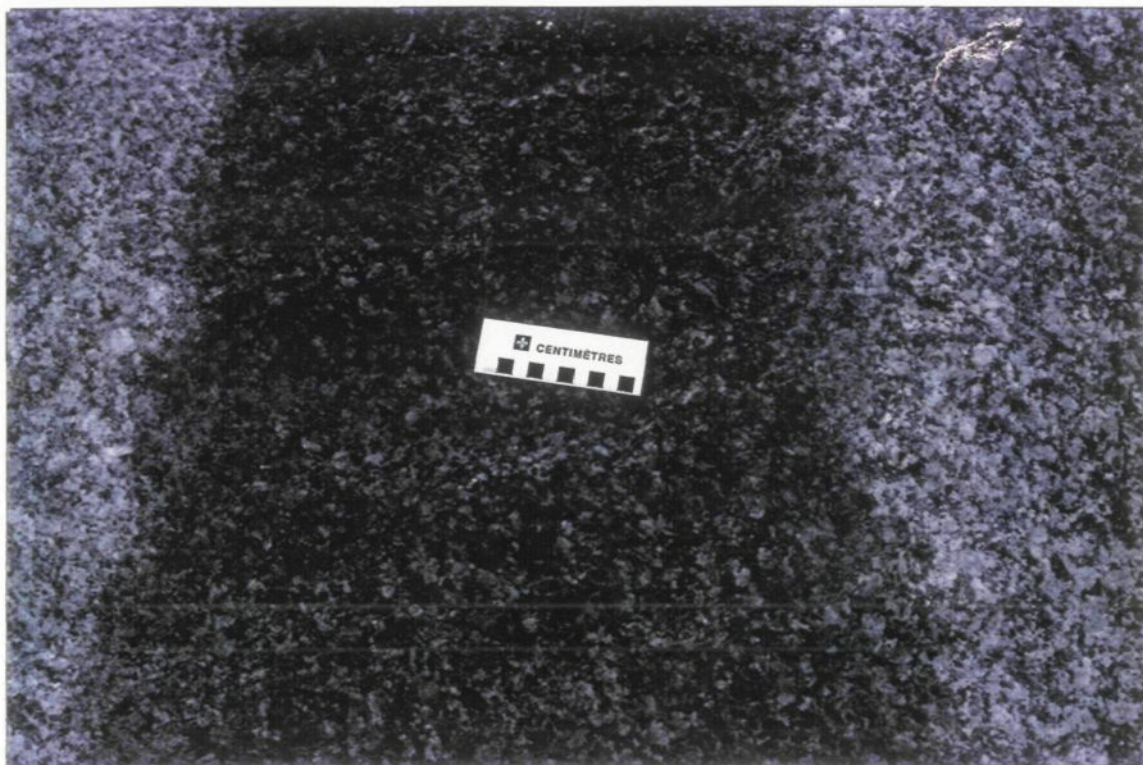
pluton is circular in form cutting, and probably emplaced along the Lacs-St-Jean-Pipmuacan lineament. It is undeformed in the solid state (plate 3.4a), and therefore most likely post-dates the deformation as well as the Du Bras Pluton bordering the anorthosite.

Typical assemblages of the Astra Pluton are summarised on table 3.3. The rock is comprised of quartz (30%), microcline (60%), with some plagioclase, arfvedsonite, apatite, magnetite and zircon; mafic minerals include hornblende and biotite (plate 3.4b). Some of the pink microcline crystals are large and rounded with plagioclase rims. Some of the plagioclase crystals have myrmekitic texture. The average grain size is 1 mm with the mantled phenocrysts up to 1 cm in diameter. There is no evidence in thin section or in the field for solid-state deformation. However, a weak foliation defined by the alignment of feldspar is thought to be magmatic in origin.

3.4 MARBLES

The marbles situated along the contact with the granite can be divided into at least three varieties: massive metadolostone, layered olivine/serpentine marble and calc-silicate marble. Typical assemblages are summarised in table 3.4.

The massive dolostone is white, massive to faintly layered and composed principally of dolomite (around 90%), the remainder being minor calcite, serpentine,

Plate 3.4a. Hand sample of undeformed Astra Pluton.

Plate 3.4b. Astra Pluton in thin section under crossed-nicols showing equigranular microcline (tartan texture), quartz (white), plagioclase (grey) and hornblende (brown-green).
Field of view = 5 mm
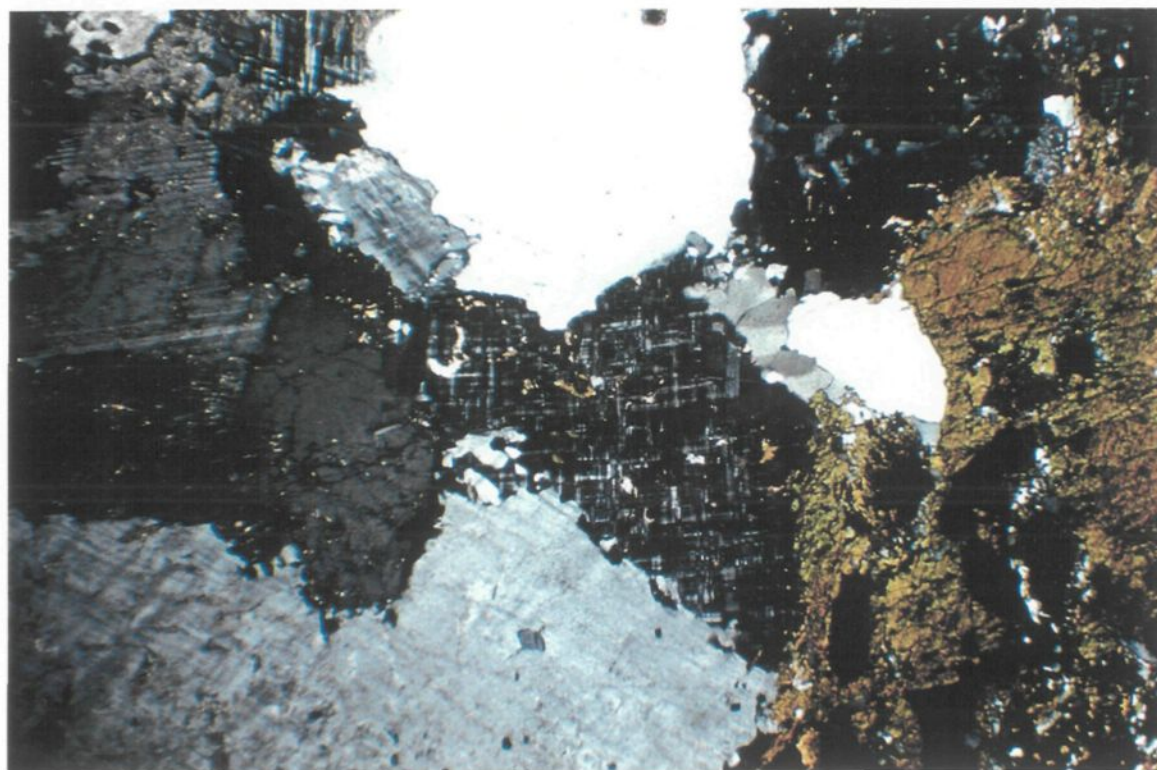
MARBLES	Metadolostones			Layered olivine-serpentine marble			
sample no.	ABM-011	ABM-089	ABM-084	ABM-050	ABM-117	ABM-122b	ABM-141
dolomite	90	80	40	2	15	5	
calcite	5	10	30	40	55	55	45
olivine	2	3		10	10		
chondrodite			27			5	5
serpentine	3	7	3	48	25	35	40
graphite					2		1
muscovite							10

	Calc-silicate marble		
sample no.	ABM-107	ABM-110	ABM-122a
calcite	70	40	
quartz	10		1
K-feldspar	3		
wollastonite		5	
biotite	2		
titanite	1	3	
pyrrhotite		2	
diopside	5	50	30
graphite	2		
olivine			25
serpentine			30
muscovite			2
orthopyroxene			10

Table 3.4. Marble mineral assemblages. Percentages determined by visual estimate.

olivine and graphite (plate 3.5). The dolomite is equant, around 1 mm in diameter with annealed triple junctions. Staining with alazarin red shows that 5% calcite fills interstices and is evenly distributed throughout the rock. Yellow chondrodite occurs in this unit with percentages ranging from 5 - 30%, but only in the samples from the south-west near the contact with the Astra pluton.

The layered serpentine/olivine marble contains 50-65% calcite with a mixture of olivine and retrograde serpentine making up around 30% of the rock (plate 3.6a). Other minor minerals are muscovite, quartz and graphite. Layering is produced by grain-size variation, as well as mineralogical contrasts between layers with more serpentine-olivine and dolomite layers. The rock is isoclinally folded on a centimetric scale which can easily be seen by the contrasting white calcite and green/black olivine/serpentine layers (plate 3.6b). The layers are continuous and can be traced along the exposure of the outcrops or trenches. Chondrodite occurs in this unit, in percentages ranging from 5 to 30% as in the dolostone but again, it only occurs in the samples from the south-west close to the contact with the Astra Pluton.

These two units are not mapable on the deposit scale, both occur in contact between the du Bras pluton to the south-east and the calc-silicates to the north-west.

Plate 3.5a. Outcrop of massive metadolostone (white) with yellow chondrodite-rich areas).

Plate 3.5b. Metadolostone in thin section under plain light showing composition of near 100% equant, annealed dolomite.
Field of view = 5 mm
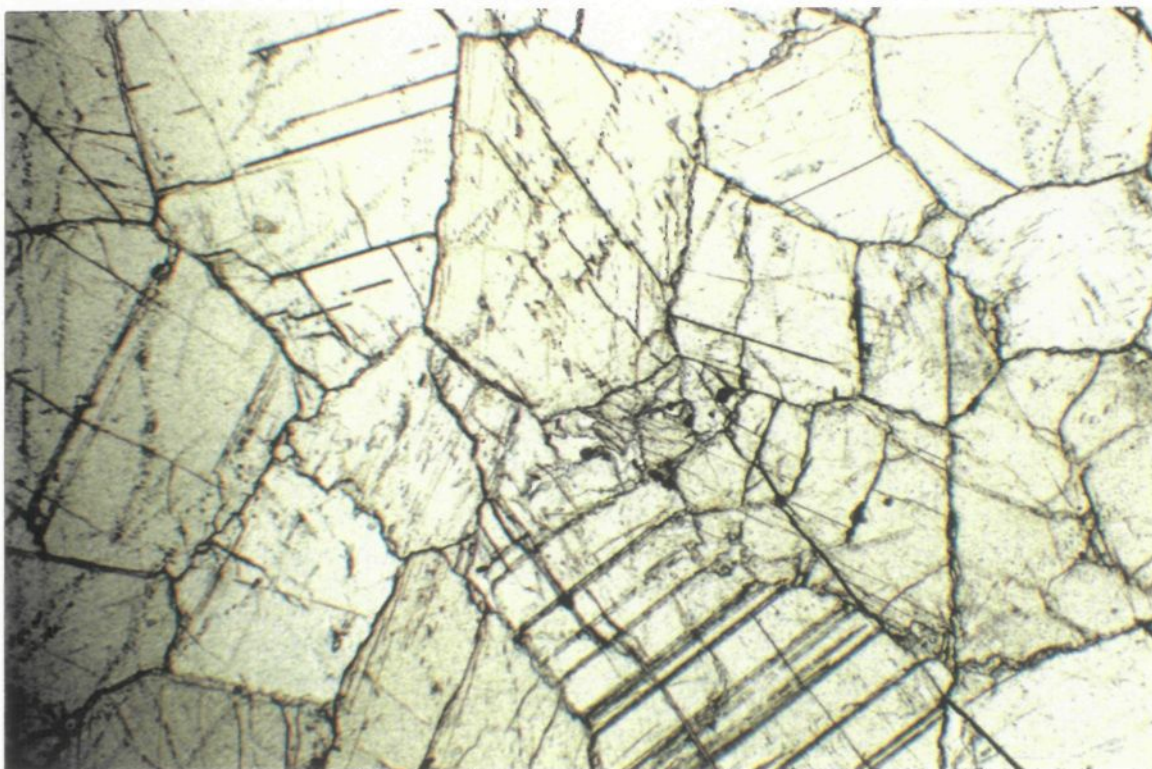
Plate 3.6a. Thin section of olivine-serpentine marble under crossed-nicols showing brown-green calcite and rounded serpentine spots containing relict olivine (yellow) centres. Field of view = 5 mm

Plate 3.6b. Outcrop of layered serpentine-olivine marble. Dark layers are rich in olivine and/or serpentine, whereas the pale layers are composed mainly of calcite. Note isoclinal folding of the layers.
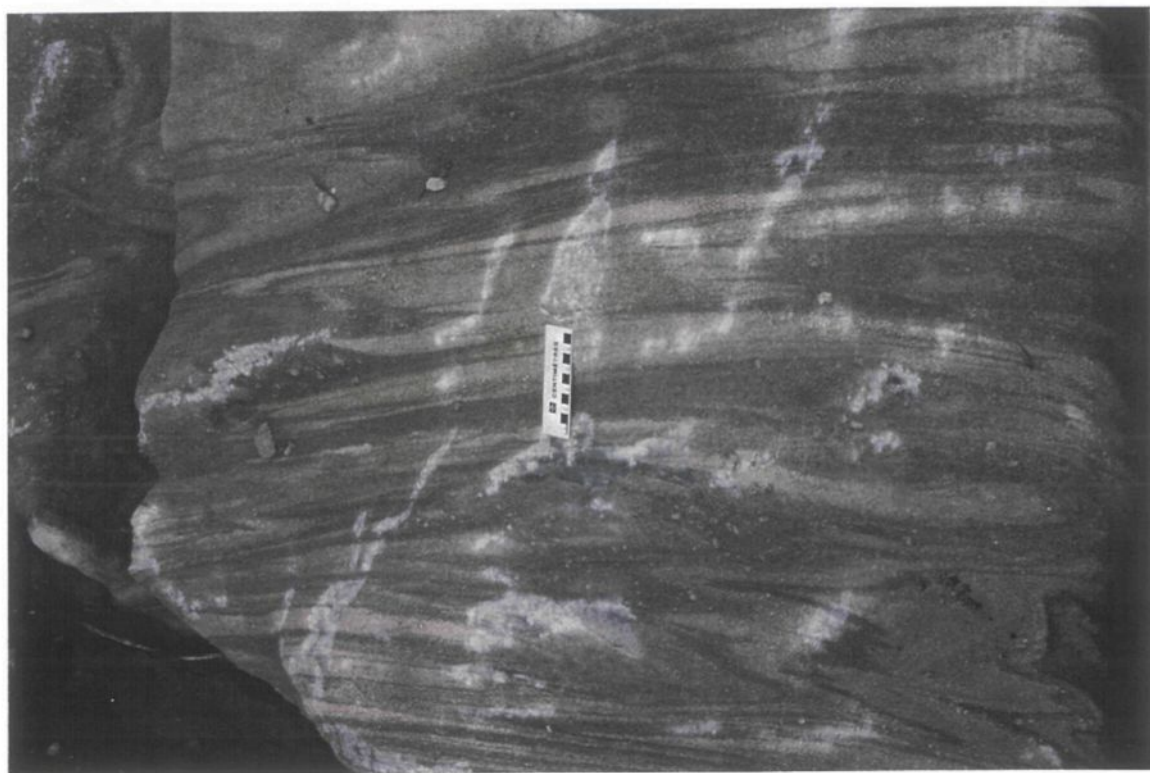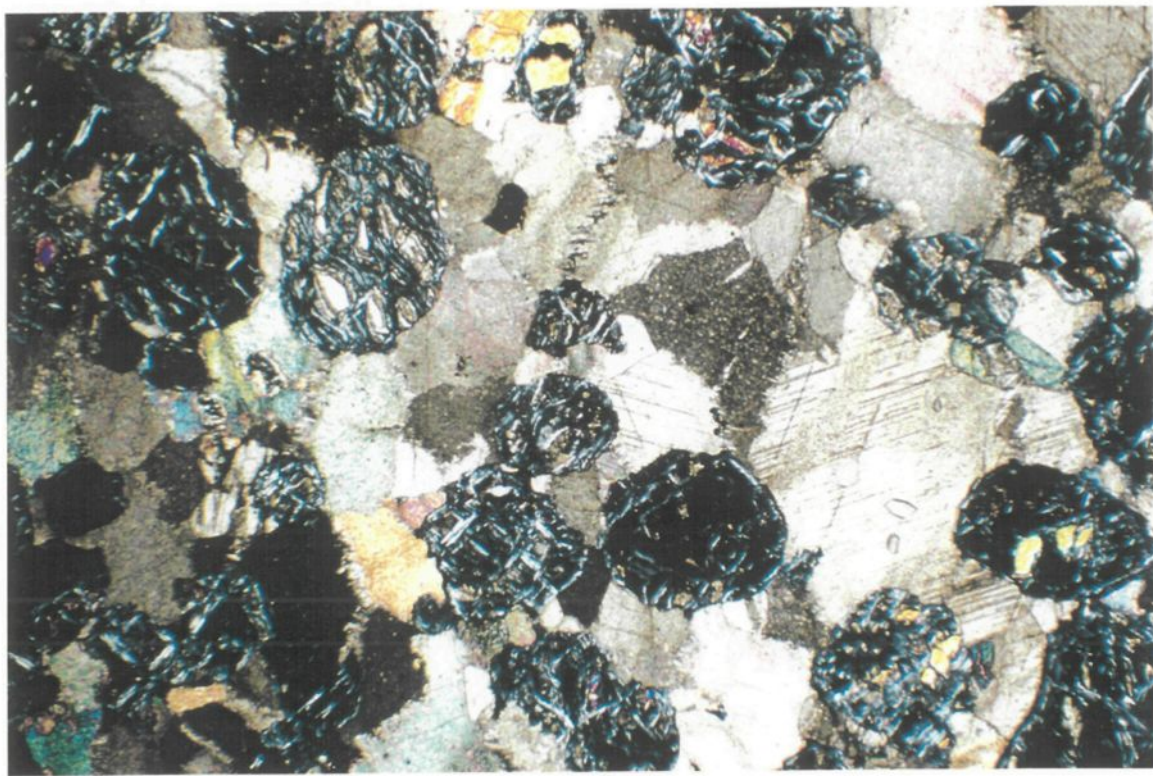
The third marble unit, the calc-silicate marble, differs from the other units by the presence of diopside (plate 3.7a). This unit is generally found near the contact between the calc-silicate rocks and the marble and, therefore, may represent a transitional stage between the two, however, it is classified as a marble because of its high calcite content (<40%). This unit is layered in some places, with layers of calcite between layers of diopside, wollastonite, and titanite. Elsewhere, it is massive, composed mainly of calcite (70%) together with quartz, diopside, perthite, graphite, biotite, and titanite.

3.5 WOLLASTONITE-BEARING CALC-SILICATE ROCKS

The calc-silicate rocks are dominated by diopside, in various forms and colours, in some areas interlayered with wollastonite (plate 3.7b). This 'layer cake' wollastonite/diopside rock is found mainly in contact with the marble, on its southern side. This layering at the millimetre to centimetre scale is easily distinguished by the difference in colour (diopside- green and wollastonite-white) as well as the preferential weathering of the wollastonite layers (plate 3.8a). The layers of quartz and diopside resist weathering whereas the wollastonite weathers easily leaving a fibrous mush.

Plate 3.7a. Thin section of calc-silicate marble under crossed-nicols showing calcite grains (brown-pink) with smaller diopside grains (blue-green).
Field of view = 5 mm

Plate 3.7b. Hand sample of wollastonite-bearing calc-silicate rock. The wollastonite is concentrated in the white layers; the green layers contain mainly diopside.

2 cm

38
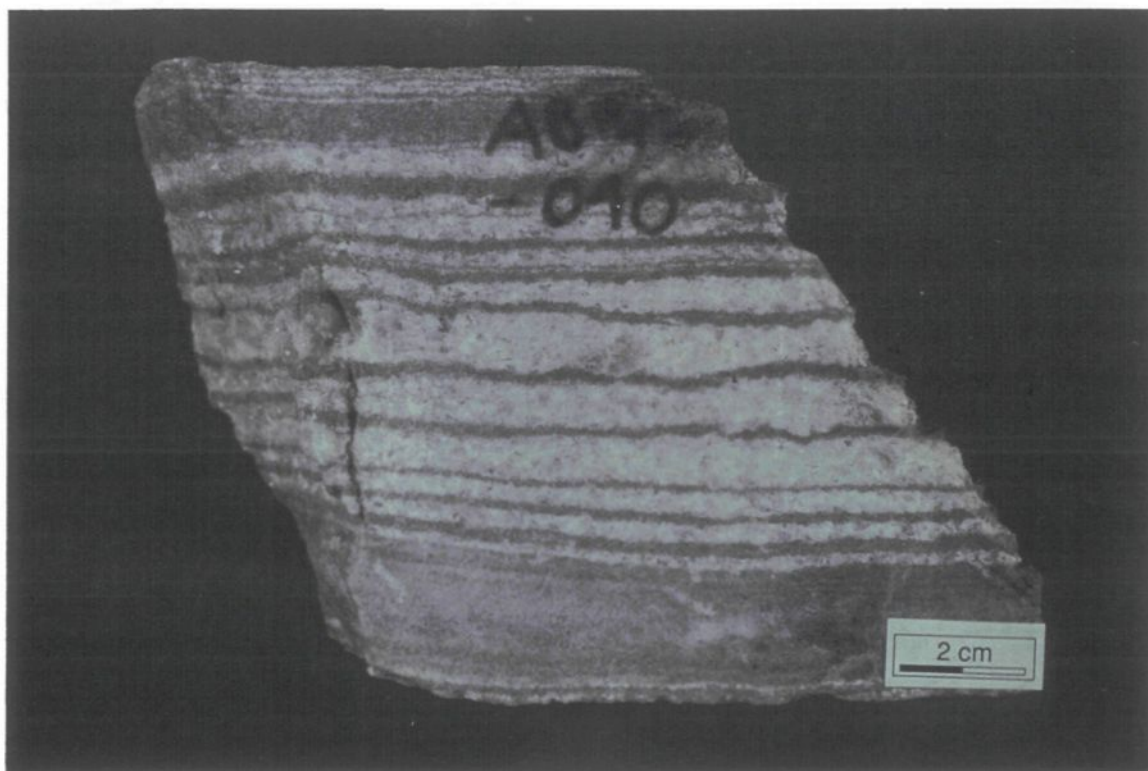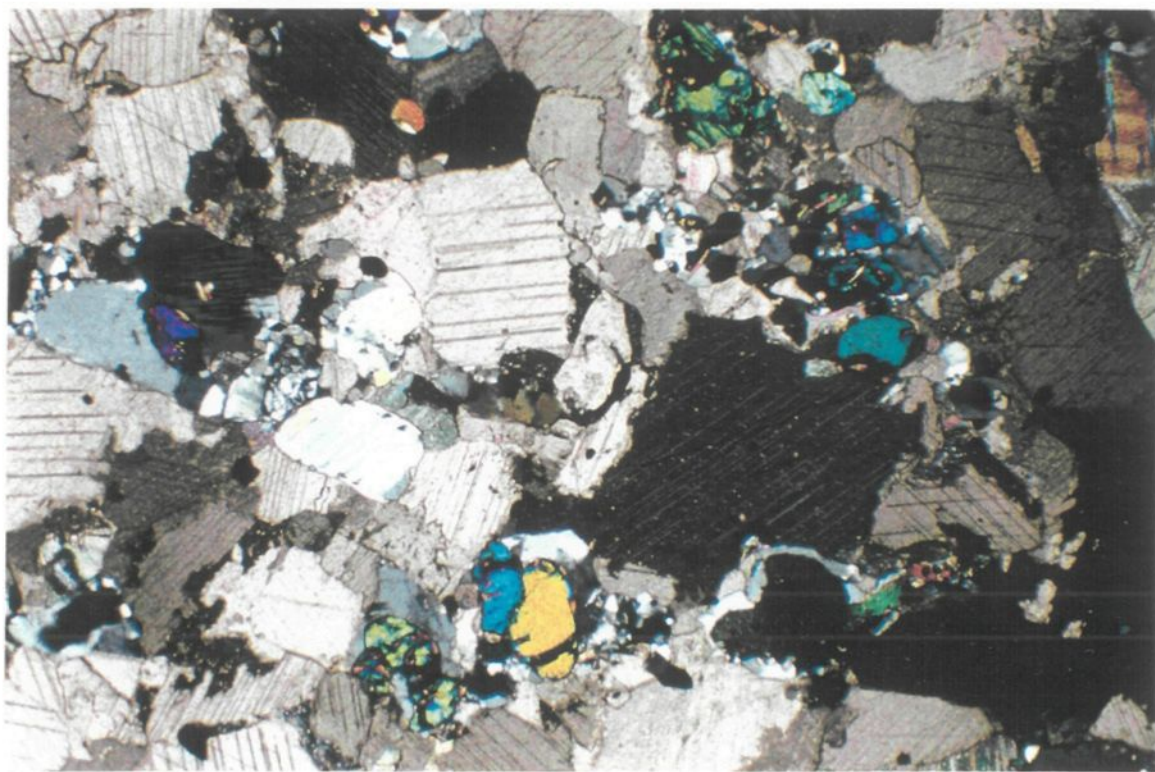
Plate 3.8a. Outcrop of wollastonite bearing calc-silicate rock showing the preferential weathering of the wollastonite -rich layers.

Plate 3.8b. Thin section of layered calc-silicate rock under crossed-nicols showing one coarse-grained wollastonite layer and the fine grained diopside rich layers.
Field of view = 5 mm
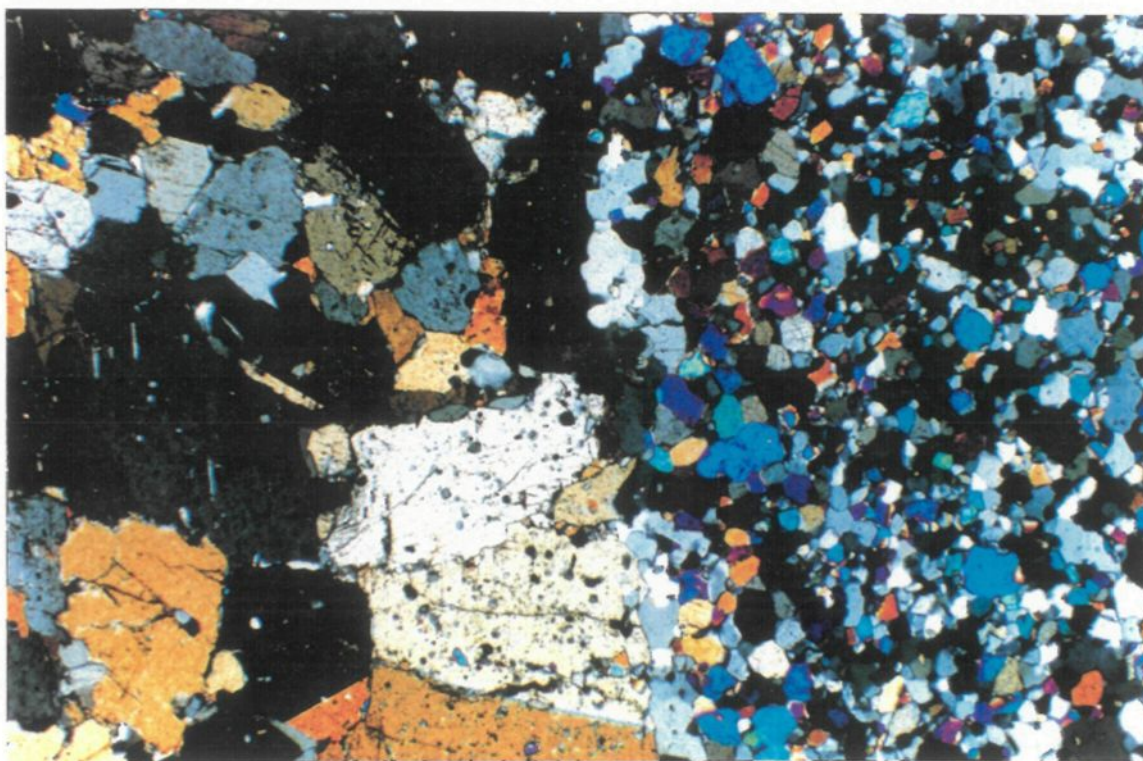
The mineral assemblages found in this unit, summarised in table 3.5, include diopside, wollastonite, quartz, titanite, and microcline (plate 3.8b). Accessory minerals include calcite, plagioclase, vesuvianite, tremolite, anthophylite, pyrrhotite and chalcopyrite.

Diopside is the most prominent mineral in the unit with quantities varying from 50 to 98%. The diopside is typically granoblastic in texture. It is generally concentrated in layers: interlayered with wollastonite as well as interlayered between coarser grained diopside (1 mm) and finer grained diopside (0.25 mm); otherwise the diopside is massive. The diopside varies in colour from green to grey to brown to white. The wollastonite seems to be more commonly associated with the green diopside.

The wollastonite is generally coarse grained, up to 6 mm long with an aspect ratio of 1:3 but is always larger than the diopside which dominates the mineral assemblage. The wollastonite laths are usually crudely aligned with the layering in the rock and are concentrated in layers alternating with the diopside rich layers. The wollastonite is usually very poikilitic with inclusions mainly of diopside and quartz.

Titanite is quite common in this unit comprising up to 30% of the sample. It is pink in colour and anhedral and therefore is easily mistaken for garnet, however, flotation experiments indicate that the deposit only contains trace quantities of garnet (Ressources

sample no.	ABM-002	ABM-005	ABM-012	ABM-034	ABM-039	ABM-040b
diopside	50	100	48	55	40	38
wollastonite				35	25	30
quartz	40		10		25	10
titanite	5		2			10
calcite	2				2	2
plagioclase	1			2		10
garnet	1					
flourite	tr					
tremolite			10			
K-feldspar				5	7	
anthophylite					1	
plagioclase				2		
phlogopite			30			

sample no.	ABM-047b		ABM-052	ABM-069	ABM-074	ABM-101
	Diopside layers	wollastonite layers				
diopside	40	20	85	50	90	70
wollastonite		60		8		20
quartz	50	2	5	10		2
titanite		10		2		3
calcite		3	5	10	10	2
plagioclase				10		
garnet						
flourite						
tremolite						
K-feldspar	10	tr	5	10		1
anthophylite						
plagioclase		5				2
phlogopite						

Table 3.5. Calc-silicate rock mineral assemblages. Percentages determined by visual estimate.

sample no.	ABM-111	ABM-140	ABM-093	ABM-031	ABM-047b
diopside	40	94	100	50	85
wollastonite	20				
quartz	10	2		30	10
titanite		2			5
calcite	20	1			
plagioclase				20	
garnet					
flourite					
tremolite					
K-feldspar	10	1			
anthophylite					
plagioclase	tr				
phlogopite					

Table 3.5. Continued

Orléans, pers.comm.). The titanite occasionally occurs as thin layers (<1 mm) in the calc-

silicate rocks or more commonly evenly distributed across the layers as an accessory

mineral.

Quartz and calcite both occur in the calc-silicate rocks. Quartz occurs concentrated

as layers as well as disseminated throughout the rock where it comprises 2-10% of the rock.

It can comprise up to 40% in this unit, and is found in areas where there is less wollastonite.

Quartz was never observed to be in contact with calcite.

Calcite is found in small quantities (<5%) in nearly all thin sections. It occurs either

as a primary phase relative to metamorphism, where it is has a subhedral to euhedral

crystalline habit as well as a secondary phase, filling in small late fractures.

Sulphide minerals in the samples include pyrite, pyrrhotite, chalcopyrite and

sphalerite. The pyrite, pyrrhotite and chalcopyrite occur disseminated throughout the rock,

although somewhat more concentrated in the diopside-rich layers, in quantities never

exceeding 2%. The sphalerite occurs only in one area (station 77 on figure 3.1) where

entire layers up to 3 centimetres thick consist of nearly massive sphalerite (plate 3.9a), with

zinc percentages up to 19.5% (Gervais, 1990) probably for chosen samples. This area was

the focus of exploration by Soquem in 1978 and 1979 (Gervais, 1991).

43

Plate 3.9a. Outcrop of zinc showing. The zinc is present in this photo as thin black layers interlayered with the wollastonite (white) and diopside (green).

Plate 3.9b. Outcrop of hornfelsic paragneiss (green) and discontinuous lenses of quartzite (blue-white).
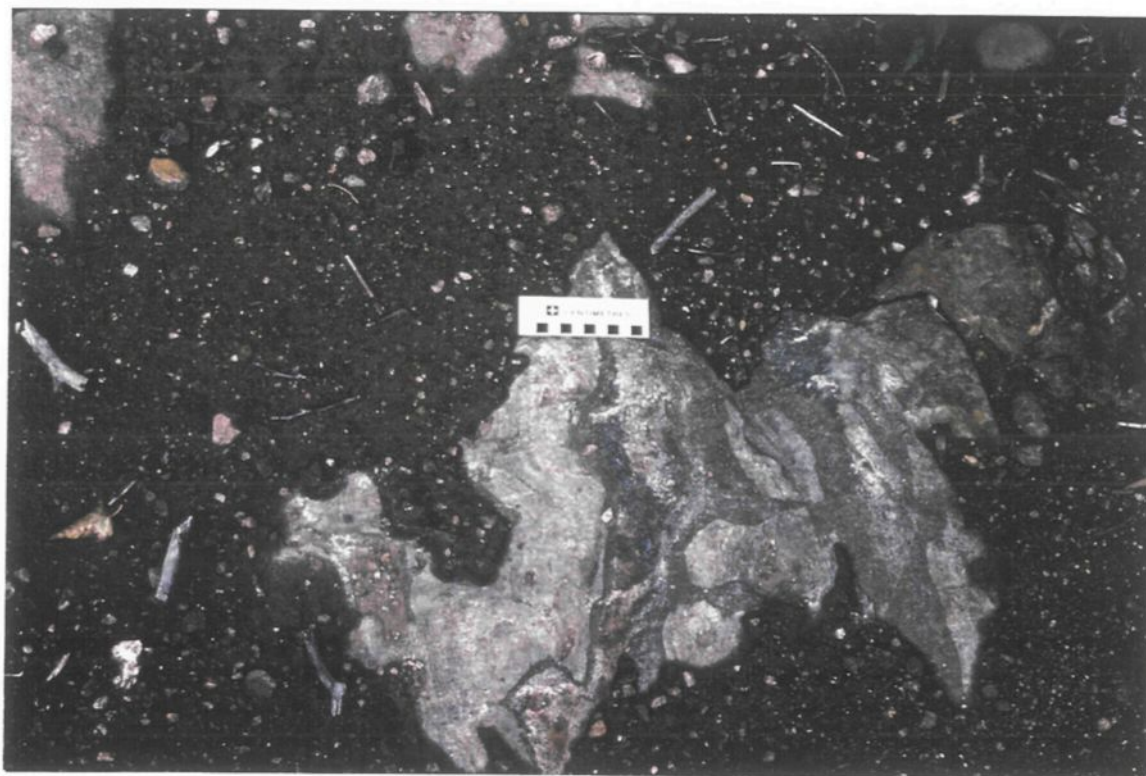
3.6 PARAGNEISSIC HORNFELS AND QUARTZITE

Other units in the area include paragneissic hornfels and quartzite, with assemblages summarised in table 3.6.

The paragneissic hornfels is found to the north of the deposit interlayered with quartzite. The paragneissic hornfels is fine-grained, grey-green, sometimes layered and contains more than 50% quartz and alkali feldspar together with augite, enstatite, biotite and hornblende.

Quartzite is most commonly found interlayered with the paragneissic hornfels as well as interlayered with the calc-silicates of the south and less commonly within the marble. The quartzite forms discontinuous lenses associated with the paragneiss and calc-silicates (plate 3.9b). It contains greater than 80% quartz and feldspar together with augite, hornblende, titanite, biotite.

3.7 DYKES

An amazonite pegmatite dyke around 5 m wide outcrops along 15 m in the south-east of the deposit. It is oriented N10°E with a shallow dip of 5° towards the west, with the host rock being the marble. The dyke is composed principally of green amazonite with

sample no.	Paragneissic hornfels			Quartzite		
	ABM-104b	ABM-112b	ABM-129	ABM-112a	ABM-130	ABM-139
quartz	50	75	30	90	95	97
biotite	20			2	2	
augite		15		7		
K-feldspar	5	5				
plagioclase	5		5			2
titanite		3	2		1	
pyrrhotite	3	2				
hornblende	7		5		3	
orthopyroxene	7					
apatite	1				tr	
pyrite	2		3	1		1
anthophylite			40			
muscovite			15			

Table 3.6. Paragneissic hornfels and quartzite mineral assemblages. Percentages determined by visual estimate.

quartz, comprising 20%, followed by cleavelandite albite, muscovite, biotite, minor garnet and fluorite. The amazonite crystals can reach a few decimetres in size, and in places exhibit graphic texture. The amazonite has been exploited for decorative stone.

There are some undeformed (late) diabase dykes within the map area. These black aphanitic dykes are around 1 m wide with black plagioclase phenocrysts a few millimetres in size comprising 20% of the rock. The dykes clearly cross cut across the stratigraphy in the calc-silicate rocks but have only been seen in small isolated outcrops were no orientation can be determined.

Some granitic dykes also occur within the map area. The dykes are around 30 cm wide, white in colour and fine-grained, average grain size is 1 mm. The dykes are granitic in composition composed mainly of quartz and microcline with minor titanite. The dykes are sub-parallel to the calc-silicate rock layering but show no contact reaction with the host calc-silicate rocks (plate 3.10).

3.8 STRUCTURE

The LSJP lineament (fig. 2.2) is a NE-trending line on a map joining lenticular plutons and shear zones (Hébert, 1991). The lineament probably represents a zone of weakness where shearing has occurred, as indicated by the solid state mineral deformation

Plate 3.10. Outcrop showing sub-parallel granitic dyke in the layered calc-silicate rocks.
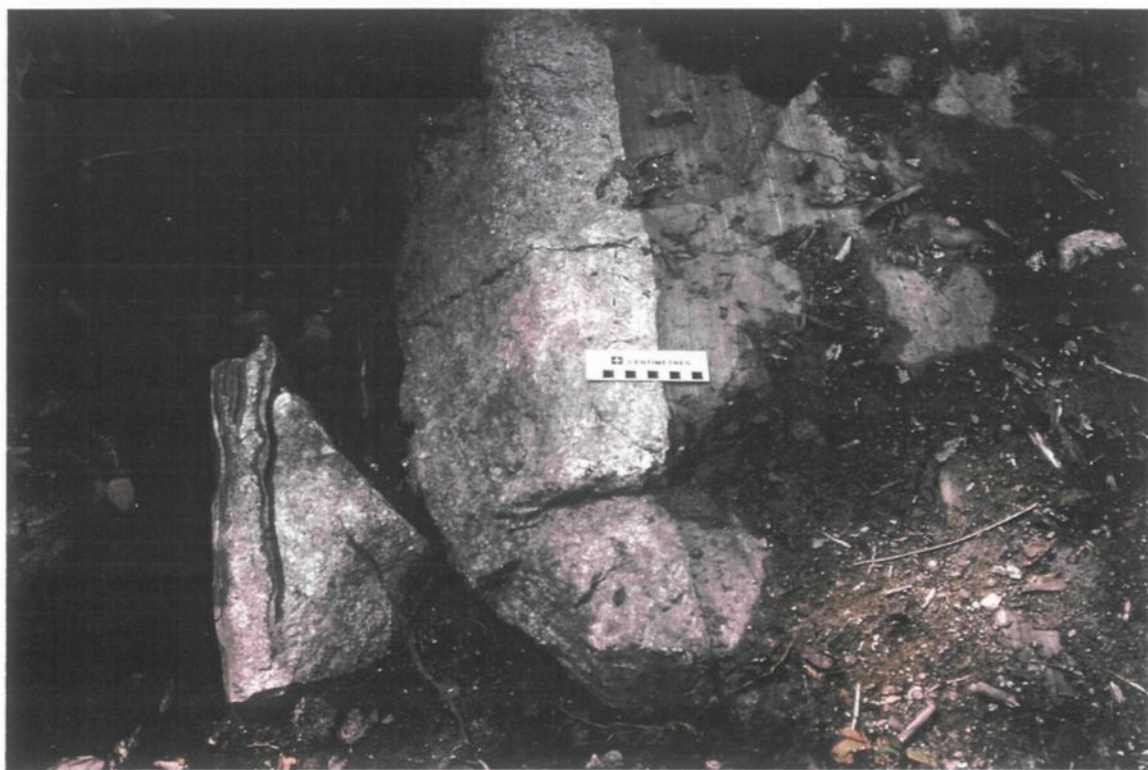
textures, and the string of undeformed plutons emplaced along the lineament. At a local scale, or at the Canton Saint-Onge wollastonite deposit field relationships indicate that the lineament is a shear zone (fig. 2.3).

The whole body of the deposit is contained within this shear zone and all the units were affected by it. The Lac Saint-Jean Anorthosite is deformed and marked by solid state deformation along the lineament but is undeformed further form it. The Du Bras Pluton judging from its lenticular shape was probably emplaced along the lineament. This pluton is deformed, as seen by a strong foliation, rotated phenocrysts and shear bands near the metasediments, or towards the lineament, whereas the unit is undeformed further away from it. This deformation may have resulted from the emplacement of the pluton but more likely results from renewed movement along the shear zone. The Astra Pluton is the only unit that appears not to be affected by the corridor of deformation since it shows no solid state deformation. However, it was emplaced along the zone of weakness following the shearing.

The metasediments also have been affected by movement along the shear zone. The calc-silicate rocks and the marbles are layered on the on the millimetre to centimetre scale these layers are generally folded and some of the straight layers in the marbles are in fact isoclinally folded. Figure 3.2 shows a Schmidt equal area stereographic projection of the poles to the measurements of the compositional layering of the metasediments appearing in appendix 1. The mean pole is at 135° 0.8°, resulting in a mean compositional layering
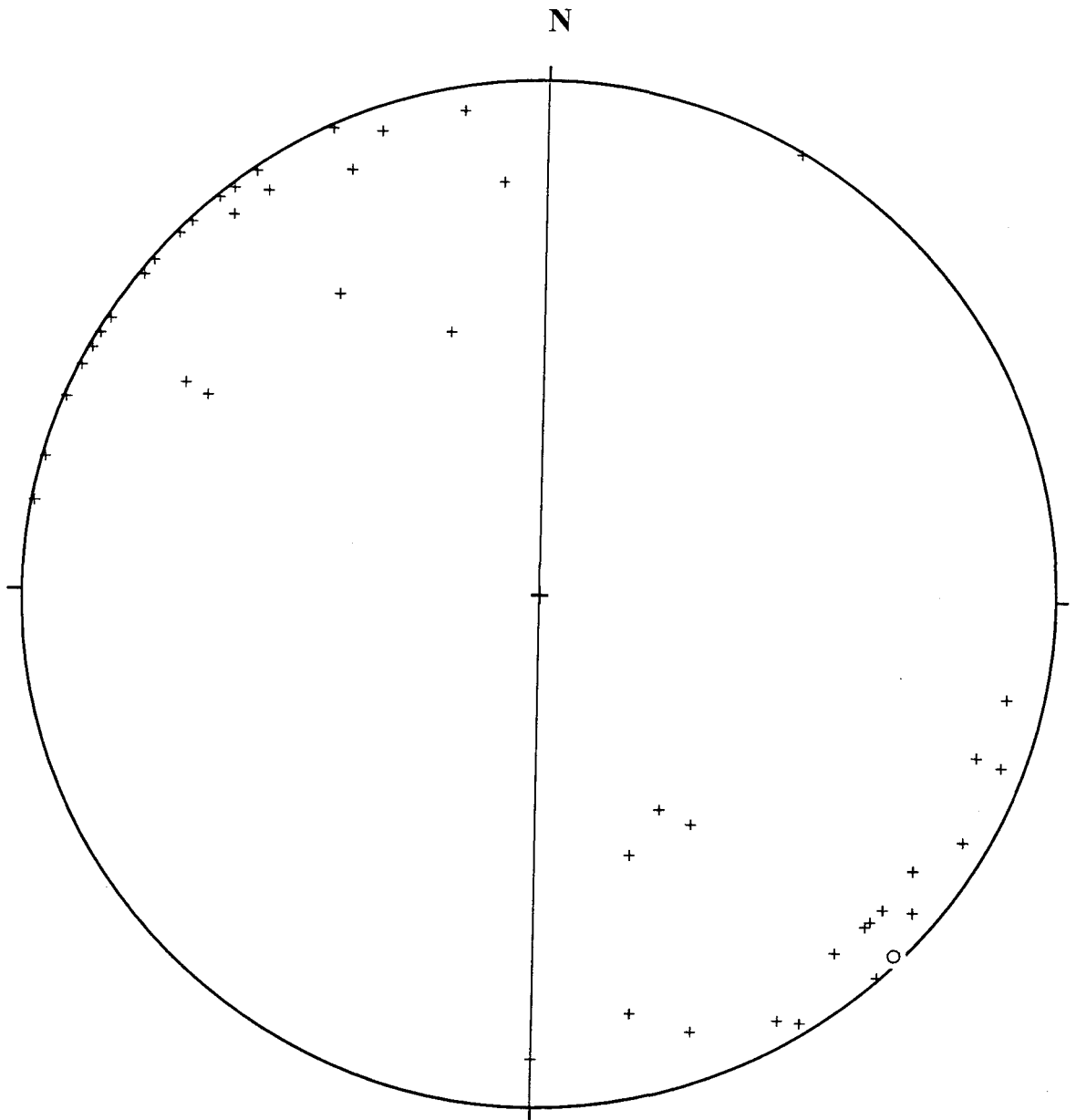
Figure 3.2. Schmidt equal area stereographic projection of poles to the compositional layering (crosses) of the metasedimentary rocks. The circle represents the mean pole to the layers.

value of 045°/89°, i.e. parallel to the orientation of the LSJP lineament. The layering could be primary, i.e. inherited from the protolith, but its orientation parallel to the lineament and its folding suggests that is was reoriented by deformation. The layering is further examined in chapter 4.

Daigneault (1994) has studied the structure of the deposit by detailed mapping of the certain stripped wollastonite-bearing calc-silicate outcrops. He found that the structural history can be divided into four events. The earliest deformation D1 is a series of isoclinal folds with a trace parallel to the Lacs-St-Jean-Pipmuacan lineament (NE) plunging to the north-east. This implies that the layering or bedding was originally oriented NW-SE. The second episode of deformation D2 produced open to closed S folds which are probably the result of sinistral movement along the shear zone. This was closely followed by some fracturing (D3) in the hinges of the folds. The final deformation episode (D4) is responsible for the formation of SW oriented shear zones that dip to the NW.

Chapter 4

MINERAL CHEMISTRY

4.1 METHODOLOGY

An ARL-SEMQ electron microprobe located at the Université du Québec à Chicoutimi was used for positive mineral identification and to determine compositions of the mineral phases. Individual minerals in polished thin sections were analysed using an energy dispersive spectrometer (EDS), and raw data were processed by the Bence-Albee matrix correction program. The electron beam was approximately 5 microns in diameter with a 10 nA current, and an acceleration voltage of 15 kV.

4.2 MINERAL COMPOSITIONS

Representative examples of microprobe results of various phases of the calc-silicate rocks, marbles and paragneissic hornfels are summarised in table 4.1 The mineral analysis showed that the calc-silicate rocks are composed principally of diopside. The diopside shows little variation in composition (fig. 4.1), with only minor iron replacing the magnesium displacing it towards hedenbergite.

The marbles consist of dolomite or calcite , olivine and serpentine. The microprobe reveals that the olivine is forsterite (Fo_{100}) with only trace iron replacing the magnesium

rock type mineral	calc-silicate rocks diopside	
Oxide	average (of 22 analysis)	std dev
SiO2	56.04	1.99
TiO2	0.18	0.32
Al2O3	0.11	0.39
FeO	0.86	0.37
MgO	21.10	2.90
MnO	0.07	0.08
CaO	19.50	5.29
Na2O	1.24	0.78
K2O	0.11	0.24
Cr2O3	0.02	0.07
Total	99.22	1.63
Ion		
Si	2.01	0.03
Ti	0.00	0.01
Al	0.00	0.02
Fe	0.04	0.07
Mg	1.12	0.14
Mn	0.00	0.00
Ca	0.76	0.21
Na	0.09	0.06
K	0.00	0.01
Cr	0.00	0.02
O	6	0

Oxide sample no. rock type mineral	92-12-01 1-2-2 calc-silicate rocks phlogopite	92-12-01 1-6-2 phlogopite	92-12-04 4-4-2 phlogopite	92-12-05 5-1-1 phlogopite	92-15-06 6-1-1 muscovite
SiO2	43.66	43.09	43.58	41.25	46.4
TiO2	0.93	0.98	1.28	1.45	0
Al2O3	11.91	11.81	11.32	15.86	9.48
FeO	2.3	1.78	0.69	0.58	0
MgO	26.45	26.73	28.34	27.57	29.97
MnO	0	0.17	0	0	0.11
CaO	0.46	0.26	0.55	0.36	0.4
Na2O	0.58	0.61	1.35	1.44	1.07
K2O	10.26	10.56	9.19	9.7	9.72
Cr2O3	0	0.11	0	0	0
Cl	0.07	0	0	0.05	0.05
Total	96.61	96.08	96.31	98.27	97.21
Ion					
Si	6.05	6.01	6.00	5.59	6.30
Ti	0.10	0.10	0.13	0.15	0.00
Al	1.95	1.94	1.84	2.53	1.52
Fe	0.27	0.21	0.08	0.07	0.00
Mg	5.46	5.56	5.82	5.57	6.07
Mn	0.00	0.02	0.00	0.00	0.01
Ca	0.07	0.04	0.08	0.05	0.06
Na	0.16	0.17	0.04	0.38	0.28
K	1.81	1.88	1.62	1.68	1.68
Cr	0.00	0.01	0.00	0.00	0.00
Cl	0.02	0.00	0.00	0.01	0.01
O	22	22	22	22	22

Oxide	92-20-13 13-2-1 paragneissic hornfels augite	92-20-13 13-3-1 augite
SiO2	52.41	52.73
TiO2	0	0
Al2O3	0	0
FeO	13.3	13.95
MgO	9.09	9.04
MnO	0.3	0.23
CaO	20.17	20.03
Na2O	2.91	3.2
K2O	0	0
Cr2O3	0.57	0
Cl	0	0
Total	98.75	99.17
Ion		
Si	2.03	2.04
Ti	0	0
Al	0	0
Fe	0.43	0.45
Mg	0.53	0.52
Mn	0.01	0.01
Ca	0.84	0.83
Na	0.22	0.24
K	0	0
Cr	0.02	0
Cl	0	0
O	6	6

Table 4.1. Some microprobe results

rock type mineral oxide	calc-silicate rocks wollastonite	
	avg (of 20 analysis)	st dev
SiO2	50.54	1.65
TiO2	0.02	0.04
Al2O3	0.00	0.00
FeO	0.04	0.07
MgO	0.03	0.05
MnO	0.39	0.10
CaO	46.33	2.36
Na2O	0.01	0.04
K2O	0.06	0.05
Cr2O3	0.12	0.12
Total	97.50	4.05
ion		
Si	2.01	0.02
Ti	0.00	0.00
Al	0.00	0.00
Fe	0.00	0.00
Mg	0.00	0.00
Mn	0.01	0.00
Ca	1.97	0.03
Na	0.05	0.23
K	0.00	0.00
Cr	0.00	0.01
O	6.00	0.00

sample no mineral rock type	92-12-02 2-4-1 anthophyllite calc-silicate rocks
SiO2	60.36
TiO2	0.09
Al2O3	0
FeO	4.32
MgO	37.65
MnO	0.17
CaO	0.44
Na2O	0.64
K2O	0
Cr2O3	0
Cl	0
Total	103.67
Ion	
Si	7.6345
Ti	0.0085
Al	0
Fe	0.457
Mg	7.0995
Mn	0.0186
Ca	0.0593
Na	0.1575
K	0
Cr	0
Cl	0
O	23

sample no. mineral rock type	92-12-05 5-2-1 serpentin marble	92-15-06 6-6-2 serpentin marble	92-12-05 5-2-1 serpentine marble	92-15-06 6-4-2 olivine marble
SiO2	42.33	41.79	42.33	35.44
TiO2	0	0	0	0.08
Al2O3	0	0	0	0
FeO	1.26	0.43	1.26	0.21
MgO	43.87	43.42	43.87	62.41
MnO	0	0	0	0
CaO	0.08	0.12	0.08	0
Na2O	0.79	0.7	0.79	0.72
K2O	0	0	0	0
Cr2O3	0.09	0	0.09	0
Cl	0.06	0.09	0.06	0
SO3	0.07		0.07	
Total	88.55	86.65	88.55	98.85
Ion				
Si	7.7853	7.8169	7.7853	0.8595
Ti	0	0	0	0.0015
Al	0	0	0	0
Fe	0.1935	0.0668	0.1935	0.0043
Mg	12.0286	12.1069	12.0286	2.2566
Mn	0	0	0	0
Ca	0.0166	0.0234	0.0166	0
Na	0.2824	0.2556	0.2824	0.0337
K	0	0	0	0
Cr	0.0135	0	0.0135	0
Cl	0.0187	0.0296	0.0187	0
S	0.0094		0.0094	
O	28	28	28	4

Oxide sample no. mineral rock type	92-15-06 6-4-1 dolomite marble	92-15-06 6-6-1 calcite marble	92-15-06 6-6-3 dolomite marble
SiO2	0	0	0
TiO2	0	0	0
Al2O3	0	0	0
FeO	0.48	0	0
MgO	23.09	3.61	22.91
MnO	0	0.11	0.15
CaO	29.07	53.38	29.24
Na2O	0	0	0
K2O	0	0	0
Cr2O3	0	0	0
Cl	0	0	0
Total	52.64	57.09	52.3
Ion			
Si	0	0	0
Ti	0	0	0
Al	0	0	0
Fe	0.0122	0	0
Mg	1.0576	0.1797	1.0463
Mn	0	0.003	0.0039
Ca	0.9569	1.9081	0.9597
Na	0	0	0
K	0	0	0
Cr	0	0	0
Cl	0	0	0
O	6	6	6

Table 4.1. Continued
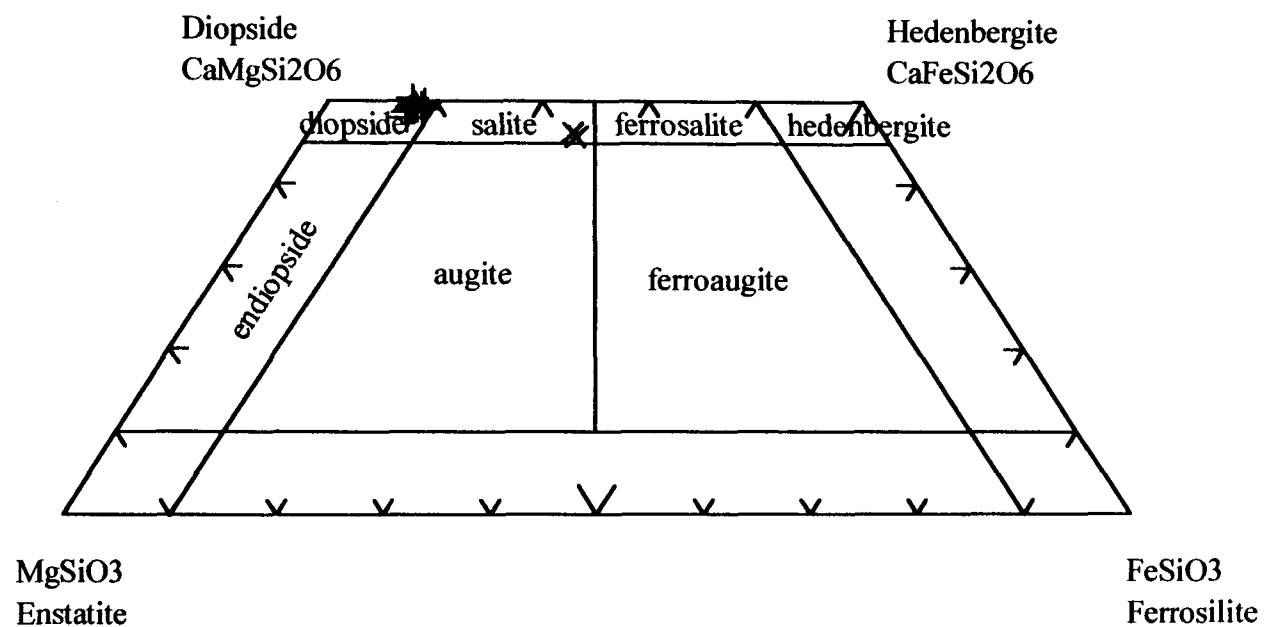
Figure 4.1. Composition of the pyroxene phases of the metasediments. The crosses in the diopside field represent the pyroxene in the calc-silicate rocks. The x's in the salite field are the pyroxenes in the hornfels assemblages.

(table 4.1). The augite of the paragneissic hornfels was also analysed. The microprobe showed that it falls within the salite field of the clinopyroxene diagram (fig 4.1).

The lack of phases limits the use of geothermobarometric programs (e.g. GeOcalc and Thermocalc) to determine equilibration temperatures and X_{CO2} values. X_{CO2} diagrams, which require a pressure assumption, cannot be used since it is not certain which pluton is responsible for the contact metamorphism, or metasomatism involved with the creation of the calc-silicates nor are any emplacement pressures known for the possible plutons. No thermobarometric pairs were discovered during microprobe analysis.

4.3 DIOPSIDE/WOLLASTONITE LAYERING CROSS-SECTION

The wollastonite-bearing calc-silicate rocks of the Canton-St-Onge wollastonite deposit are layered on a millimetre scale. The layers are dominated either by diopside or by wollastonite. The two minerals are similar in structure (both inosilicates) and formula, the only difference being the cation ratio between wollastonite and diopside.

A cross-section of one sample was made to examine closely the cation ratio of the minerals in the layers and to determine if there was a composition change in either the diopside or the wollastonite near the layer boundaries. A slight increase in calcium with respect to magnesium in the diopside towards the wollastonite layers could suggest that textural equilibrium had not been reached nor the layers had been reequilibrated where no change should be seen along the layers. This determined by analysing the wollastonite and diopside along a transect across a representative thin section of the layered calc-silicate rocks. The thin section chosen for closer examination was ABM-077, a calc-silicate rock

which displays the wollastonite/diopside layering and is typical of the rocks in the deposit area.

4.3.1 Petrography

The thin section examined (ABM-077)contains one 8 mm thick layer of wollastonite surrounded by diopside (plate 4.1). The wollastonite layer contains 85% wollastonite with the remainder being composed of quartz. The wollastonite grains are approximately 2 mm in size, elongate to equant, and are poikilitic with inclusions of diopside and some quartz. Within the wollastonite layer, there is a 5 mm thick layer which is rich in quartz (25%) and contains smaller wollastonite grains (0.4 mm) which are much more elongate (aspect ratio of 20:1) and randomly oriented.

The diopside-rich layers which are made up of finer grained equant diopside grains (0.25 mm in size) make up 60% of the minerals with the remainder being quartz (37%) and minor sphalerite (3%). Within the diopside-rich zones there are thin layers, 1-4 mm thick, of coarser grained (0.5 mm in size) diopside without significant quantities of other minerals.

4.3.2 Compositional Profiling Results

The wollastonite and diopside grains were analysed systematically along a line crossing the thin-section lengthwise to determine if there was a variation in the cation ratio of the minerals. Fifty analyses were done with an approximate spacing of 0.5 mm between analyses. These values were then plotted on a Mg/Ca cation versus distance graph to see

Plate 4.1. Diopside (fine-grained) and wollastonite (coarse-grained) layering in calc-silicate rocks (sample ABM-077).
Field of view = 2 cm
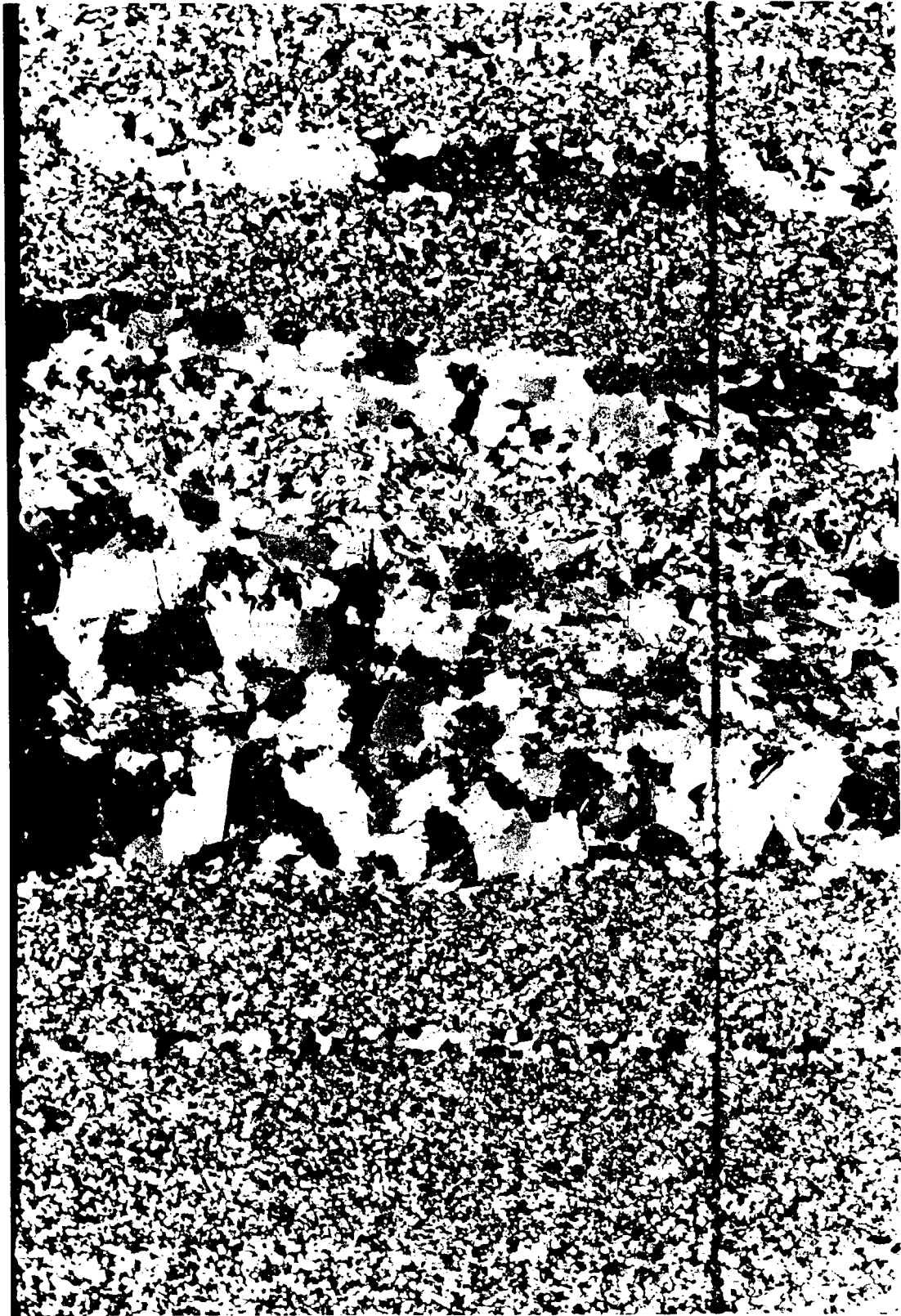
the variation of the magnesium to calcium in the diopside, relative to the wollastonite as well as to the coarse grained diopside layers (fig. 4.2).

These studies revealed that the wollastonite is relatively pure with on average 1.6% impurities of magnesium and iron replacing the calcium (table 4.1). The diopside contains on average 55:45 mol% magnesium to calcium. Impurities in this mineral include iron with 5 mol% on average and sodium with 2 mol% on average.

The plot of Mg/Ca cation versus distance is shown on figure 4.2. This illustrates that there is no increase in calcium relative to magnesium close to the sharp wollastonite contacts. The Mg/Ca ratio varies little in the diopside with most values falling between 0.8 and 0.9. For a closer examination of the cation ratio in the diopside, figure 4.3 shows an expanded scale to see if there is any variation in the coarser grained layers. The graph shows that the cation ratio is not related to the grain size of the diopside.

4.3.2 Cross-Section Conclusions

Figures 4.1 and 4.2 show that there is little variation in the cation ratio within the alternating diopside-wollastonite layers in the calc-silicates. This could be the result of two possibilities either the layers were formed with the different cation ratios, i.e. the sedimentary protolith contained alternating layers with the different cation ratios, or were reequilibrated by diffusion or metamorphism, which evened out the cation ratio within the respective layers.
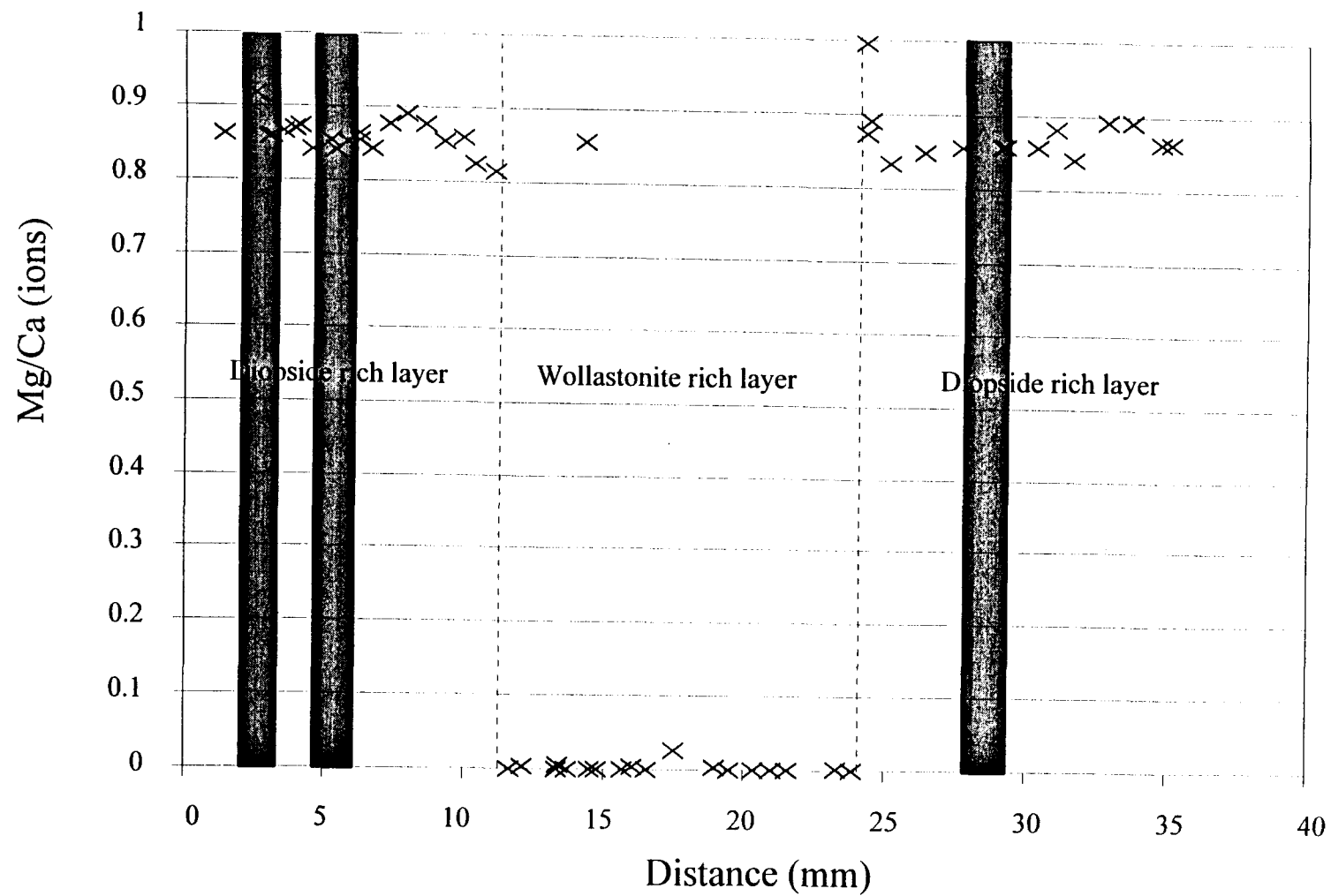
Figure 4.2. Probe cross section of sample Abm-077. Shaded areas represent coarse grained diopside layers within the diopside layers.
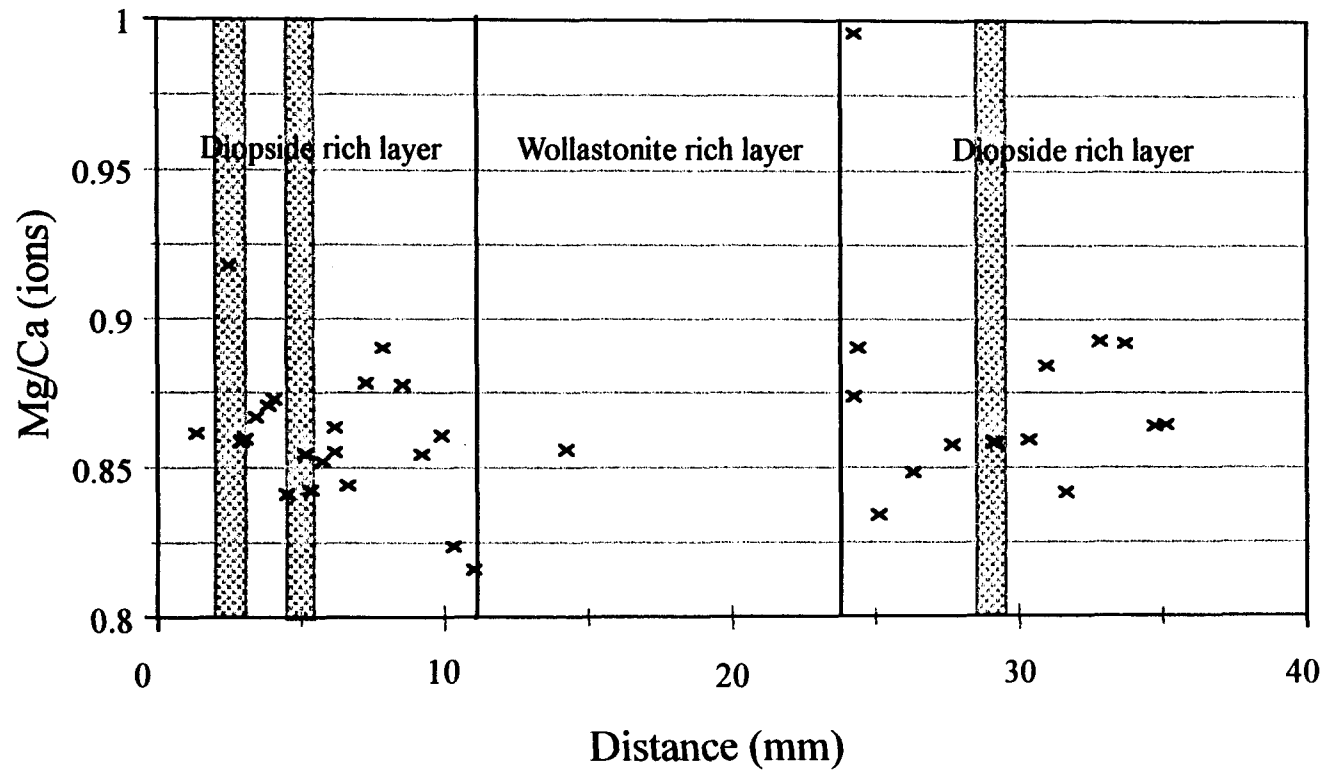
Figure 4.3. Same microprobe cross section of sample Abm-077 but with expanded ordinate, shaded areas represent coarse grained diopside layers. The figure shows there is no subtle variation in the diopside composition within the layers.

Chapter 5

Whole Rock Geochemistry

5.0 INTRODUCTION

Whole rock geochemical analyses were used to compare the various units and determine which elements were mobile and also to characterise the plutons using discrimination diagrams. In total, 70 samples were analysed for major and trace elements by X-ray florescence (XRF) and inductively coupled plasma emission spectrometry (ICPES). Sixty of the samples represent different lithological units from the Canton-St-Onge wollastonite deposit, three are from a nearby smaller deposit, four from the Harrrisville deposit in New York, one internal standard (SH-19), and 2 duplicate analyses (of sample ABM-068). Forty-eight samples were analysed by neutron activation, 46 of which are from the Canton-St-Onge wollastonite deposit, the remaining two being the same internal standard as was used for the XRF and ICPES.

5.1 METHODOLOGY

For all samples used for geochemical analysis, the surface alteration and weathering were removed by saw or hammer. They were first crushed in a steel jaw-crusher and were then passed through a rotary ceramic crusher (BICO) to reduce the samples to sand-sized particles. The samples analysed by XRF and ICPES were reduced to a fine powder in a

tungsten-carbide shatter-box, the samples analysed by neutron activation in a ceramic shatter-box.

The X-ray florescence and ICPES analyses were carried out at the Centre de recherches minérales (CRM) in Quebec City. Elements analysed and their detection limits are shown in table 5.1. Other trace elements, including the rare earth elements were analysed by instrumental neutron activation (INAA). These samples were irradiated at the École Polytechnique in Montreal were counted at the Université du Québec à Chicoutimi.

5.1.1 Precision

The precision of the ICPES and XRF analyses are shown on table 5.1. The analysis of the internal standard (SH-19) for this study is compared with analyses done at the Geological Survey of Canada as well as the Centre de Recherches Minerals (CRM). One sample, ABM-068, was analysed three times for this study to determine the variance in the results. The table shows that all elements posses low standard deviation and acceptable percentage differences for the repeats and the standard with the exception of gallium, vanadium, barium and zinc. Therefore, these elements will not be considered in the discussion of the results.

The precision of the neutron activation results are shown in table 5.2. The table shows the average, standard deviation, variance and standard error of the internal standard SH-19 by previous analyses, as well as two analyses of the same sample for this study with their averages and percentage differences from the average of the previous analyses. Those

Majors XRF	detection limit (%)	shale standard (SH-19)	analysis1 shale	% diff	abm-068	abm-068	abm-068	standard deviation	100*std div./ Mean
SiO2	0.04	57.02	56.60	0.74	46.10	46.20	46.30	0.08	0.18
Al2O3	0.02	13.13	12.80	2.51	3.59	3.58	3.61	0.01	0.35
Fe2O3t	0.02	3.27	3.63	9.92	1.35	1.52	1.50	0.08	5.26
MgO	0.05	2.79	2.78	0.47	6.82	6.88	7.03	0.09	1.28
CaO	0.02	1.68	1.63	2.74	30.20	30.70	30.60	0.22	0.71
Na2O	0.1	1.06	0.89	16.27	1.14	1.21	1.19	0.03	2.49
K2O	0.01	6.39	6.17	3.40	1.53	1.53	1.53	0.00	0.00
TiO2	0.01	0.90	0.88	1.79	0.36	0.37	0.37	0.00	1.29
MnO	0.01	0.04	0.04	11.11	0.04	0.04	0.04	0.00	0.00
P2O5	0.01	0.08	0.08	0.00	n.d.	n.d.	n.d.		
LOI		12.50	13.60	8.80	7.84	7.73	7.74	0.05	0.64
minors XRF	detection limit (ppm)								
Ga	3	20	16	20.00	0	4	3	1.70	72.84
Sn	10	n.d.	n.d.		n.d.	n.d.	n.d.		
Sr	3	62	56	9.68	1100	1100	1100	0.00	0.00
Te	10	n.d.	n.d.		n.d.	n.d.	n.d.		
Y	3	43	35	18.60	10	11	10	0.47	4.56
Zr	3	184	180	2.17	130	130	130	0.00	0.00
ICPES	detection limit (ppm)								
Ba	1	666	449	32.58	910	1000	1000	42.43	4.37
Be	1	n.d.	n.d.		n.d.	n.d.	n.d.		
Cd	2	n.d.	n.d.		n.d.	n.d.	n.d.		
Co	3	33	31	6.06	11	9	8	1.25	13.36
Cu	1	30	28	6.67	22	23	24	0.82	3.55
Li	1	44	39.00	11.36	15.00	16.00	16.00	0.47	3.01
Mo	4	n.d.	n.d.		n.d.	n.d.	n.d.		
Pb	12	27	30	11.11	48	51	56	3.30	6.39
Pr	10	n.d.	n.d.		n.d.	n.d.	n.d.		
V	2	391	387	1.02	36	75	106	28.64	39.59
Zn	2	30	80	166.67	147	162	164	7.59	4.81

n.d. = not detected

Table 5.1. Detection limit and precision of XRF and ICPES analyses.

Neutron Activation Elements	standard SH-19 (of 25 analyses)				Analysis of SH-19 for this study			
	mean	std-dev	variance	std/err	analysis1	analysis2	mean	% diff
Cr	116.69	5.22	27.22	4.47	123.79	124.29	124.04	6.30
Ni	61.95	18.76	351.85	30.28	90.68	97.00	93.84	51.48
Sc	19.38	0.54	0.29	2.8	19.98	20.11	20.05	3.43
W	147.33	10.39	1.07	7.05	154.37	150.55	152.46	3.48
As	23.17	1.48	2.18	6.38	23.41	23.29	23.35	0.78
Sb	1.41	0.1	0.01	6.99	1.60	1.79	1.70	20.21
Au	0.01	0.00	0.00	31.60	0.01	0.01	0.01	0.00
Rb	128.63	7.41	54.9	5.76	131.31	120.64	125.98	2.06
Ta	1.39	0.17	0.03	12.27	1.29	0.67	0.98	29.50
Hf	3.68	1.01	1.02	27.5	4.09	4.81	4.45	20.87
Th	8.98	0.39	0.16	4.4	9.29	8.85	9.07	1.00
U	4.87	0.31	0.1	6.47	4.98	4.61	4.80	1.54
La	31.23	1.11	1.23	3.55	32.45	32.55	32.50	4.07
Ce	62.22	3.67	13.47	5.9	66.24	67.53	66.89	7.50
Nd	28.39	5.01	25.14	17.67	29.46	30.58	30.02	5.74
Sm	5.55	0.41	0.16	7.3	5.84	5.5	5.67	2.16
Eu	1.17	0.13	0.02	11.04	1.14	1.44	1.29	10.26
Tb	0.83	0.13	0.02	15.8	0.76	0.77	0.77	7.83
Yb	2.84	0.1	6.2	3.41	2.63	2.92	2.78	2.29
Lu	0.52	0.03	0	6.2	0.50	0.54	0.52	0.00

Table 5.2. Precision of neutron activation analysis. %age difference represents the percentage difference between the mean of the analysis of SH-19 for this study and the mean from the previous 25 analysis.

elements with a percentage difference over 10 % were ignored for this study. Such elements include: nickel, antimony, tantalum, and hafnium.

5.2 RESULTS

The geochemical results for all the lithologies are summarised according to rock type in tables 5.3 to 5.9. The calc-silicate rocks are divided into wollastonite bearing calc-silicates (table 5.8) and barren calc-silicates for those samples lacking wollastonite (table 5.9).

5.2.1 Major Element Analyses

The results of the LSJ Anorthosite summarised on table 5.3 are divided into anorthosite and anorthositic gabbro. The unit is composed mainly of silica , ~ 50 wt% for both sub-units. Alumina in the anorthosite varies from 18 to 19 wt% and is understandably lower in the anorthositic gabbro since it contains less plagioclase. The anorthositic gabbro is richer in iron relative to magnesium and, therefore, has a lower Mg number (15) than that of the anorthosite (from 30 to 51). Both units show little loss on ignition (<1%) suggesting little retrograde metamorphism took place which would have introduced hydrous minerals resulting in a higher value.

The Du Bras Pluton analyses are summarised on table 5.4. The analyses show that the unit is rich in silica (~ 77 wt%) due to the high percentage of quartz present in the rock. The granite also shows high iron to magnesium ratios, revealed by the low Mg numbers. This unit also has low loss on ignition, due to the low percentage of hydrous minerals.

Sample #	ANORTHOSITE				ANORTHOSITIC GABBRO
	abm-132	abm-666	abm-136	abm-135	abm-131
Mg Number	30.78	35.63	48.18	51.65	15.78
SiO2 (%)	53.00	53.10	52.90	54.00	49.00
TiO2 (%)	2.02	0.89	0.12	0.74	2.41
Al2O3 (%)	17.90	22.60	28.70	20.20	14.70
Fe2O3t (%)	11.00	4.85	0.49	6.58	20.30
MnO (%)	0.16	0.06	n.d.	0.10	0.32
MgO (%)	2.47	1.35	0.23	3.55	1.92
CaO (%)	8.02	8.85	11.40	8.41	7.05
Na2O (%)	3.89	4.41	4.44	3.87	3.47
K2O (%)	1.66	1.44	0.50	1.20	1.50
P2O5 (%)	0.57	0.38	0.01	0.09	1.13
LOI (%)	n.d.	0.73	0.32	0.56	n.d.
Cr (ppm)	18	7	2	52	16
Ni (ppm)	5	16	7	18	3
Co (ppm)	54	41	45	52	48
Sc (ppm)	19	8	1	16	35
V (ppm)	107	70	7	75	14
Cu (ppm)	34	21	8	15	41
Pb (ppm)	18	44	41	32	n.d.
Zn (ppm)	129	63	19	66	200
Cd (ppm)	n.d.	n.d.	n.d.	n.d.	2.00
Sn (ppm)	n.d.	n.d.	n.d.	n.d.	n.d.
W (ppm)	1.63	n.d.	n.d.	n.d.	3.28
As (ppm)	0.67	0.59	n.d.	0.56	0.64
Sb (ppm)	0.52	0.37	0.52	0.68	1.00
Ag (ppm)	n.d.	n.d.	n.d.	n.d.	n.d.
Rb (ppm)	30	28	7	17	21
Cs (ppm)	0.62	0.84	n.d.	n.d.	0.73
Ba (ppm)	610	370	139	318	351
Sr (ppm)	370	460	540	410	280
Ga (ppm)	21	21	18	22	27
Li (ppm)	13.00	22.00	8.00	13.00	9.00
Nb(ppm)	19	6	n.d.	5	36
Ta (ppm)	1.44	0.26	n.d.	n.d.	1.59
Hf (ppm)	6.59	4.34	n.d.	3.41	12.56
Zr (ppm)	290	260	31	200	570
Y (ppm)	53	25	n.d.	17	94
Th (ppm)	1.54	2.00	n.d.	0.89	1.98
U (ppm)	0.57	0.48	n.d.	0.21	0.77
La (ppm)	22.73	14.65	1.95	9.04	51.04
Ce (ppm)	55.83	35.22	3.02	20.26	128.05
Nd (ppm)	37.67	18.87	4.08	8.50	84.39
Sm (ppm)	8.86	4.82	0.38	2.84	19.74
Eu (ppm)	3.26	1.76	0.73	1.44	5.14
Tb (ppm)	1.63	0.73	n.d.	0.56	3.07
Dy (ppm)	2.00	9.00	3.00	2.00	1.00
Ho (ppm)	1.25	0.21	n.d.	0.37	2.62
Yb (ppm)	4.33	1.95	n.d.	1.57	7.24
Lu (ppm)	0.79	0.35	n.d.	0.28	1.32
Be (ppm)	n.d.	n.d.	n.d.	n.d.	n.d.

n.d. = not detected; blank space = not analysed

Table 5.3. Analyses of some Lac-Saint-Jean Anorthosite samples.

Sample #	abm-134	abm-126	abm-120	abm-124	abm-121	abm-145
Mg Number	11.17	15.93	n.d.	8.62	15.01	26.28
SiO2 (%)	77.10	77.90	79.60	79.60	76.40	77.20
TiO2 (%)	0.14	0.26	0.11	0.12	0.16	0.19
Al2O3 (%)	12.50	11.40	10.90	11.10	12.90	11.40
Fe2O3t (%)	1.26	2.09	2.08	1.47	1.57	1.00
MnO (%)	0.01	0.02	n.d.	n.d.	0.01	n.d.
MgO (%)	0.08	0.20	n.d.	0.07	0.14	0.18
CaO (%)	0.63	0.55	0.56	0.14	0.54	0.48
Na2O (%)	2.98	2.75	2.90	2.79	3.50	2.84
K2O (%)	5.72	5.10	4.93	5.02	5.23	5.17
P2O5 (%)	n.d.	0.03	n.d.	n.d.	n.d.	0.02
LOI (%)	0.36	0.33	0.27	0.50	0.27	0.36
Cr (ppm)	n.d.	n.d.	n.d.	3	4	n.d.
Ni (ppm)	4	5	4	42	4	12
Co (ppm)	74	102	104	112	n.d.	87
Sc (ppm)	1	3	n.d.	1	2	3
V (ppm)	3	6	n.d.	3	3	14
Cu (ppm)	7	12	5	8	5	13
Pb (ppm)	37	41	n.d.	46	37	41
Zn (ppm)	28	27	23	38	33	20
Cd (ppm)	n.d.	n.d.	n.d.	n.d.	n.d.	n.d.
Sn (ppm)	n.d.	n.d.	n.d.	n.d.	n.d.	n.d.
W (ppm)	n.d.	1.22	n.d.	1.26	n.d.	0.99
As (ppm)	0.36	0.34	0.62	0.43	0.36	0.53
Sb (ppm)	0.63	0.77	0.67	0.09	0.57	0.38
Ag (ppm)	n.d.	0.6	n.d.	n.d.	n.d.	n.d.
Rb (ppm)	319	225	322	351	271	291
Cs (ppm)	3.16	1.60	0.83	0.99	1.78	2.58
Ba (ppm)	301	416	49	87	500	336
Sr (ppm)	39	56	13	20	72	49
Ga (ppm)	23	22	26	25	26	25
Li (ppm)	23.00	16.00	22.00	16.00	23.00	14.00
Nb(ppm)	13	13	14	25	6	15
Ta (ppm)	1.06	0.91	0.76	1.41	n.d.	1.75
Hf (ppm)	7.36	10.62	12.17	17.93	9.49	11.72
Zr (ppm)	270	410	250	430	250	280
Y (ppm)	33	20	71	49	25	23
Th (ppm)	2.91	2.51	3.49	7.66	2.31	4.55
U (ppm)	1.54	1.12	2.26	3.69	1.35	2.07
La (ppm)	16.82	7.04	18.55	16.31	8.25	18.22
Ce (ppm)	29.03	17.87	39.36	40.15	16.11	37.56
Nd (ppm)	14.23	7.43	11.37	12.00	9.18	14.75
Sm (ppm)	3.09	2.75	3.89	4.11	3.09	5.22
Eu (ppm)	0.88	0.80	0.25	n.d.	1.36	1.28
Tb (ppm)	0.56	0.36	0.96	0.77	0.40	0.70
Dy (ppm)	4.00	5.00	5.00	7.00	3.00	12.00
Ho (ppm)	0.42	0.41	1.14	1.03	0.51	0.67
Yb (ppm)	1.64	1.50	3.66	4.84	1.81	2.08
Lu (ppm)	0.31	0.26	0.66	0.91	0.31	0.35
Be (ppm)	2.00	n.d.	n.d.	n.d.	1.00	2.00

n.d. = not detected; blank space = not analysed

Table 5.4. Analyses of some of the Du Bras Pluton samples.

Sample #	abm-137	abm-138
Mg Number	13.74	14.55
SiO2 (%)	67.80	68.80
TiO2 (%)	0.53	0.49
Al2O3 (%)	14.30	13.90
Fe2O3t (%)	4.60	4.07
MnO (%)	0.09	0.09
MgO (%)	0.37	0.35
CaO (%)	2.02	1.39
Na2O (%)	3.41	3.34
K2O (%)	4.79	5.69
P2O5 (%)	0.10	0.09
LOI (%)	0.37	0.45
Cr (ppm)	8	2
Ni (ppm)	6	54
Co (ppm)	73	72
Sc (ppm)	7	7
V (ppm)	8	6
Cu (ppm)	14	14
Pb (ppm)	61	55
Zn (ppm)	167	118
Cd (ppm)	n.d.	n.d.
Sn (ppm)	n.d.	n.d.
W (ppm)	3.11	n.d.
As (ppm)	n.d.	n.d.
Sb (ppm)	0.41	0.43
Ag (ppm)	n.d.	n.d.
Rb (ppm)	133	100
Cs (ppm)	1.12	0.44
Ba (ppm)	1800	2000
Sr (ppm)	340	200
Ga (ppm)	30	25
Li (ppm)	26.00	16.00
Nb (ppm)	51	30
Ta (ppm)	2.43	1.64
Hf (ppm)	21.40	20.90
Zr (ppm)	770	730
Y (ppm)	98	55
Th (ppm)	12.55	5.45
U (ppm)	1.89	1.03
La (ppm)	148.61	82.38
Ce (ppm)	351.22	175.64
Nd (ppm)	185.96	90.78
Sm (ppm)	29.97	16.73
Eu (ppm)	5.52	5.48
Tb (ppm)	3.64	2.06
Dy (ppm)	15.00	10.00
Ho (ppm)	1.60	1.38
Yb (ppm)	7.67	4.36
Lu (ppm)	1.27	0.77
Be (ppm)	2.00	n.d.

n.d. = not detected; blank space = not analysed

Table 5.5. Analyses of some Astra Pluton samples.

Sample #	METADOLOSTONE			OLIVINE-SERPENTINE MARBLE				CALC-SILICATE MARBLE
	abm-011	abm-084	abm-089	abm-117	abm-050	abm-141	abm-122b	abm-107
Mg Number	100.00	100.00	99.40	100.00	98.48	99.17	98.60	76.14
SiO2 (%)	0.85	14.40	3.73	10.30	18.40	14.50	14.90	10.90
TiO2 (%)	n.d.	0.01	n.d.	n.d.	0.10	0.03	n.d.	0.23
Al2O3 (%)	0.16	0.20	0.06	0.10	1.89	0.13	0.19	2.12
Fe2O3t (%)	n.d.	n.d.	0.27	n.d.	0.83	0.26	0.62	1.08
MnO (%)	0.02	0.02	n.d.	n.d.	0.03	0.03	0.04	0.03
MgO (%)	19.60	23.70	22.60	18.90	27.20	15.60	22.10	1.74
CaO (%)	32.70	31.10	29.30	34.10	22.30	35.70	28.80	45.50
Na2O (%)	n.d.	n.d.	n.d.	n.d.	n.d.	n.d.	n.d.	0.56
K2O (%)	n.d.	0.02	n.d.	n.d.	n.d.	0.04	n.d.	0.99
P2O5 (%)	n.d.	n.d.	n.d.	n.d.	n.d.	0.04	n.d.	0.02
LOI (%)	45.60	31.10	44.00	36.80	30.20	33.60	33.30	34.90
Cr (ppm)	1	1	n.d.	1	7	n.d.	n.d.	15
Ni (ppm)	4	6	n.d.	7	21	6	n.d.	11
Co (ppm)	4	10	4	6	5	n.d.	6	6
Sc (ppm)	n.d.	n.d.	n.d.	n.d.	1	n.d.	n.d.	3
V (ppm)	n.d.	n.d.	n.d.	9	n.d.	6	n.d.	22
Cu (ppm)	n.d.	1	n.d.	5	n.d.	5	10	16
Pb (ppm)	n.d.	n.d.	n.d.	n.d.	18	n.d.	n.d.	n.d.
Zn (ppm)	39	37	54	36	100	191	151	59
Cd (ppm)	n.d.	n.d.	n.d.	n.d.	n.d.	n.d.	n.d.	n.d.
Sn (ppm)	n.d.	n.d.	n.d.	n.d.	n.d.	n.d.	n.d.	n.d.
W (ppm)	n.d.	n.d.	n.d.	n.d.	0.82	0.96	0.18	n.d.
As (ppm)	0.19	0.46	0.07	0.04	n.d.	0.33	0.16	1.06
Sb (ppm)	0.48	0.43	2.70	0.42	0.56	0.79	0.71	0.64
Ag (ppm)	n.d.	0.1	n.d.	n.d.	n.d.	0.2	n.d.	0.2
Rb (ppm)	n.d.	5	n.d.	n.d.	n.d.	7	n.d.	13
Cs (ppm)	n.d.	0.78	n.d.	n.d.	n.d.	1.00	n.d.	0.29
Ba (ppm)	14	39	24	17	51	71	52	569
Sr (ppm)	310	220	180	210	380	190	200	1200
Ga (ppm)	n.d.	n.d.	n.d.	n.d.	3	n.d.	n.d.	n.d.
Li (ppm)	3.00	4.00	3.00	4.00	2.00	3.00	2.00	3.00
Nb(ppm)	n.d.	n.d.	n.d.	n.d.	n.d.	3	n.d.	n.d.
Ta (ppm)	n.d.	n.d.	0.08	n.d.	0.09	0.17	n.d.	n.d.
Hf (ppm)	n.d.	n.d.	n.d.	n.d.	0.96	0.13	n.d.	1.35
Zr (ppm)	21	23	18	19	49	29	20	80
Y (ppm)	n.d.	n.d.	n.d.	n.d.	n.d.	3	4	6
Th (ppm)	n.d.	0.17	n.d.	n.d.	0.24	0.90	n.d.	1.87
U (ppm)	n.d.	0.05	n.d.	n.d.	0.36	0.77	n.d.	1.16
La (ppm)	0.64	0.66	0.24	0.37	2.28	7.24	3.96	5.25
Ce (ppm)	1.58	0.96	n.d.	n.d.	4.49	11.03	8.56	12.16
Nd (ppm)	1.57	0.93	1.90	2.83	4.52	3.96	6.74	4.14
Sm (ppm)	0.19	0.12	0.06	0.07	0.44	0.65	0.50	1.30
Eu (ppm)	0.04	0.04	n.d.	n.d.	n.d.	n.d.	0.90	0.27
Tb (ppm)	0.01	n.d.	n.d.	n.d.	n.d.	n.d.	n.d.	0.17
Dy (ppm)	n.d.	n.d.	n.d.	3.00	n.d.	4.00	n.d.	3.00
Ho (ppm)	0.03	n.d.	n.d.	n.d.	0.04	0.05	0.78	0.18
Yb (ppm)	0.06	0.68	n.d.	0.05	0.15	0.36	0.54	0.78
Lu (ppm)	0.01	0.01	n.d.	0.01	0.03	0.06	0.08	0.15
Be (ppm)	n.d.	1.00	n.d.	n.d.	n.d.	2.00	n.d.	n.d.

n.d. = not detected

Table 5.6. Analyses of some marbles samples.

Sample #	PARAGNEISSIC HORNFELS		QUARTZITE		
	abm-104b	abm-112b	abm-130	abm-139	abm-112a
Mg Number	48.97	68.02	61.24	91.85	73.66
SiO2 (%)	55.70	57.80	96.30	94.50	91.60
TiO2 (%)	1.35	1.04	0.11	0.03	0.34
Al2O3 (%)	15.20	9.41	0.31	1.05	0.88
Fe2O3t (%)	9.35	5.95	0.89	0.26	1.53
MnO (%)	0.08	0.12	0.02	n.d.	0.04
MgO (%)	4.53	6.39	0.71	1.48	2.16
CaO (%)	3.13	11.10	0.89	2.12	2.95
Na2O (%)	4.62	1.76	0.37	0.26	0.20
K2O (%)	4.34	5.37	0.10	0.52	0.43
P2O5 (%)	0.21	0.16	n.d.	0.01	0.05
LOI (%)	0.24	0.33	0.11	0.14	0.19
Cr (ppm)	84	59	3	n.d.	21
Ni (ppm)	63	27	14	7	10
Co (ppm)	50	39	142	116	145
Sc (ppm)	21	15	1	n.d.	4
V (ppm)	96	70	13	8	43
Cu (ppm)	19	19	9	7	10
Pb (ppm)	51	59	n.d.	n.d.	13
Zn (ppm)	87	103	28	46	36
Cd (ppm)	3.00	2.00	n.d.	n.d.	n.d.
Sn (ppm)	n.d.	13.00	n.d.	n.d.	n.d.
W (ppm)	n.d.	9.09	0.32	n.d.	1.34
As (ppm)	n.d.	1.84	0.17	n.d.	1.74
Sb (ppm)	0.39	0.89	0.52	0.04	1.13
Ag (ppm)	n.d.	n.d.	0.3	n.d.	0.2
Rb (ppm)	85	76	4	16	11
Cs (ppm)	n.d.	1.04	0.21	0.28	0.36
Ba (ppm)	497	1900	35	110	139
Sr (ppm)	96	450	3	160	29
Ga (ppm)	23	12	n.d.	n.d.	n.d.
Li (ppm)	73.00	133.00	5.00	8.00	47.00
Nb(ppm)	12	9	4	3	5
Ta (ppm)	0.66	0.82	0.17	n.d.	n.d.
Hf (ppm)	5.90	4.65	3.72	0.39	1.47
Zr (ppm)	230	180	130	36	67
Y (ppm)	29	41	11	n.d.	15
Th (ppm)	0.99	4.84	0.87	0.57	1.72
U (ppm)	0.54	0.71	0.99	0.18	0.43
La (ppm)	25.05	35.52	3.93	0.98	8.36
Ce (ppm)	53.11	80.61	10.82	1.31	19.56
Nd (ppm)	23.48	34.62	4.83	n.d.	10.71
Sm (ppm)	5.43	7.86	1.50	0.12	2.41
Eu (ppm)	1.70	1.91	0.20	n.d.	0.47
Tb (ppm)	0.76	1.08	0.27	n.d.	0.47
Dy (ppm)	n.d.	4.00	4.00	5.00	4.00
Ho (ppm)	n.d.	n.d.	0.33	n.d.	0.26
Yb (ppm)	2.40	3.51	1.01	n.d.	1.15
Lu (ppm)	0.41	0.62	0.19	n.d.	0.20
Be (ppm)	n.d.	n.d.	n.d.	n.d.	n.d.

n.d. = not detected

Table 5.7. Some analyses of the paragneissic hornfels and quartzite units.

Table 5.8. Analyses of some of the wollastonite-bearing calc-silicate rock samples.

n.d. = not detected; blank space = not analysed

Sample #	abm-034	abm-039	abm-040b	abm-101	abm-111	abm-015	abm-068	abm-104a
Mg Number	92.52	92.26	91.98	92.14	91.36	94.70	90.00	88.57
SiO2 (%)	57.80	55.00	56.50	53.90	44.00	77.20	46.10	53.90
TiO2 (%)	0.16	0.16	0.18	0.16	0.11	0.05	0.36	0.07
Al2O3 (%)	2.05	2.50	2.23	1.97	1.64	0.71	3.59	3.02
Fe2O3t (%)	1.07	1.30	1.36	1.02	0.88	0.37	1.50	1.84
MnO (%)	0.05	0.04	0.12	0.08	0.04	0.03	0.04	0.03
MgO (%)	6.68	7.83	7.88	6.04	4.70	3.34	6.82	7.20
CaO (%)	30.20	29.60	30.20	34.80	38.80	16.40	30.20	30.90
Na2O (%)	0.61	0.72	0.94	0.43	0.30	0.17	1.14	0.56
K2O (%)	0.88	1.21	0.58	0.95	0.81	0.35	1.53	1.07
P2O5 (%)	0.05	0.02	0.05	0.14	0.04	0.02	n.d.	0.03
LOI (%)	0.68	1.17	0.51	0.90	8.29	1.15	7.84	0.87
Cr (ppm)	10	13			8	2	21	
Ni (ppm)	10	14			12	3	13	
Co (ppm)	16	15	20	14	9	30	11	14
Sc (ppm)	3	3			2	1	5	
V (ppm)	18	54	27	44	39	6	36	53
Cu (ppm)	7	9	9	14	13	30	22	14
Pb (ppm)	14	20	28	14	25	n.d.	48	38
Zn (ppm)	197	161	307	83	40	16	147	25
Cd (ppm)	n.d.	n.d.	n.d.	n.d.	n.d.	n.d.	n.d.	n.d.
Sn (ppm)	n.d.	n.d.	n.d.	n.d.	n.d.	n.d.	n.d.	n.d.
W (ppm)	n.d.	n.d.				n.d.	n.d.	n.d.
As (ppm)	n.d.	n.d.				0.38	0.21	n.d.
Sb (ppm)	0.46	1.23				0.48	0.10	0.22
Ag (ppm)	n.d.	n.d.				n.d.	n.d.	n.d.
Rb (ppm)	26	40				22	9	36
Cs (ppm)	n.d.	0.64				n.d.	n.d.	0.81
Ba (ppm)	283	272	154	380	568	69	910	1000
Sr (ppm)	900	1700	440	1100	1700	430	1100	290
Ga (ppm)	3	n.d.	n.d.	3	4	n.d.	n.d.	5
Li (ppm)	10.00	7.00	18.00	17.00	19.00	5.00	15.00	15.00
Nb(ppm)	n.d.	n.d.	4	n.d.	n.d.	n.d.	n.d.	5
Ta (ppm)	n.d.	n.d.				n.d.	0.12	0.21
Hf (ppm)	1.08	1.20				0.79	0.53	2.66
Zr (ppm)	66	100	56	75	79	45	130	89
Y (ppm)	7	5	6	8	4	8	10	
Th (ppm)	0.51	0.45				0.69	0.81	0.43
U (ppm)	0.14	0.16				0.16	0.41	0.22
La (ppm)	3.95	4.73				13.03	3.83	12.42
Ce (ppm)	11.66	11.93				23.96	10.25	25.19
Nd (ppm)	6.86	3.39				9.27	6.33	10.53
Sm (ppm)	1.48	1.29				1.65	1.38	2.25
Eu (ppm)	0.28	0.16				0.28	0.23	0.47
Tb (ppm)	0.14	0.11				0.17	0.23	0.25
Dy (ppm)	n.d.	2.00	n.d.	n.d.	3.00	n.d.	n.d.	2.00
Ho (ppm)	0.11	0.08				0.09	0.19	n.d.
Yb (ppm)	0.62	0.62				0.54	0.64	0.99
Lu (ppm)	0.11	0.11			0.10	0.11	0.18	n.d.
Be (ppm)	n.d.	n.d.	n.d.	n.d.	n.d.	n.d.	n.d.	n.d.

Sample #	abm-022	abm-024	abm-054	abm-077	abm-047a	abm-027	abm-040a
Mg Number	90.11	91.52	92.94	84.53	100.00	88.46	92.41
SiO2 (%)	57.90	56.90	62.50	62.60	59.10	55.50	59.70
TiO2 (%)	0.23	0.19	0.17	0.29	0.15	0.23	0.17
Al2O3 (%)	3.28	2.96	1.06	2.38	2.00	2.33	1.93
Fe2O3t (%)	1.38	1.48	1.27	2.73	0.97	1.69	0.94
MnO (%)	0.06	0.10	0.05	0.34	0.02	0.05	0.08
MgO (%)	6.35	8.07	8.44	7.53	6.00	6.54	5.78
CaO (%)	26.40	26.40	25.40	22.20	29.10	30.50	29.60
Na2O (%)	0.98	0.73	0.33	0.48	0.98	0.82	0.69
K2O (%)	1.41	1.55	0.52	1.20	0.58	0.69	0.49
P2O5 (%)	0.07	0.09	0.06	0.07	0.02	0.09	0.08
LOI (%)	0.78	1.30	1.04	0.22	0.66	1.46	0.51
Cr (ppm)	15	15		15			10
Ni (ppm)	12	18		15			9
Co (ppm)	19	26	17	25	15	13	31
Sc (ppm)	4	4		4			2
V (ppm)	27	26	23	32	163	21	19
Cu (ppm)	6	9	35	10	7	6	46
Pb (ppm)	16	18	224	972	17	39	38
Zn (ppm)	200	267	103	3700	88	153	271
Cd (ppm)	n.d.	n.d.	n.d.	15.00	n.d.	n.d.	n.d.
Sn (ppm)	n.d.	n.d.	n.d.	n.d.	n.d.	n.d.	n.d.
W (ppm)	n.d.	0.18		1.40			n.d.
As (ppm)	n.d.	0.42		n.d.			0.34
Sb (ppm)	0.17	0.57		1.25			0.65
Ag (ppm)	n.d.	n.d.		1.3			0.2
Rb (ppm)	34	33		27			10
Cs (ppm)	0.49	0.30		0.25			n.d.
Ba (ppm)	247	430	109	188	106	156	106
Sr (ppm)	1000	1100	940	640	1800	1800	660
Ga (ppm)	4	3	n.d.	4	3	n.d.	n.d.
Li (ppm)	15.00	16.00	20.00	18.00	11.00	5.00	9.00
Nb(ppm)	n.d.	n.d.	n.d.	n.d.	n.d.	n.d.	n.d.
Ta (ppm)	0.20	0.27		0.22			n.d.
Hf (ppm)	1.21	1.28		1.14			0.97
Zr (ppm)	80	85	48	64	83	110	56
Y (ppm)	15	11		11			9
Th (ppm)	2.46	4.94		1.59			1.37
U (ppm)	1.11	2.65		0.38			0.46
La (ppm)	9.54	15.08		8.30			7.85
Ce (ppm)	23.69	27.40		18.90			18.28
Nd (ppm)	6.19	11.16		8.15			5.54
Sm (ppm)	2.75	2.39		1.85			1.48
Eu (ppm)	0.46	0.52		0.55			0.39
Tb (ppm)	0.47	0.26		0.24			0.20
Dy (ppm)	n.d.	n.d.	n.d.	n.d.	n.d.	n.d.	n.d.
Ho (ppm)	0.35	0.30		n.d.			0.11
Yb (ppm)	1.39	1.01		0.82			0.55
Lu (ppm)	0.24	0.19		0.15			0.10
Be (ppm)	n.d.	n.d.	n.d.	n.d.	n.d.	n.d.	n.d.

n.d. = not detected; blank space = not analysed

Table 5.8. Continued

Sample #	abm-002	abm-005	abm-012	abm-052	abm-069	abm-074	abm 140	abm-031	abm-047b	abm-093	abm-056
Mg Number	93.35	97.96	95.34	90.87	91.33	99.16	96.06	91.51	87.86	99.71	88.53
SiO2 (%)	66.20	54.90	54.70	56.20	55.00	52.60	54.30	68.40	52.20	56.00	74.90
TiO2 (%)	0.18	0.06	0.43	0.18	0.21	0.01	0.09	0.28	0.68	n.d.	0.20
Al2O3 (%)	2.56	0.90	4.95	2.30	3.62	0.08	0.96	3.24	7.20	n.d.	2.63
Fe2O3t (%)	1.07	0.75	1.81	2.11	1.74	0.33	1.34	1.82	3.12	0.11	1.87
MnO (%)	0.04	0.04	0.04	0.04	0.07	0.03	0.14	0.04	0.06	0.05	0.03
MgO (%)	7.58	18.20	18.70	10.60	9.25	19.60	16.50	9.90	11.40	19.00	7.29
CaO (%)	19.80	23.80	14.20	25.40	27.30	24.80	25.10	14.90	22.40	25.60	11.20
Na2O (%)	0.62	0.33	1.09	0.56	1.02	n.d.	0.25	1.15	1.35	n.d.	0.76
K2O (%)	1.32	0.05	2.65	1.18	1.10	n.d.	0.44	1.16	0.27	n.d.	1.35
P2O5 (%)	0.06	0.03	0.08	0.23	n.d.	n.d.	n.d.	0.04	n.d.	0.02	0.08
LOI (%)	1.14	0.58	1.46	1.48	0.47	2.10	1.39	0.11	1.68	0.27	0.09
Cr (ppm)	10		30				2	14	35	n.d.	
Ni (ppm)	9		15				7	12	n.d.	5	
Co (ppm)	24	18	22	19	14	12	13	45	31	10	92
Sc (ppm)	3		7		5	n.d.	2	4	8	n.d.	5
V (ppm)	19	8	40	26	66	3	64	31	50	n.d.	72
Cu (ppm)	5	4	16	8	22	2	6	8	14	1	21
Pb (ppm)	21	13	n.d.	62	n.d.	34	n.d.	29	44	n.d.	30
Zn (ppm)	102	84	185	326	447	94	223	195	125	189	74
Cd (ppm)	n.d.	n.d.	n.d.	2.00	n.d.	n.d.	n.d.	n.d.	n.d.	n.d.	n.d.
Sn (ppm)	n.d.	n.d.	n.d.	n.d.	20.00	n.d.	n.d.	n.d.	n.d.	35.00	n.d.
W (ppm)	0.48		n.d.				n.d.	n.d.	1.78	n.d.	
As (ppm)	0.31		0.57				1.57	n.d.	n.d.	0.27	
Sb (ppm)	0.43		0.80				0.83	0.39	0.90	0.48	
Ag (ppm)	0.1		n.d.				0.7	n.d.	n.d.	0.1	
Rb (ppm)	32		100				15	26	4	n.d.	
Cs (ppm)	0.41		5.14				0.58	0.33	0.70	n.d.	
Ba (ppm)	195	16	627	371	452	18	228	234	264	3	187
Sr (ppm)	800	270	250	1200	1900	110	660	1100	1300	100	570
Ga (ppm)	3	n.d.	4	3	6	n.d.	3	4	8	n.d.	3
Li (ppm)	14.00	42.00	127.00	28.00	25.00	5.00	32.00	22.00	41.00	5.00	17.00
Nb(ppm)	n.d.	3	6	n.d.	n.d.	n.d.	n.d.	n.d.	5	n.d.	3
Ta (ppm)	0.29		n.d.				n.d.	0.23	0.45	n.d.	
Hf (ppm)	0.72		2.52				0.75	1.40	5.22	n.d.	
Zr (ppm)	55	31	110	60	87	18	59	83	260	27	61
Y (ppm)	10	n.d.	17	9	n.d.	3	n.d.	n.d.	5	n.d.	4
Th (ppm)	0.96		2.64				0.32	0.36	3.77	0.21	
U (ppm)	0.31		1.06				0.19	0.10	1.19	0.22	
La (ppm)	4.26		14.16				2.64	1.53	6.38	0.80	
Ce (ppm)	11.47		28.83				5.70	3.93	15.93	1.78	
Nd (ppm)	6.54		16.35				2.21	2.32	15.44	n.d.	
Sm (ppm)	1.55		2.85				0.47	0.55	2.26	0.27	
Eu (ppm)	0.30		0.58				0.15	0.11	0.40	0.06	
Tb (ppm)	0.25		0.40				n.d.	n.d.	0.26	n.d.	
Dy (ppm)	n.d.	n.d.	n.d.	n.d.	n.d.	n.d.	n.d.	n.d.	1.00	n.d.	n.d.
Ho (ppm)	0.22		0.28				n.d.	n.d.	0.17	n.d.	
Yb (ppm)	0.83		1.34				0.15	0.20	0.54	0.18	
Lu (ppm)	0.13		0.23				0.03	0.06	0.15	0.04	
Be (ppm)	n.d.	2.00	n.d.	n.d.	n.d.	1.00	n.d.	n.d.	n.d.	1.00	n.d.

n.d. = not detected; blank space = not analysed

Table 5.9. Analyses of some of the barren calc-silicate rock samples.

The Astra Pluton analyses are summarised on table 5.5. They show that the unit is rich in silica: ~ 68%, this value is lower than that of the Du Bras pluton since this unit contains less quartz. Like the du Bras pluton this unit has low Mg numbers due to a higher percentage of iron relative to magnesium.

The analyses for the marbles, summarised on table 5.6, are separated into three groups: metadolostone, olivine-serpentine marble and calc-silicate marble. The olivine-serpentine and calc-silicate marbles have more silica than the dolostones due to the fact that they contain diopside and olivine respectively. All three have high (~ 30 wt%) calcium and high loss on ignition (~35 wt%) due to the high percentage of calcite. The metadolostone and the olivine-serpentine both have around the same quantity of magnesium (~20 wt%) despite their differing mineralogies, the magnesium in the former is contained in the dolomite, in the latter it is in the olivine or serpentine. All sub-units are poor in iron with high magnesium numbers (near 100).

Table 5.7 summarises the results of the paragneissic hornfels and the quartzite. The paragneissic hornfels is the only metasedimentary unit containing iron. The unit contains roughly equal amount of iron and magnesium (~ 7wt%). The unit is rich in silica with around 55% silica due, in this case, to the presence of quartz.

The quartzite consists primarily of silica (>90%) due to its high content of quartz. It contains little iron relative to magnesium as shown by its high Mg number ~80.

Table 5.8 summarises the analytical results for the wollastonite-bearing calc-silicate rocks. They show that the unit is composed principally of the silica, calcium, and

magnesium oxides. The Mg number is very high (~ 95). This unit is rich in silica with around 55% of SiO$_2$ due to the presence of silicate minerals such as wollastonite, diopside and quartz. Samples Abm-068 and Abm-111 have higher than normal loss on ignition (~7 %) because both samples contain around 20% calcite. Sample Abm-077 has anomalously high zinc, 3.7 wt%, this sample represents the zinc showing on the property.

The analytical results from the barren calc-silicate rocks are represented in table 5.9, and are similar to those of the wollastonite-bearing calc-silicates both for silica (around 55 wt%, as well as for the Mg number (~95). However this unit contains more magnesium (10% versus 7% for the wollastonite-bearing calc-silicate rocks), and less calcium (20% versus 28% for the latter). This difference is probably due to the lack of wollastonite in this unit compared to the other.

5.2.2 Rare Earth Element Diagrams

Rare earth element (REE) diagrams were made to compare rare earth elements and their mobility between the lithological units. On these diagrams, the analyses are normalised to chondrite values from Taylor and McLennan (1985).

5.2.2.1 The Plutons

The normalised rare earth patterns for the three plutons, namely the LSJ anorthosite, the du Bras Pluton and the Astra Pluton, are shown on figure 5.1, and each show fairly different signatures.

The chondrite normalised rare earth element patterns of the LSJ anorthosite show more variation than the other plutons (fig. 5.1a). They have medium values as compared to the other plutons, i.e. REE_N 12-200 and they only show a gentle slope with little enrichment in light REE. Sample abm-136 deviates somewhat from the general pattern with much lower rare earth values and a positive rare earth anomaly. This is probably due to the fact that it is richer in plagioclase than the other anorthositic samples

The Astra Pluton shows a different rare earth pattern (Figure 5.1b). In general, the chondrite normalised rare earth values are higher, La_N in the 50 to 300 range. It also shows a steeper slope revealing a stronger enrichment in light rare earth elements. The samples of the Astra syenite analysed here do not have a significant europium anomaly.

For the Du Bras Pluton, the REE patterns all fall within a narrow range. Figure 5.1c shows a relatively flat pattern with a small enrichment in light REE. Only one sample (abm-120) has a negative europium anomaly with a value of 3. The chondirite normalised values are lower than the other two plutons, i.e. La_N =10-80.

5.2.2.2 The Metasediments

Similar plots of chondrite normalised rare earth elements of the metasediments were made (figs 5.2 and 5.3). The patterns show that on the whole, these units are more depleted in rare earth elements than the plutons.
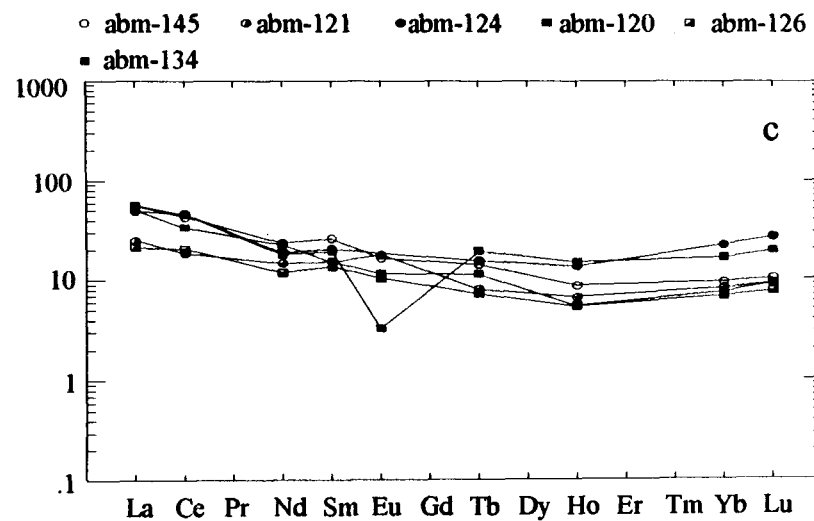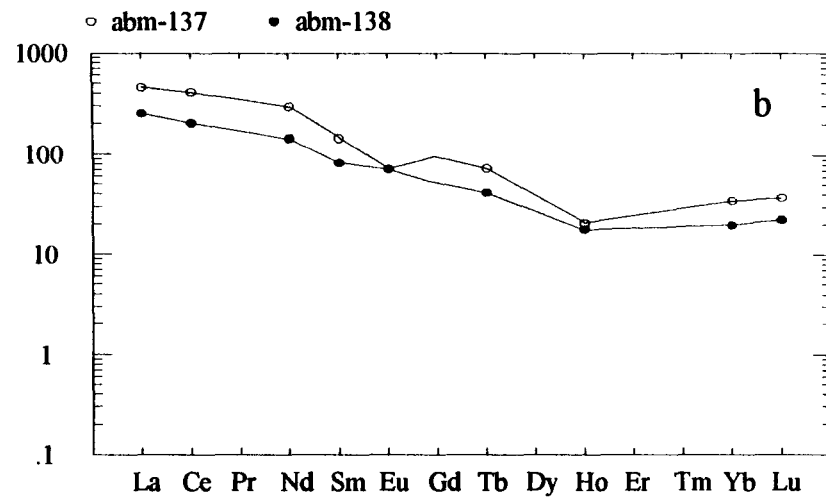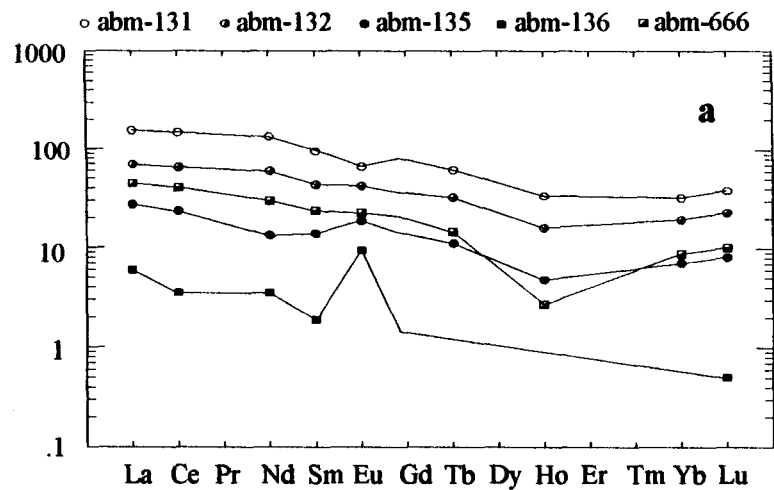
Figure 5.1. Chondrite normalised rare earth element diagrams of the Plutons: a) for the LSJ anorthosite; b) Astra Pluton; c) Du Bras Pluton. Gadolinium values for the LSJ anorthosite and the Astra Pluton are extrapolated from a projection from the samarium to the terbium values to accentuate possible europium anomalies.

77
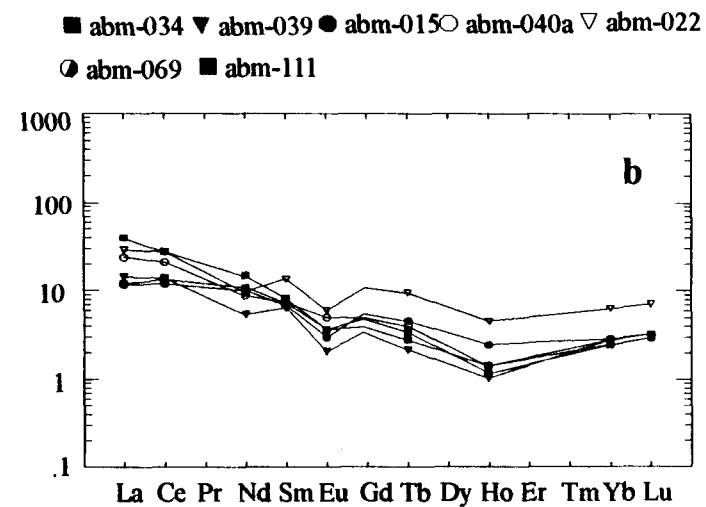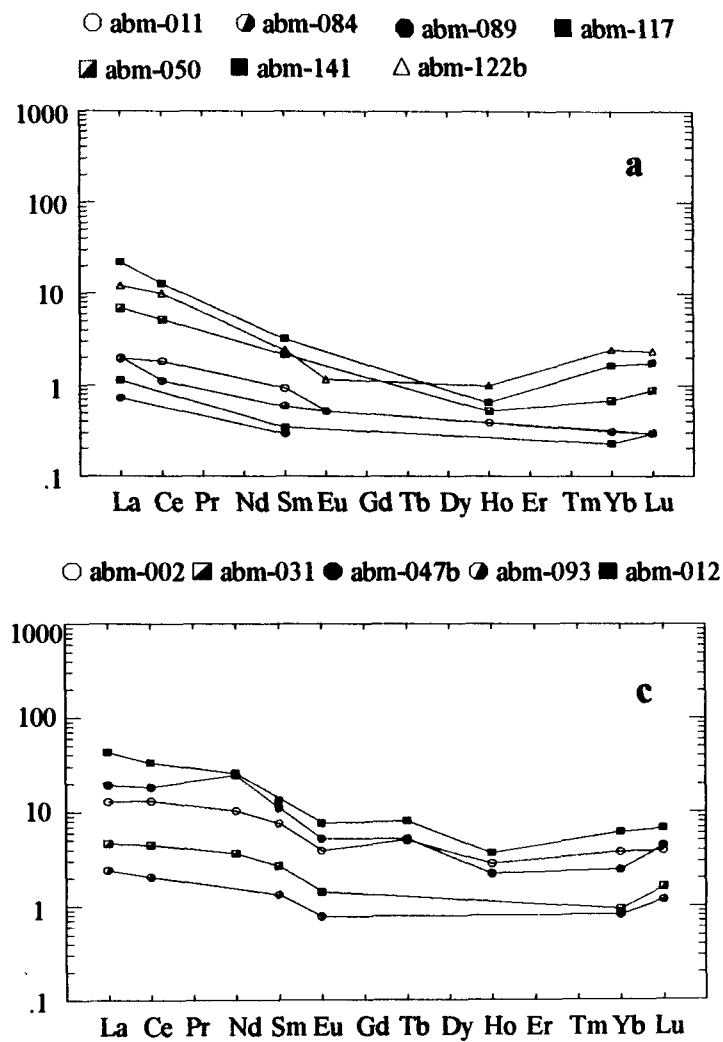
Figure 5.2. Chondrite normalised rare earth element diagrams for the metasediments: a) the marbles; b) the barren calc-silicate rocks and c) the wollastonite-bearing calc-silicate rocks. Gadolinium values for the wollastonite-bearing calc-silicate rocks are extrapolated from a projection from the samarium to the terbium values to accentuate possible europium anomalies.

◇ abm-104b ○ abm-112b

○ abm-139 ◑ abm-130 ● abm-112a
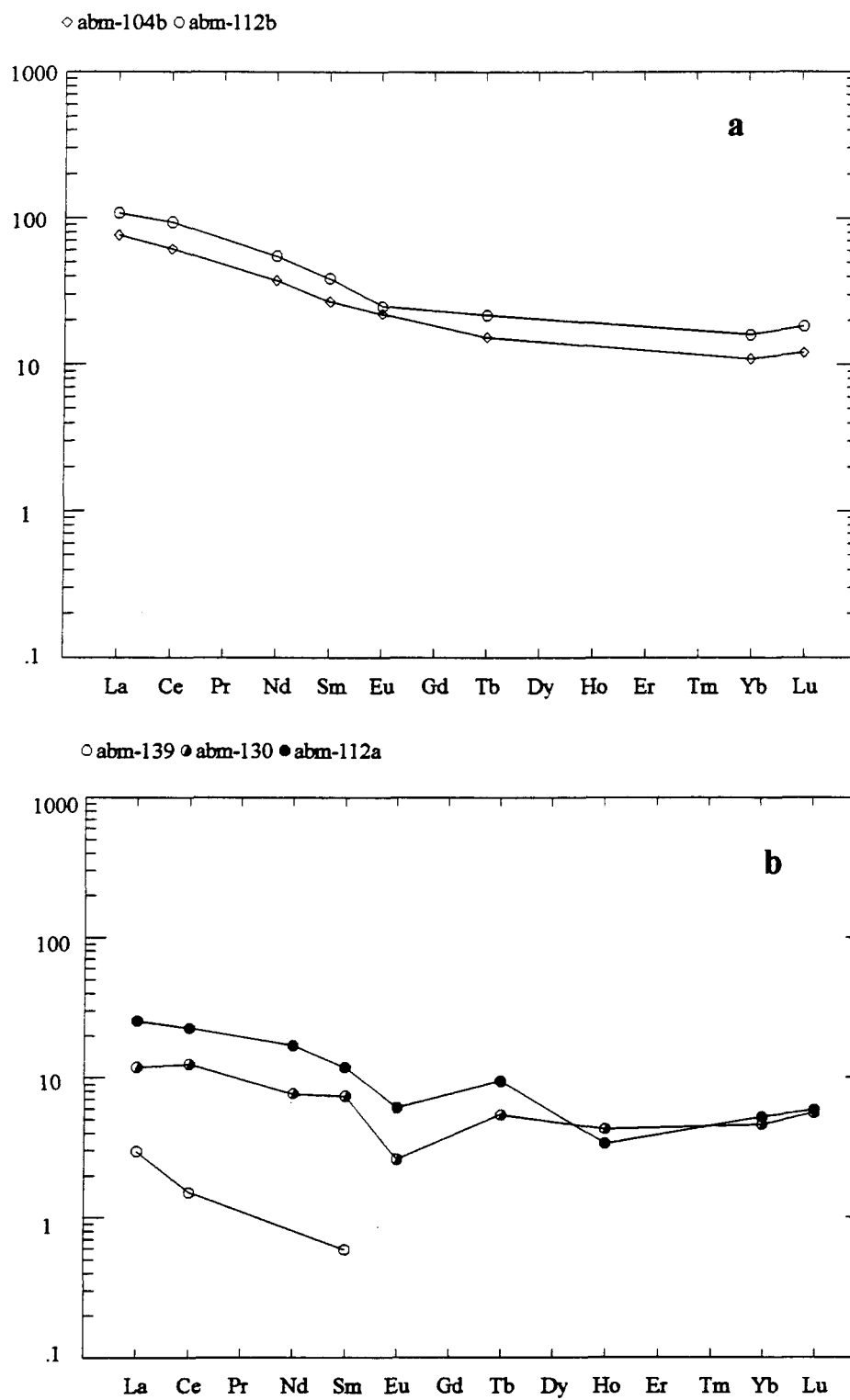
Figure 5.3. Chondrite normalised rare earth element diagrams of the metasediments: a) the paragneissic hornfels; b) the quartzite.

The marbles have the lowest chondrite normalised REE values, with slight depletion in heavy REE (fig. 5.2a). The values show some variation with a range from 0.1 to 20. The samples analysed have no significant europium anomaly.

The calc-silicate rocks were divided into two groups: barren calc-silicate rocks and calc-silicate rocks containing wollastonite. The calc-silicate rocks with wollastonite (fig. 5.2b) show a narrow range of values between 10 and 40, with only a gentle slope showing slight heavy REE depletion. All samples have a negative europium anomaly. In contrast the barren calc-silicate rocks show more dispersion (fig. 5.2c) extending downwards towards value similar to those of the marble, with values ranging between 1 and 45 between the range of the marbles and the calc-silicate rocks with wollastonite.

The hornfelsic paragneiss and the quartzite are the two other metasedimentary lithological units in the area and their rare earth patterns are represented on figures 5.3a and 5.3b respectively. The chondrite normalised paragneiss REE values are significantly higher than the values of the marbles and the calc-silicate rocks with values around 100 and they show less depletion of heavy REE. The quartzite has a normalised REE pattern that is similar to that of the barren calc-silicate rocks.

5.3 DISCUSSION

If the calc-silicate rocks at the Canton-Saint-Onge wollastonite deposits formed as a result of the infiltration of aqueous silica in a skarn process, as discussed in section 1.4, the resulting rock should not only show a change in silica content but the concentration of other

elements should change as well. Unfortunately standard mass transfer diagrams (e.g. Greisens diagrams) do not prove to be useful because of the concentrations of the most elements in the protolith is too low to be measured as will be shown further in this section.

In order to characterise the mobility of the elements during the skarn process certain assumptions must be made. The first being the nature of the protolith. For this section we have used the marbles in contact with, and enveloping, the calc-silicate rocks. This is justified as a probable protolith because of their position neighbouring the calc-silicate rocks, probably representing an untransformed facies. The second assumption is that of the open system behavior, where silica is introduced in a fluid and CO_2 is removed. Using the reactions:

$$CaCO_3 + SiO_2 \rightarrow CaSiO_3 + CO_2 \qquad\qquad 1$$
$$\text{rock} \qquad \text{fluid} \qquad \text{rock} \qquad \text{fluid}$$

and
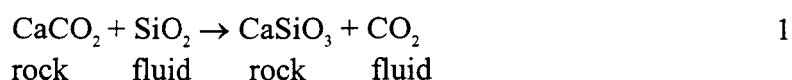
$$CaMg(CO_3)_2 + 2SiO_2 \rightarrow CaMgSi_2O_6 + 2CO_2 \qquad\qquad 2$$
$$\text{rock} \qquad\qquad \text{fluid} \qquad\quad \text{rock} \qquad\qquad \text{fluid}$$
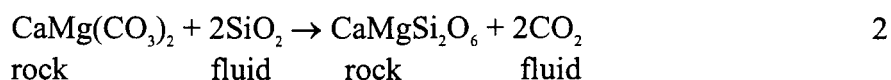
the principal reactions forming the wollastonite and diopside bearing calc-silicate rocks. The mass change, therefore, principally involves the addition of silica, and since the CO_2 is driven off during the reaction some oxygen is removed. Therefore based on the atomic mass the mass change is of 16% and 17% respectively for the two reactions. This mass change is minimal and therefore ignored in the subsequent discussion.

5.3.1 Mass Transfer

The mass transfer for the different elements was examined by plotting individual samples over the mean wollastonite value for certain elements, these values are organised according to rock type and are plotted on figure 5.4. This diagram was used to distinguish the concentration of different elements in the metasediments. Since the values were examined with respect to the mean wollastonite-bearing calc-silicates values around 1.0 represent little change.

Silica is the element with the most mass transfer as shown by the reactions above. This is also shown on figure 5.4 where the marbles have near zero silica with respect to the calc-silicate rocks. Therefore the silica has been added. There is no significant difference between the wollastonite bearing and barren calc-silicate rocks.

The titanium also appears mobile, with low values, near zero for the marbles and much higher values for the calc-silicate rocks. The large variance for this element especially in the barren calc-silicates is probably dependant on the presence of titanite in this unit which tends to be concentrated in layers therefore the samples with higher TiO_2 ratios represent sampling of the titanite layers. This increase in titanium suggests that it was involved in a possible skarn process, mentioned in the opening of this section.

Figure 5.4 also shows an increase in alumina and iron in the calc-silicate rocks as compared to the marbles. The values of the marbles fall mainly near zero with one alumina
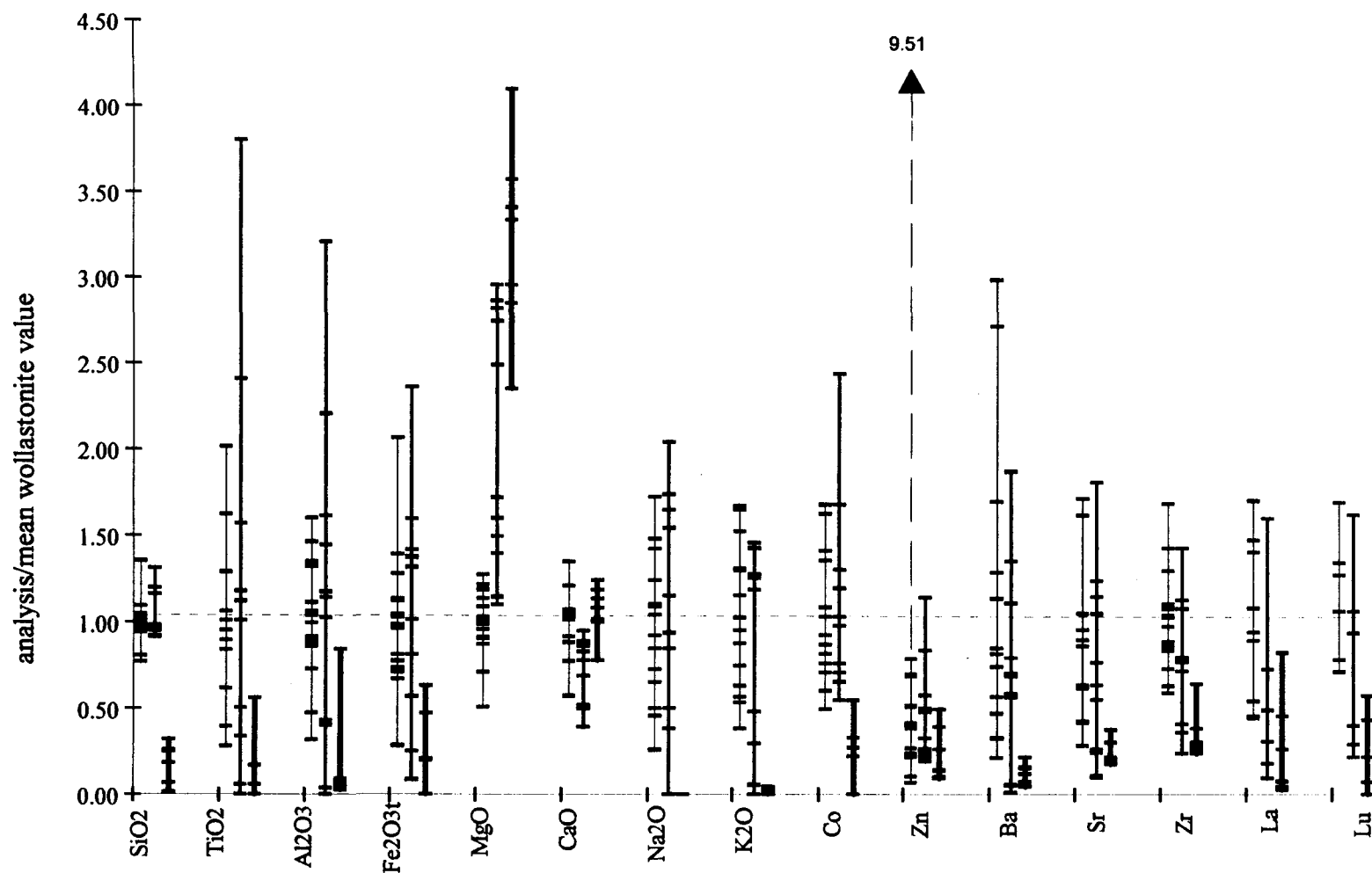
Figure 5.4. Mass transfer of the different elements between lithological units. For each element the first thin line represents wollastonite-bearing calc-silicate rock analyses values over the mean wollastonite-bearing calc-silicate value; the second thicker line, the barren calc-silicate rocks; and the third thickest line the marbles.
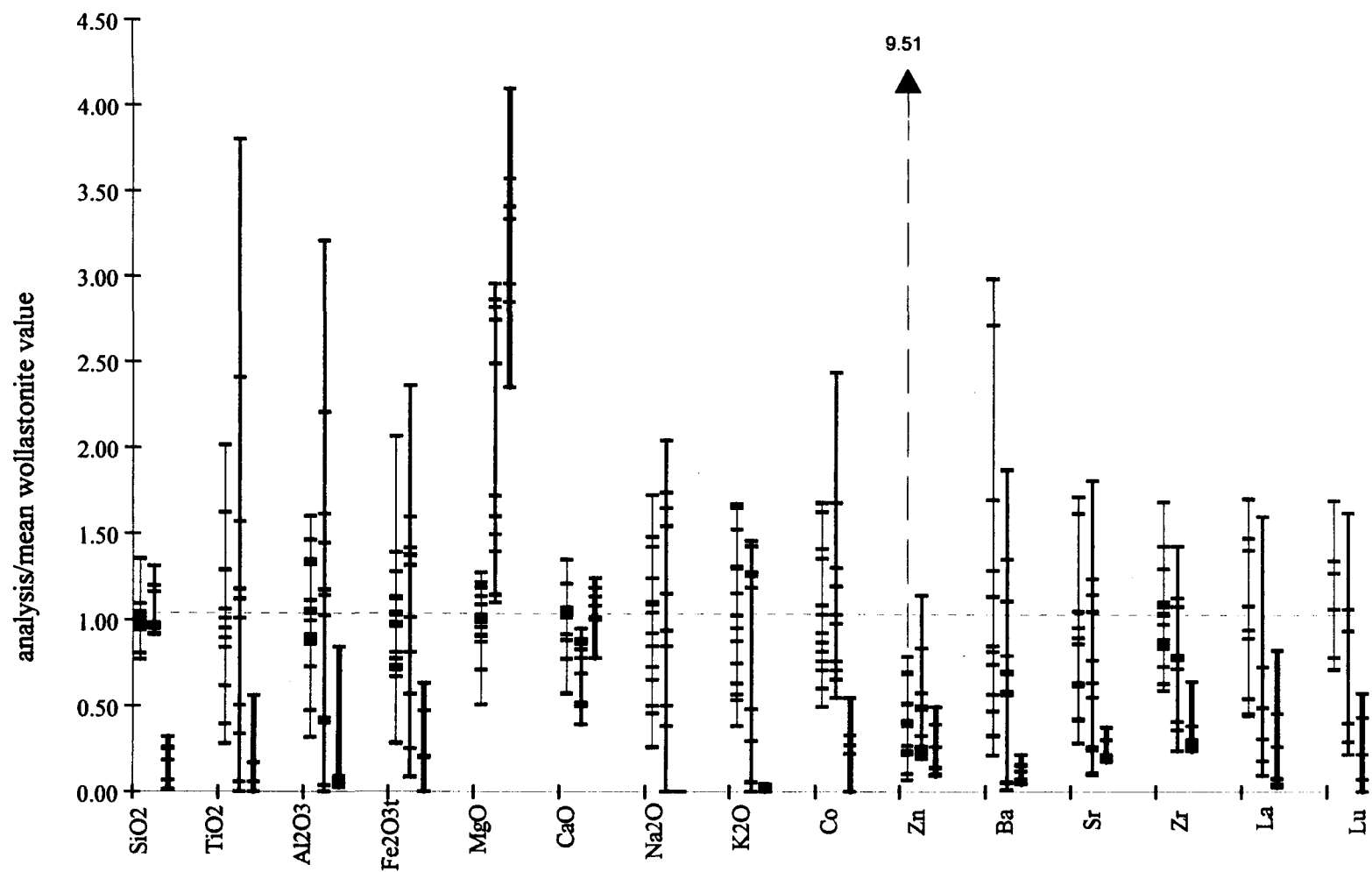
Figure 5.4. Mass transfer of the different elements between lithological units. For each element the first thin line represents wollastonite-bearing calc-silicate rock analyses values over the mean wollastonite-bearing calc-silicate value; the second thicker line, the barren calc-silicate rocks; and the third thickest line the marbles.

outlier at 0.8 with the calc-silicate rocks having varying values averaging one. This suggests that alumina and iron was also introduced during the skarn process.

The magnesium seems to be the only element that shows a significant decrease in concentration from the marbles to the calc-silicate rocks. The marbles have the highest values followed by the barren calc-silicate rocks and the wollastonite-bearing calc-silicate rocks have the lowest values. This suggests that the magnesium was leached from the marble protolith leading to low values for the resulting calc-silicate rocks, and this process was more advanced in the wollastonite-bearing calc-silicate rocks during the skarn process.

Calcium seems to be the element that shows the least change. All the units have ratios around one. The barren calc-silicates have slightly lower values this is due to their larger quantity of diopside relative to the calcium-rich wollastonite. This relationship suggests that little exchange of calcium took place during the skarn process.

The sodium and potassium show similar relationships. In both cases the marbles have near zero or zero ratios. In contrast the calc-silicate rocks have similar wide ranging values averaging around one. This suggests that the two elements were introduced during the skarn process. None of the units contain much potassium nor sodium however the slightest increase is measurable because of the near total lack of them in the marbles.

There is an increase in cobalt from the marbles to the calc-silicate rocks, but there is little difference between the different calc-silicate rocks. This suggests that the cobalt as well was introduced in the skarn fluids during the ore-forming process.

The average wollastonite-bearing calc-silicate value for zinc is somewhat skewed due to the presence of sample abm-077, representing the zinc showing on the property. Other than this sample the rest of the unit seems to have similar values to that of the marble and the barren calc-silicate rocks. The concentration of zinc at this one site seems to have no relation to the skarn process forming the wollastonite and therefore might be post-skarn.

The barium, strontium and zirconium show similar relationships. The marble ratios are well clustered with values between 0.5 and 0. The barren calc-silicate rocks have wider ranging values with the lowest being in the range of the marbles and the highest values in the range of the wollastonite-bearing calc-silicates. These start with values slightly higher than the barren calc-silicates but have the same range of values. This relationship suggests that barium, strontium and zirconium were present in the marble protolith, but more was introduced during the skarn reactions increasing their abundance in the product, however the increase was not uniform.

Lanthanum and lutetium represent the light and heavy rare earth elements respectively on the diagram. There is an increase in both rare earth elements from the marbles to the barren calc-silicates to the wollastonite-bearing calc-silicate rocks, as depicted by the rare earth diagrams from section 5.2.2. The fact that the wollastonite-bearing calc-silicate rocks have higher REE values suggests that these rocks were even more effected by the fluids as compared to the barren calc-silicate rocks. This increase in REE in the calc-silicates suggests that the components of these rocks were also influenced by externally derived material and therefore probably were not the result of a simple isochemical reaction history. The diagram shows that the wollastonite-bearing calc-silicate rocks were clearly enriched in REE, whereas the barren calc-silicate rocks were enriched to

varying degrees. The barren calc-silicate rocks show much variation, from low REE, with values around that of the marble, to the highest wollastonite values.

The REE plots are not sufficient, however, to determine the nature and the source of the fluids. The most likely source is that of the plutons, since they all have higher normalised REE patterns than those of the marbles and the calc-silicate rocks. Whether the source pluton is the Astra, du Bras or LSJ anorthosite cannot be determined from the geochemistry alone.

5.4 DISCRIMINATION DIAGRAMS

Data from the Astra and du Bras plutons were plotted on various discrimination diagrams to investigate their paragenesis. Petrogenesis was examined using the discrimination diagrams of Maniar and Piccoli (1989), Bachelor and Bowden (1985), Pearce *et al.* (1984), and Whalen *et al.* (1987).

On Shand's Index from Maniar and Piccoli (1989) represented by figure 5.5, the two plutons fall approximately within separate ranges. The Astra Pluton is slightly metaluminous falling near the edge of the metaluminous field. Most of the Du Bras samples fall within the peraluminous field with one exception which falls in the metalumious field.

On the petrogenetic discrimination diagram of Batchelor and Bowden's (1985; fig.10) (fig. 5.6) the two plutons cluster well within different fields. The Astra Pluton falls
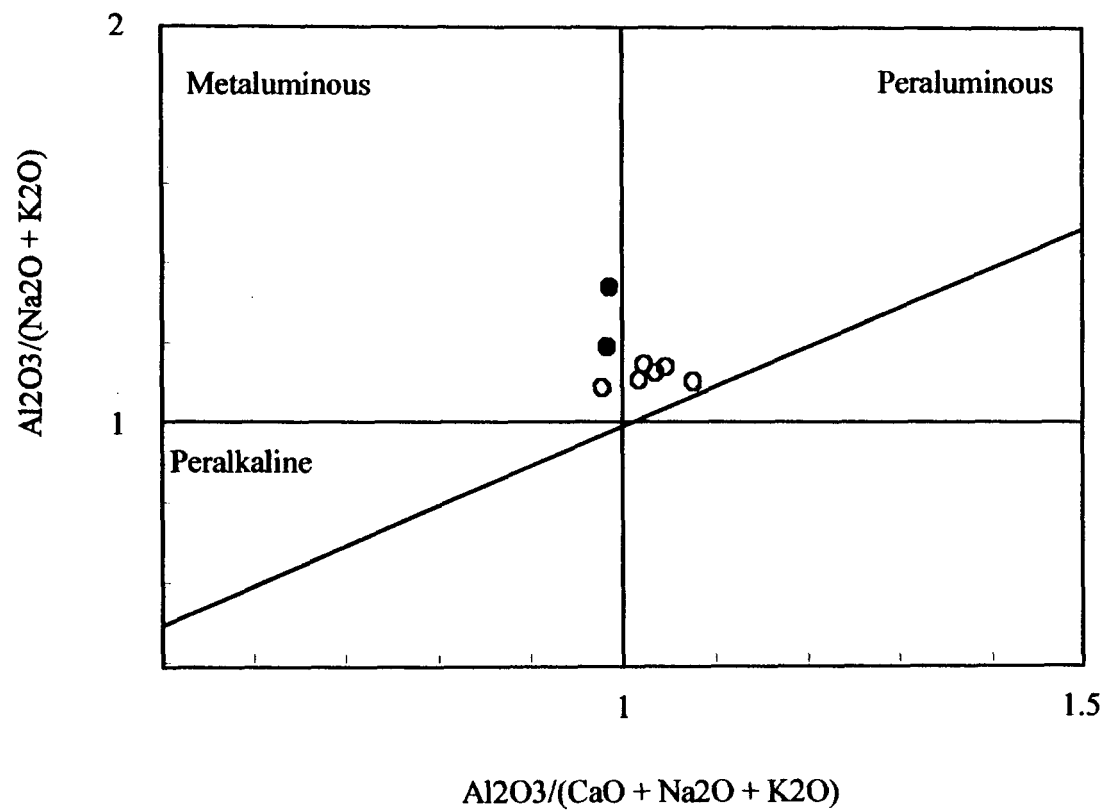
Figure 5.5. Granite discrimination diagram of Shand's index from Maniar and Piccoli (1989). Astra Pluton samples (solid circles) fall in the metaluminous field, whereas the Du Bras Pluton samples (open circles) fall mainly in the peraluminous field.
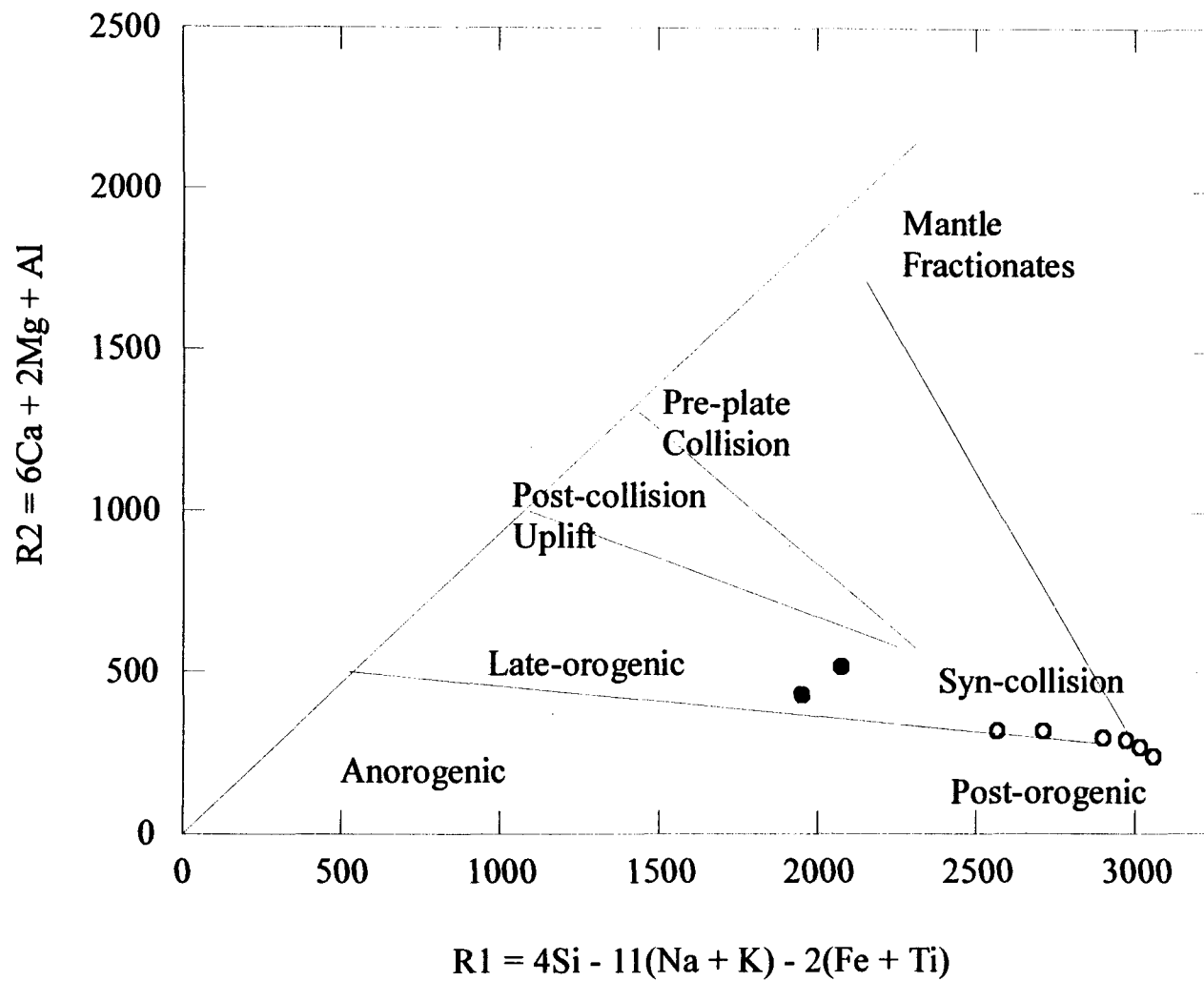
Figure 5.6. Granite petrogenitic diagram after Batchelor and Bowden (1985; fig. 10). Astra Pluton (solid circles) fall in late-orogenic granite field whereas the Du Bras Pluton samples (open circles) fall in the syn-collisional to post-orogenic granite fields.

within the range of late orogenic plutons whereas the Du Bras Pluton falls within the range of post-orogenic to syn-collisional plutons. The discrimination diagram of Pearce *et al.* (1984; fig. 4) reveals similar petrogenetic traits as the plutons again cluster well within different fields (fig. 5.7). The Du Bras Pluton falls within the syn-collisional granites whereas the Astra Pluton falls in the within-plate-granite field.

On the discrimination diagrams of Whalen et al. (1987; fig 5b) the relationships is less clear. The Astra Pluton clearly falls within the anorogenic granite field, whereas the Du Bras Pluton samples fall in or towards the fractionated felsic granite field. This suggests that the latter is transional between the two granite types whereas the Astra Pluton clearly is anorogenic.

The petrogenetic discrimination diagrams suggest that the Astra Pluton is metaluminous and formed as a late-orogenic to anorogenic, within plate pluton, whereas the same diagrams suggest that the du Bras Pluton is peraluminous and shows a more transitional petrogenesis as a fractionated syn-collisional to a post-collisional pluton. This is in accordance with the field relationships, since the du Bras granite is sheared and foliated in certain places, suggesting the rock has undergone some deformation and could be of syn-collisional or late collisional petrogenesis. In contrast, the Astra syenite is pristine and undeformed, thus suggesting that the pluton was emplaced following deformation, as a late, within plate pluton.
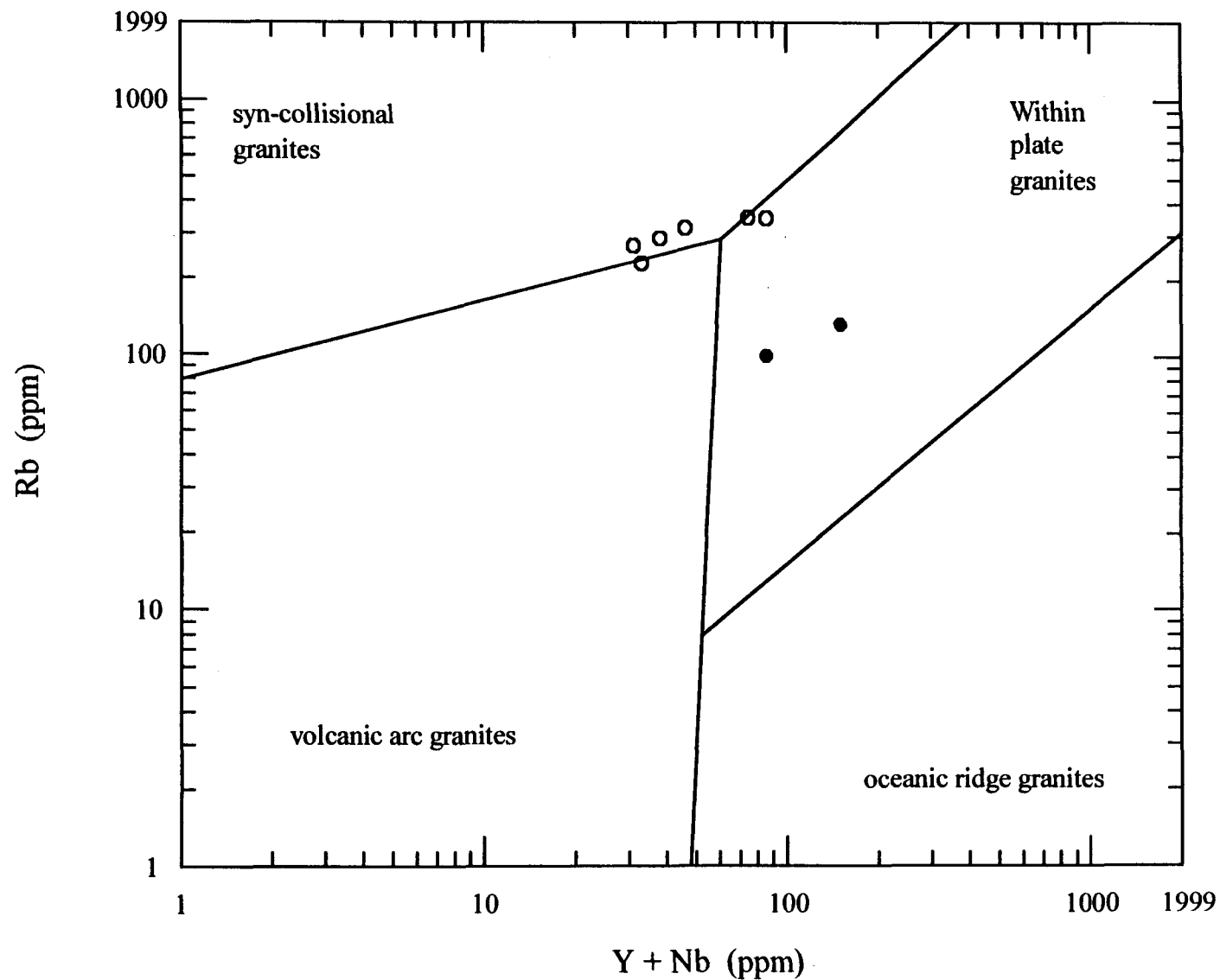
Figure 5.7. Granite petrogenetic discrimination diagram from Pearce (1984; fig.4) Astra Pluton samples (solid circles) fall in the within plate granite field whereas the Du Bras Pluton samples (open circles) appear transitional falling between the syn-collisional granites and the within plate granites fields.
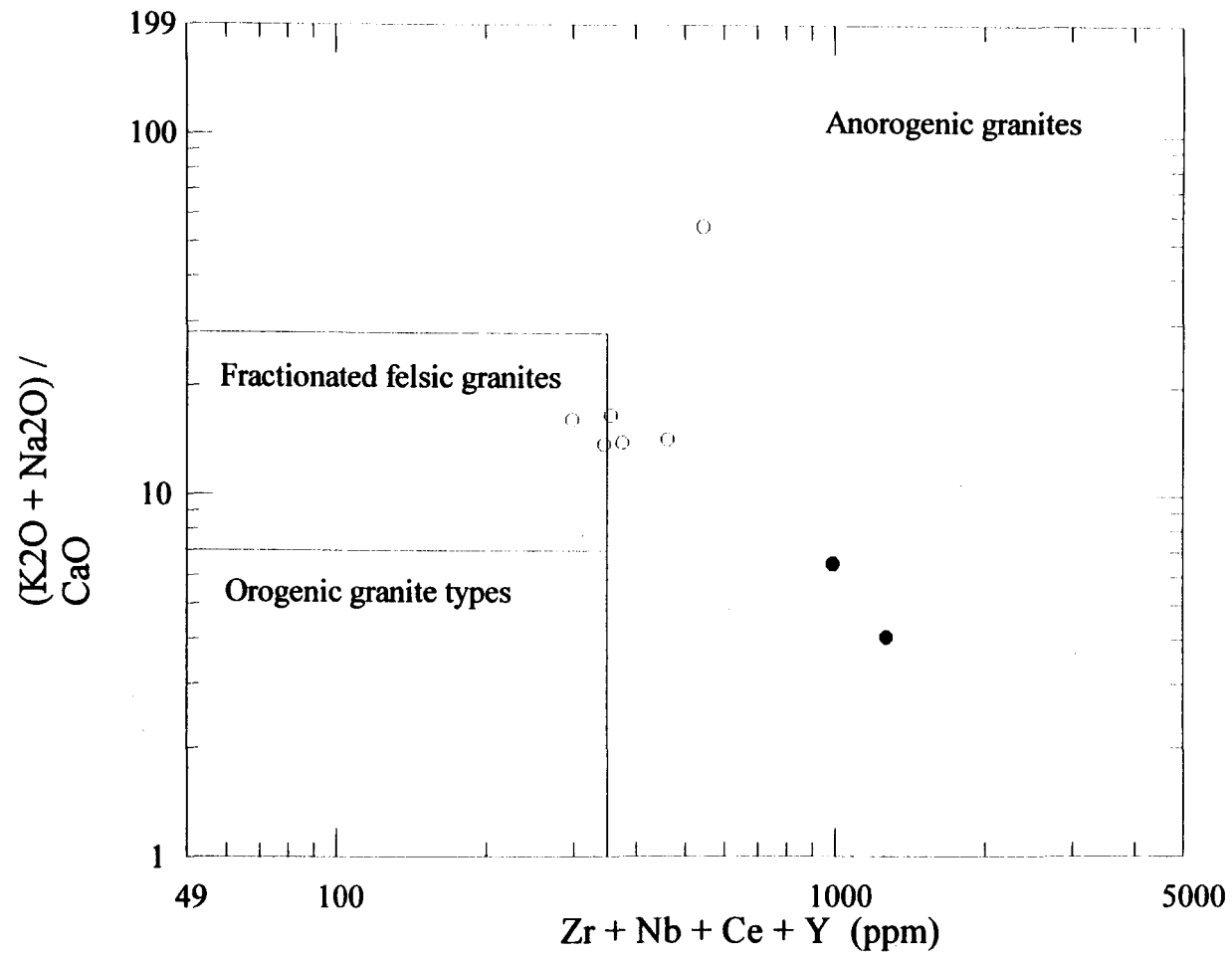
Figure 5.8. Granite petrogenetic discrimination diagram after Whalen *et al.* (1987; fig. 5b). Astra Pluton samples (solid circles) fall in the anorogenic granite field, whereas the DuBras Pluton samples are more transitional falling the anorogenic to fractionated felsic granites fields.

Chapter 6

Stable Isotopes

6.1 INTRODUCTION

Stable isotopes have been used to study skarns (Gerdes and Valley, 1994; Cartwright and Weaver, 1993; Valley, 1986; Bowman *et al.*, 1985; Valley and O'Neil, 1982;) and can be very effective because of the large difference in isotopic ratios between limestone and most plutons: the $\delta^{18}O$ of limestone is 20-28 $^o/_{oo}$ (parts per thousand) and the $\delta^{18}O$ of most plutons is around 6-13 $^o/_{oo}$. These studies have also been effective because the assumed unmetasomatised equivalent of the skarned rock can be analysed for comparison.

Oxygen isotopes were used in particular in this study since during the wollastonite forming reaction:

$$CaCO_3 + SiO_2 \rightarrow CaSiO_3 + CO_2 \qquad\qquad 1$$
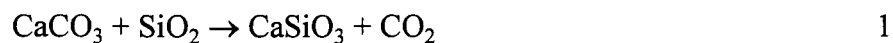
the reaction of interest, oxygen is involved in all phases of the reaction and therefore its change in isotopic ratio can reveal information on its source. Carbon isotopes were also used, but its presence only in the reactant (or marble protolith) allows for no comparison with other units.

Since the stable isotope composition of a metamorphic rock is controlled by the following four factors:

1) the composition of the pre-metamorphic protolith

2) the effects of volatilisation

3) the exchange with infiltrating fluids

4) the temperature of exchange (independent of pressure)

important information on protolith, fluid composition and sources can be revealed by their study.

6.1.1 Composition of the pre-metamorphic protolith

Although the protolith itself cannot be determined using stable isotopes alone, the study of the stable isotopes can determine by comparison if an assumed protolith is a valid choice. For this study the pre-metamorphic protolith concerned is assumed to be the pre-metasomatised protolith of the marble or limestone. It is used because of its position neighbouring the calc-silicate rocks; the stable isotopes can show whether this is a reasonable protolith.

6.1.2 Effects of volatilisation

Since the wollastonite forming reaction causes the liberation of CO_2, which fractionates the heavy oxygen and carbon isotope (O'Neil, 1986), its evolution will affect the remaining rock by lowering its heavy to light isotopic ratio. Valley (1986) examined

the evolution of a rock through an open and closed volatilisation process. Figure 6.1 shows

how a rock and the CO_2 would evolve during a batch volatilisation (closed system) where
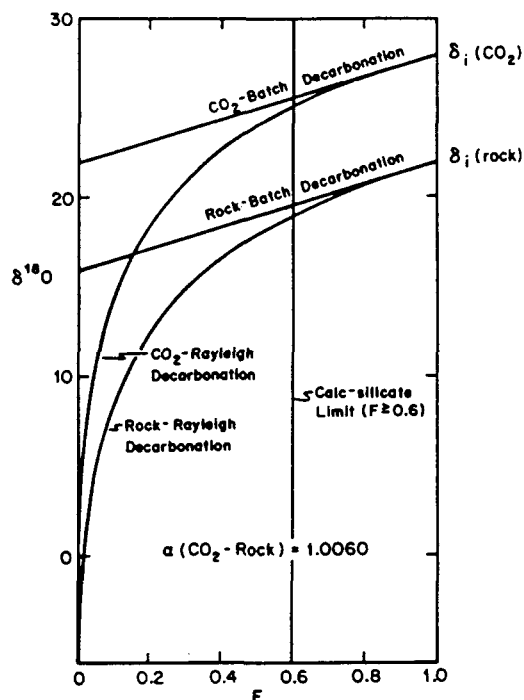
Figure 6.1. Lowering of $\delta^{18}O$ resulting from batch decarbonation (straight line) and Rayleigh decarbonation (curves). F is the mole fraction of oxygen remaining in the rock (after Valley, 1986).

the evolved fluid remains in contact with the rock and Rayleigh volatilisation (open system)

where the CO_2 is continually removed. The diagram shows that during Rayleigh

decarbonation the $\delta^{18}O$ tends toward - ∞ if all the oxygen is volitilised, but a calc-silicate

limit exists at $F \geq 0.6$ because of the stoichiometry of most metamorphic reactions (Valley,

1986). Therefore, this graph shows that through normal volatilisation there is a limit to the

amount the $\delta^{18}O$ can be lowered.

6.1.3 Exchange with infiltrating fluids

Bowman *et al.* (1985) further studied the effects of volatilisation by introducing the effect of fluid infiltration using the contact aureole and skarn formation at the Black Butte Stock at Elkhorn, Montana as an example. The Elkhorn stock is a quartz-diorite pluton surrounded by skarned carbonates consisting of calc-silicates, followed by marbles in the periphery to the pluton.

The authors completed sampling cuts at the contact between the stock and the skarn to study the isotopic variation. They found the $\delta^{18}O$ isotopic values of the skarn to be around 8 to 12 $^o/_{oo}$, and decreasing on approaching the pluton (fig. 6.2). The surrounding marble, however, records $\delta^{18}O$ values around 22 $^o/_{oo}$ indicating that there was significant removal of heavy isotopes during metasomatism, more than can be explained by volatilisation.

Using the decarbonation reaction of:

$$CaMg(CO_3)_2 + 2SiO_2 \leftrightarrow CaMgSi_2O_6 + 2CO_2 \qquad\qquad 2$$
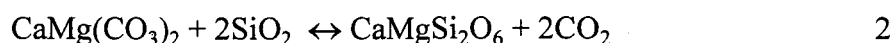
Bowman *et al.* (1985) modelled the various processes which could bring about such a drop in $\delta^{18}O$ and $\delta^{13}C$ values. They plotted (see fig 6.3) the three metasedimentary lithologies of the area: sedimentary dolostone, marble and skarn. The marble shows a slight decrease in $\delta^{18}O$ which can be explained by the decarbonation, or volatilisation, brought about by
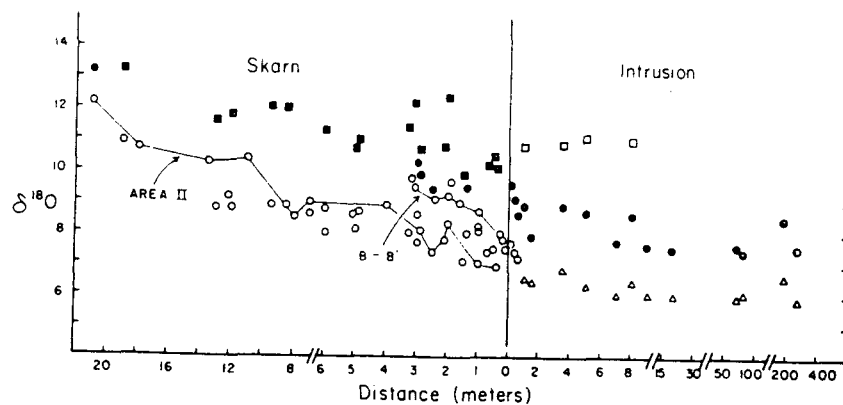
Figure 6.2. Plot of the $\delta^{18}O$ values of minerals from the Black Butte stock and skarns as a function of distance from the intrusive contact (after Bowman *et al.*, 1985).
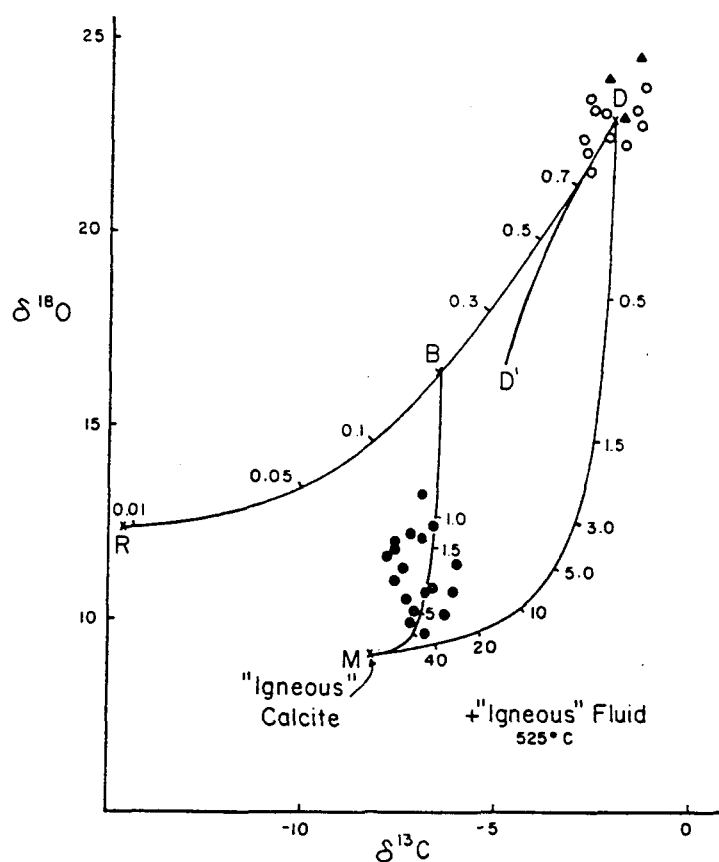
Figure 6.3. Plot of $\delta^{18}O$ versus $\delta^{13}C$ values form calcite and dolomites from sedimentary dolostone (solid triangles), marble (open circles), and skarn (solid circles) from Elkhon, Montana (after Bowman *et al.*, 1985).

contact metamorphism of the intruding pluton, however, the low $\delta^{18}O$ values of the skarn rock cannot be explained by contact metamorphism alone.

If one considers decarbonation in a closed system (Batch volatilisation) represented by the curve D-D', the $\delta^{18}O$ cannot be lowered by fractionation before the system reaches equilibrium and there is very little lowering of $\delta^{13}C$.

Volatilisation in an open system represented by the curve D-R shows how the $\delta^{13}C$ can be further lowered but again the $\delta^{18}O$ will not be lowered sufficiently by this process. Exchange with a magmatic fluid, represented by curve D-M, is one possible explanation to significantly lower the $\delta^{18}O$ and $\delta^{13}C$ values to arrive at "igneous" calcite. The scattering of the skarn $\delta^{18}O$ values higher than those of the "igneous" calcite can be explained by an actual path of reaction that was a combination decarbonation and magmatic exchange reaction represented by path DBM.

6.1.4 Temperature of exchange

In order to use stable isotopes to determine equilibrium temperature, isotopic analyses of mineral pairs must be used. For this study whole rock powders were used for isotopic analysis since no phase was common to all units analysed and therefore the temperature of exchange cannot be determined.

6.2.0 METHODOLOGY

Twenty-nine bulk rock samples were analysed to determine their isotopic ratios at the stable isotope lab of the École Polytechnique in Montreal. All units were analysed; 2 samples from each pluton; 3 from the anorthosite; 6 from the marble; and 13 calc-silicates (fig. 6.4). Criteria for sample selection for isotopic analysis included minimal alteration as well as geographical dispersion. The same powders used for geochemistry were used for isotopic analysis.

6.2.1 Oxygen From Silica

The method used for isotopic analysis is that of Clayton and Mayeda (1963). Between 4 and 6 mg of rock powder was reacted with bromine pentaflouride (BrF_5) to release the oxygen. A typical reaction being:

$$KAlSi_3O_8 + 8BrF_5 \rightarrow KF + AlF_3 + 3SiF_4 + 4O_2 + 8BrF_3 \qquad\qquad 3$$

The reactions were run for at least 12 hours (overnight) in nickel tubes at around $600°C$. With this process the samples are loaded and heated for one hour open to the high vacuum line. This step is used to remove absorbed air and water acquired during sample loading. However, this step was avoided for samples containing feldspars (i.e. the du Bras and Astra Plutons) following the discovery of low yields probably due to premature reactions with residual fluorine attached to the nickel reaction tubes. Once this was corrected adequate oxygen yields were obtained.

Figure 6.4. Location of samples used for δ18O analysis with their values.
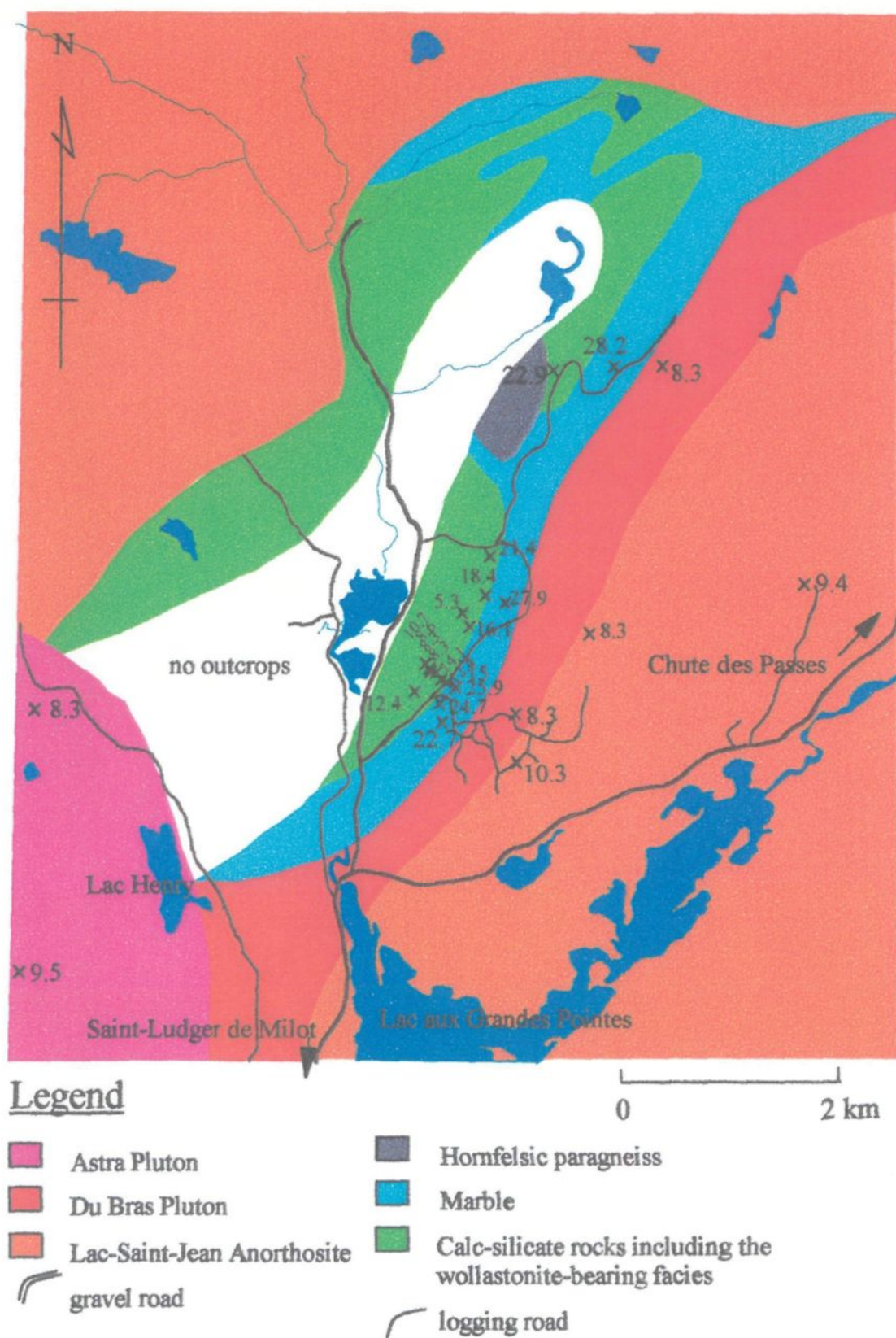
The BrF_5 was expanded into the reaction tubes with an approximately 5 fold excess of reagent over stoichiometric requirements. The apparatus at the École Polytechnique allowed for 10 simultaneous reactions, however, only nine reaction tubes were working at the time. Following the 12 hour reaction with BrF_5 the volatiles from each reaction tube were passed through a cold trap where of the possible products of O_2, BrF_5, BrF_3, Br_2, and SiF_4 only the oxygen passes through.

After collection and measurement of the oxygen (to determine yield), the gas is passed over hot carbon to convert it quantitatively to carbon dioxide by the reaction:

$$C + O_2 \rightarrow CO_2$$ 4

The carbon dioxide is then collected in bottles at the end of the line. It is the carbon dioxide that is then analysed by a mass spectrometer to determine the isotopic ratios.

6.2.2 Oxygen and Carbon From Carbonates

The marble samples were analysed differently, in order to determine both the oxygen and carbon isotopic ratios in the individual minerals. Since the samples contained both calcite and dolomite the technique of Al-Aasm *et al.* (1990) was used to separate the two. Rather than mechanical separation of the minerals, they were separated chemically based on their different reaction rates.

With this method the samples were reacted with phosphoric acid at 25°C to liberate the oxygen. Around 50 mg of each sample mixed with phosphoric acid in a glass reaction vessel were heated in a bath. A typical reaction occurring is:

$$CaCO_3 + H_3PO_4 \rightarrow CO_2 + H_2O + CaHPO_4 \qquad \qquad 5$$
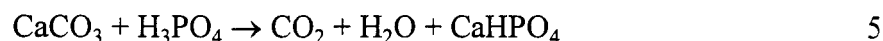
After allowing for 3 hours of reaction time the gases (H_2O and CO_2) were driven out of the reaction tubes. This should allow enough time for all of the calcite to react but not the dolomite. The gases evolved after 24 hours represent the dolomite products. As with the previous technique the gasses were analysed by the mass spectrometer to determine the isotopic ratios.

6.3 RESULTS

The location of the samples used for isotope analysis are shown on figure 6.4. The results for $\delta^{18}O$ are summarised in table 6.1 and the results for the carbonates are summarised in table 6.2. All $\delta^{18}O$ are calculated with respect to SMOW and the $\delta^{13}C$ with respect to PDB.

Figure 6.5 shows the isotopic results with respect to rock type. The marbles have $\delta^{18}O$ values between +22 and +28 ‰ and $\delta^{13}C$ values between 5 and 0 ‰, typical of sedimentary limestones (Faure, 1986). This implies isochemical metamorphism with no interaction of external oxygen to alter the $\delta^{18}O$ values from the original sedimentary values. The Du Bras Pluton and the Astra Pluton have $\delta^{18}O$ values between 8 to 10 ‰, typical of plutonic granites (Taylor and Sheppard, 1986), implying no contamination from high $\delta^{18}O$

Lithological unit	Sample #	$\delta^{18}O(\text{‰} \pm 0.5)$
LSJ Anorthosite	abm-666	10.3
	abm-136	9.4
	abm-131	8.3
Astra Pluton	abm-137	9.5
	abm-138	8.3
Du Bras Pluton	abm-120	8.3
	abm-120	8.3
Barren calc-silicate	abm-002	14.1;13.8
rocks	abm-031	8.3
	abm-047b	16.1
	abm-093	18.6;18.3
	abm-012	15.3;15.9
Wollastonite-bearing	abm-101	21.4
calc-silicate rocks	abm-034	8.6
	abm-036	10.7
	abm-111	22.9
	abm-015	12.4
	abm-068	12.4
	abm-040b	5.3
	abm-022	8.3
Marbles	abm-011	25.9
	abm-050	24.7;24.7
	abm-084	27.9
	abm-117	28.2
	abm-141	22.7

Table 6.1. $\delta^{18}O$ results for the different lithological units.

Sample#	mineral	$\delta^{13}C(\text{‰}\pm0.1)$	$\delta^{18}O(\text{‰}\pm0.1)$
abm-011	calcite	11.9	25.9
	dolomite	2.3	27.7
abm-050	calcite	0.02;-0.07	24.7;24.7
abm-084	calcite	1.16	27.9
abm-117	calcite	1.9	28.2
	dolomite	4.3	34.4
abm-141	calcite	-0.08	22.7

Table 6.2. $\delta^{13}C$ and $\delta^{18}O$ analysis of the carbonates in the marbles.
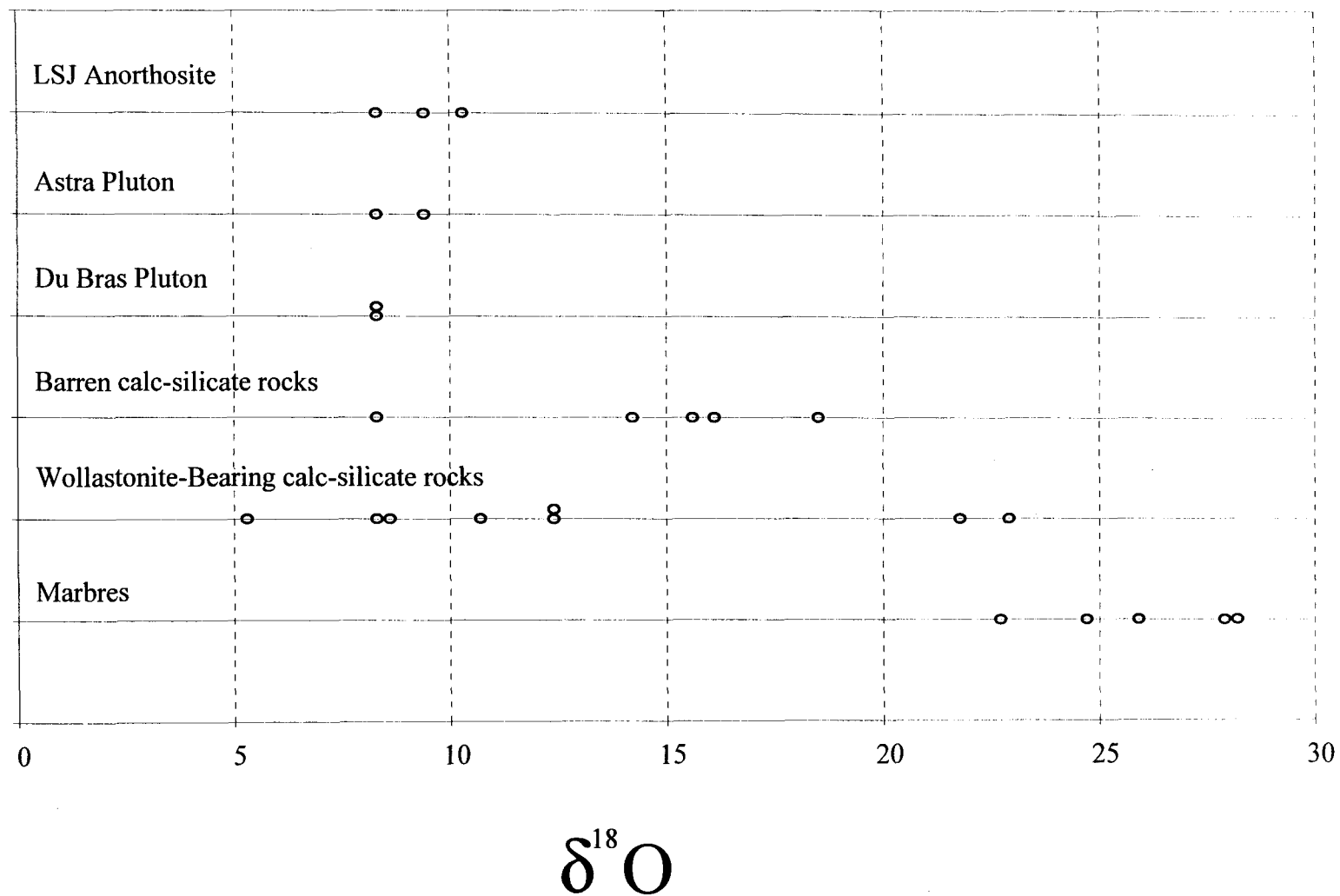
Figure 6.4.δ18O results with respect to the different lithological units

crustal sources. The LSJ Anorthosite has $\delta^{18}O$ values ranging from 8 to 11 ‰. These values are high for a mafic rock but typical of Grenvillian anorthosites which probably originated as high $\delta^{18}O$ magmas (Valley *et al.*, 1990).

The calc-silicate rocks have $\delta^{18}O$ values ranging from 8 to 22 ‰, with the lowest values similar to those of the plutons and the highest similar to those of the marbles. There is one exception, however, sample Abm-040b with lower than normal isotopic ratios, $\delta^{18}O$ = 5.3 ‰, however, this sample is strongly weathered and altered deeply and therefore its isotopic ratio could have been affected by later fluid flow.

On figure 6.5 the calc-silicate rocks were separated into two groups: wollastonite-bearing calc-silicate rocks and barren calc-silicate rocks to see if there was a relation between the oxygen isotopic ratios and the presence of wollastonite. It shows the wollastonite bearing calc-silicate rocks tend to have somewhat lower $\delta^{18}O$ values, in the range of 8 to 13 ‰, than their barren counter parts, with the exception of two outliers, samples Abm-101 and Abm-111 at 21.4 and 22.9 ‰ respectively. These two represent samples taken from the north-eastern end of the deposit. The barren calc-silicate rocks, however, have higher values from 14 to 18 ‰, with one exception, sample Abm-031 at 8.3 ‰.

6.4 DISCUSSION OF ISOTOPIC RESULTS

6.4.1 Volatilisation Versus Fluid Infiltration

The dispersion of the calc-silicate rock $\delta^{18}O$ values between those of the marbles and those of the plutons (from 8 to 23 ‰) suggests that the calc-silicate rocks could initially

have had values in the range of the marbles, but that they were reequilbrated with a fluid that was in equilibrium with the plutons to varying degrees.

Considering the marbles as the protolith to the calc-silicate rocks then the low values of most of the later ($\delta^{18}O$ between 8-14) cannot be explained by volatilisation or decarbonation alone. The studies of Bowman et al. (1985, fig. 6.2) and Valley et al. (1984, fig. 6.1) show that decarbonation will only reduce the $\delta^{18}O$ by about 5 ‰, not explaining the significantly lower values of the calc-silicate rocks with respect to the marbles. By continuous-removal-decarbonation (Rayleigh distillation) the values cannot be significantly lowered because of the stoichiometry considerations (Valley, 1986) since not all the oxygen atoms initially present in the dolomite or calcite can be removed as CO_2; some fraction of the original oxygen remains in the newly formed silicate minerals, buffering the final $\delta^{18}O$. During the conversion of dolomite marble to massive diopside skarn, one third of the oxygen originally present in the dolomite remains in the diopside (Bowman et al. 1985). If one considers oxygen derived from SiO_2, and SiO_2 in the form of quartz originally in the rock, as would be the case for isochemical contact metamorphism, then only 40% of the original oxygen can be removed in CO_2 (Bowman et al. 1985). Only a fluid in equilibrium with the plutons, having $\delta^{18}O$ around 8 ‰ could have resulted in sufficient lowering of the $\delta^{18}O$ values of the calc-silicate rocks to this observed low level. The higher $\delta^{18}O$ values (in the 20's) to the north of the deposit could be the result of simple volatilisation and continuous removal of CO_2.

Also of note is that no lithological unit has $\delta^{18}O$ values lower than 8 ‰. This implies no interaction with meteoric water, or reequilibration afterwards, since meteoric water typically has $\delta^{18}O$ values lower than zero, as in the case of the Adirondack Aureole

(Valley and O'Neil, 1982) where its implication brought the $\delta^{18}O$ values of the rocks into the negative range. If there was interaction with meteoric water the isotopic ratios of the waters were re-equilibrated with the intrusions prior to interaction with the calc-silicate rocks. Because of the narrow range of the isotopic ratios of the three plutons it cannot be determined with which pluton-derived fluids the calc-silicate rocks interacted, since all three plutons have values around 8 ‰, which is the lowest isotopic value of the pristine calc-silicate rocks.

6.4.2 Geographical distribution

In order to examine the geographical representation of the isotopic ratios two cross-sections were made transecting the different lithological units from the south-west to the north-east represented by line A-A', and south-east to north-west section represented by line B-B' in figure 6.6.

The $\delta^{18}O$ values for the A-A' section are plotted on figure 6.7 with respect to distance from the samples of the Astra Pluton. This section cuts through the Astra Pluton to the south-west through the calc-silicate rocks to the marbles in the north-east (fig. 6.6). The different values were projected onto the line A-A' with averages used from the areas where there were many calc-silicate rock values.

The linear relationship between $\delta^{18}O$ and distance is clear on figure 6.7. The low values for the Astra pluton grade into the high values for the marble through the intermediate values of the calc-silicates. This relation suggests that fluids in equilibrium
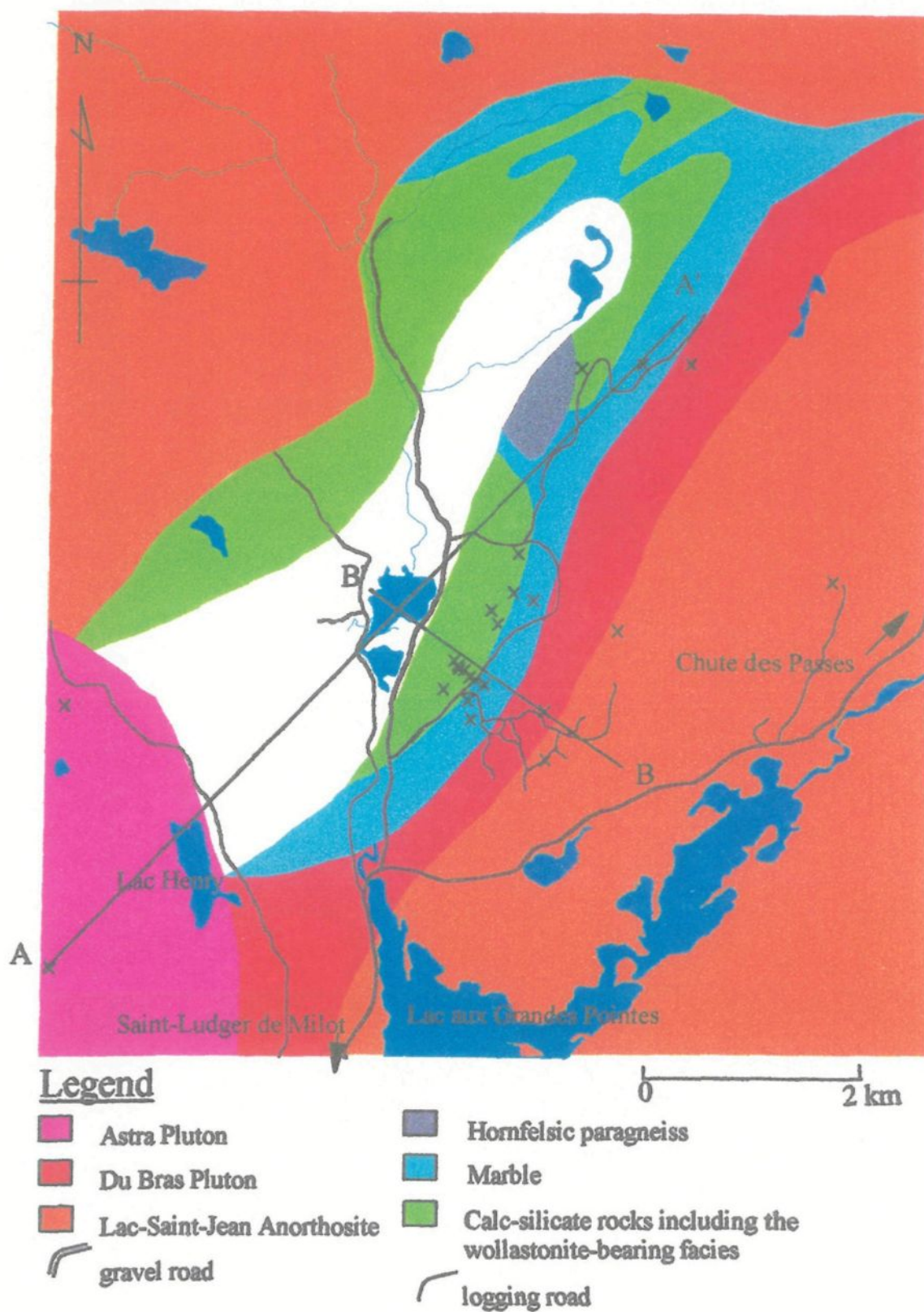
Figure 6.6. δ18O sample locations with cross-section lines A-A' and B-B'.

Legend

- Astra Pluton
- Du Bras Pluton
- Lac-Saint-Jean Anorthosite
- gravel road
- Hornfelsic paragneiss
- Marble
- Calc-silicate rocks including the wollastonite-bearing facies
- logging road
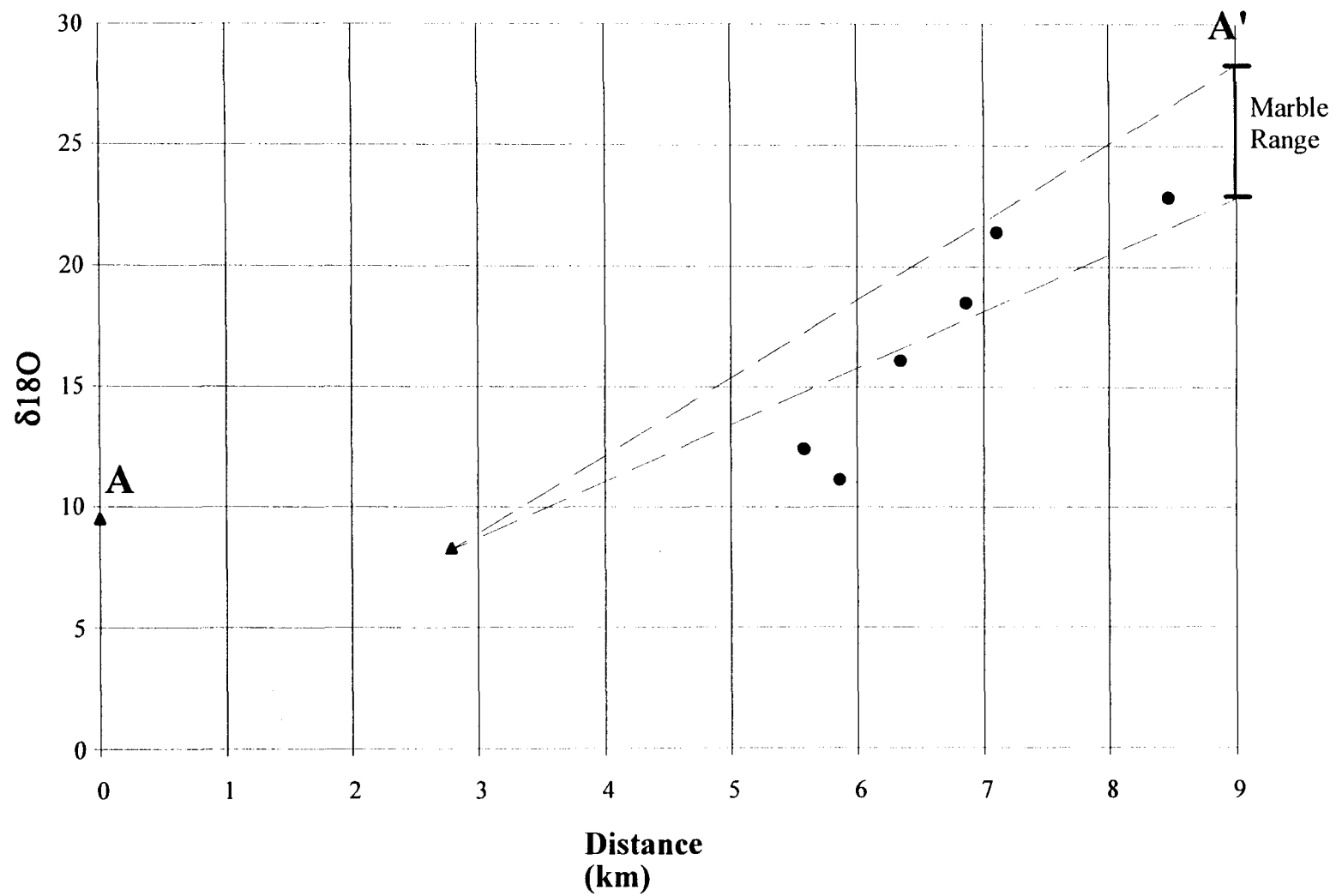
Figure 6.7. Section A-A', SW-NE cross-section of isotopic ratio with respect to distance. The triangles represent the Astra Pluton samples and the circles, the calc-silicate rocks.
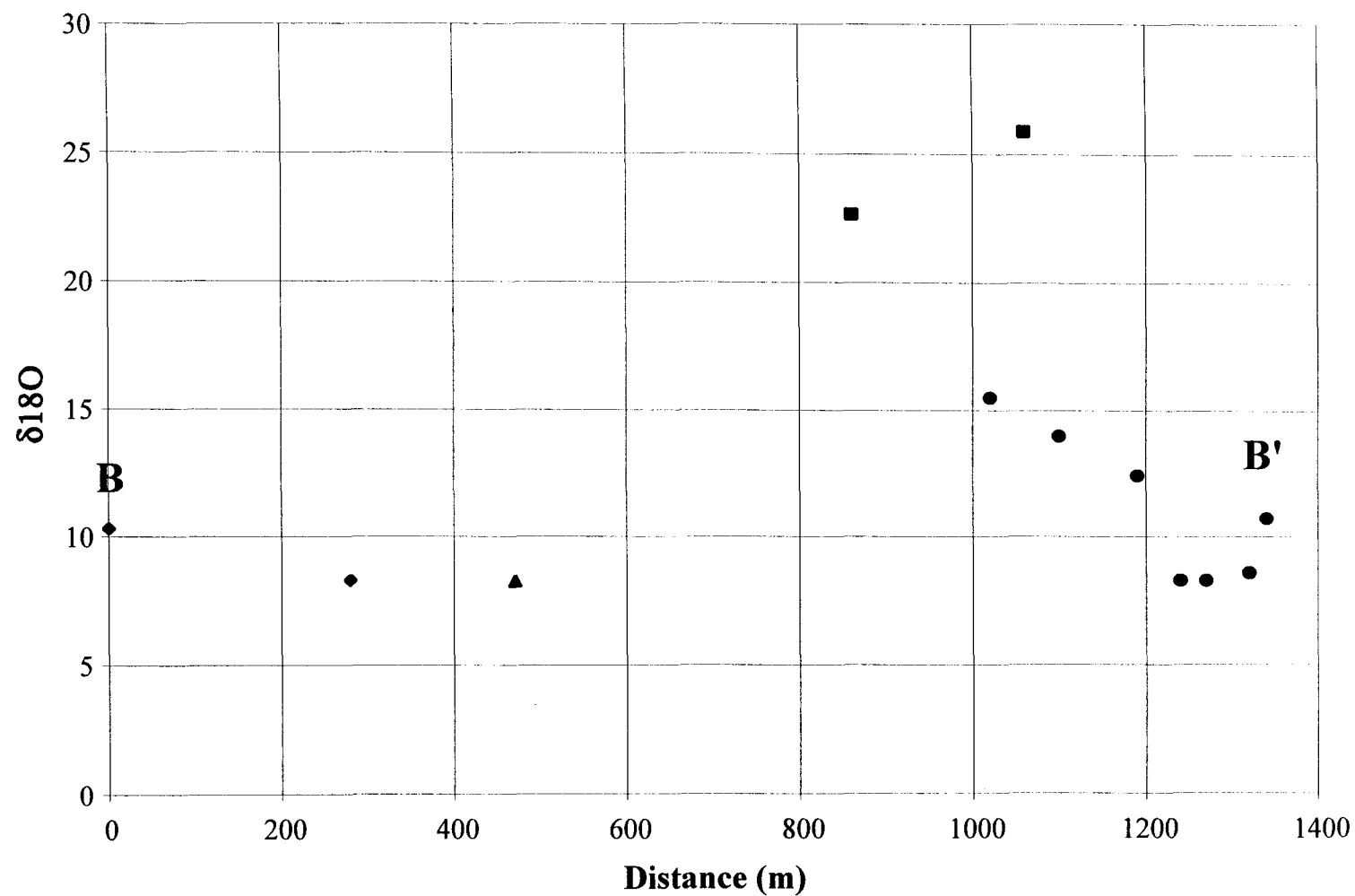
Figure 6.7. Section B-B', SE-NW cross-section of isotopic ratio with respect to distance. Diamonds represent LSJ Anorthosite samples; traingle, the Du Bras Pluton sample; the circles, the calc-silicate rocks; and the squares the marble samples.

with the Astra Pluton infiltrated and interacted principally with the calc-silicate rocks near its contact and that the marbles were largely untouched by these fluids.

The B-B' section plotted in figure 6.8 begins at the LSJ Anorthosite, passing through the du Bras Granite, through the marbles and ends in the calc-silicate rocks. The relation of the isotopic ratios with respect to distance is less clear. The low anorthosite and granite values and the intermediate calc-silicate values are separated by the high marble values. This relationship makes the anorthosite and Du Bras Plutons less likely candidates as fluid source of metasomatism, in addition to the geological relationship where these plutons are not in contact with any calc-silicate rocks. However, since hot magmatic fluids tend to flow upwards it would depend on the distribution of the rocks underlying the calc-silicate rocks, either pluton could be in contact with the calc-silicate rocks at depth. This seems unlikely, however, since the limited drilling by Ressources Orléans (Khobzi, K., pers. comm) on the property has intersected marble beneath the calc-silicate rocks.

Because of the linear relationship between distance from the Astra Pluton and isotopic ratio (figure 6.7), this pluton seems a more likely fluid source. This is possible considering some lateral fluid flow channelled along a zone of weakness. The lack of outcrop in along a line trending N040° crossing the deposit most probably represents a brittle fault associated with the LSJP lineament, or a conduit for fluids emanating from the Astra Pluton during skarn formation.

Chapter 7

DISCUSSION

7.1 INTRODUCTION

The goal of this thesis is to develop a petrogenetic model for the Canton Saint-Onge wollastonite deposit. The petrogenetic model should include determination the protolith of the wollastonite bearing calc-silicates as well as the process by which the wollastonite was formed. The model also should encompass the timing of the events that led up to the formation of the wollastonite. With the petrogenetic model established the deposit can then be compared to other wollastonite deposits in the Grenville Province and exploration criteria can be developed for finding similar wollastonite deposits elsewhere.

7.2 ORE FORMING PROCESS

7.2.1 Protolith

The first problem to resolve is to find the protolith of the wollastonite. The wollastonite is contained within the calc-silicate rocks which are comprised mainly of diopside and wollastonite with minor quartz, sphene and trace calcite and vesuvianite. It is the protolith to this rock unit that needs to be found.

In pure siliceous carbonates, wollastonite is usually formed from calcite by the reaction:

$$CaCO_3 + SiO_2 \rightarrow CaSiO_3 + CO_2 \qquad 1$$
$$\text{calcite} \quad \text{silica} \quad \text{wollastonite}$$
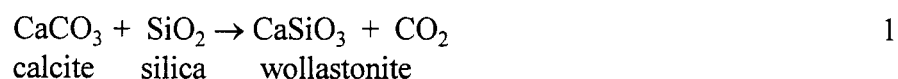
Similarly diopside is usually formed by the reaction:

$$(Ca,Mg)CO_3 + 2(SiO_2) \rightarrow CaMgSi_2O_6 + 2CO_2 \qquad 2$$
$$\text{Dolomite} \qquad\qquad \text{Diopside}$$
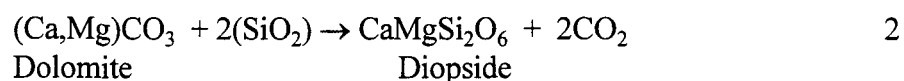
Therefore, a likely candidate for the protolith to the wollastonite bearing calc-silicates is a marble since that would be the only rock that would contain sufficient calcite and/or dolomite necessary for the reaction creating the observed volumes wollastonite and diopside. The silica in the reaction can be provided in the form of quartz or aqueous silica introduced by circulating fluids, this is discussed further in the following section. Therefore, the protolith can range from a siliceous marble to a pure calcite marble.

Adjacent to the wollastonite bearing calc-silicate rocks is the marble lithological unit which could be the protolith to the wollastonite and calc-silicate rocks. This unit contains sufficient quantities of calcite and dolomite for the reactions to form large quantities of wollastonite and diopside. There is little quartz and siliceous minerals and, therefore, most of the silica in the reaction probably is derived from an external source, or the actual protolith is a

more silica-rich marble, and the marble left represents a more refractory, or inert, starting composition.

Figure 7.1 shows the Mg/Mg+Ca atomic ratio versus $\delta^{18}O$ for the calc-silicate rocks and the marbles. The marbles, represented by **D** on figure 7.1, appear dolomitic with a Mg/Mg+Ca ratio of 0.5, the magnesium in this unit is derived either from the dolomite in the rocks or from the forsterite but both cases have the same Mg/Mg+Ca ratio. The barren calc-silicates, represented by **B** on the diagram, have a similar Mg/Mg+Ca ratio but with lower $\delta^{18}O$ values suggesting that the dolomitic marbles are the protolith of the barren calc-silicates with the isotopic ratio lowered by interaction with fluids with a lower isotopic ratio. The wollastonite bearing calc-silicates, represented by **W** on the diagram, however, have lower Mg/Mg+Ca ratios, i.e. enriched in Ca compared to Mg, with no equivalent marble at this cation ratio range. One possible explanation is that the light oxygen-rich fluids that lowered the $\delta^{18}O$ ratio for the calc-silicates also contained significant quantities of calcium for enrichment of the wollastonite bearing calc-silicates. The other explanation is that the calcite marbles with the same cation ratio have all been transformed leaving no neighbouring protolith.

7.2.2 Ore-Forming Process

If the protolith to the wollastonite is the marble adjacent to the calc-silicate rocks the source of the silica must also be determined. The silica can be provided in the form of quartz
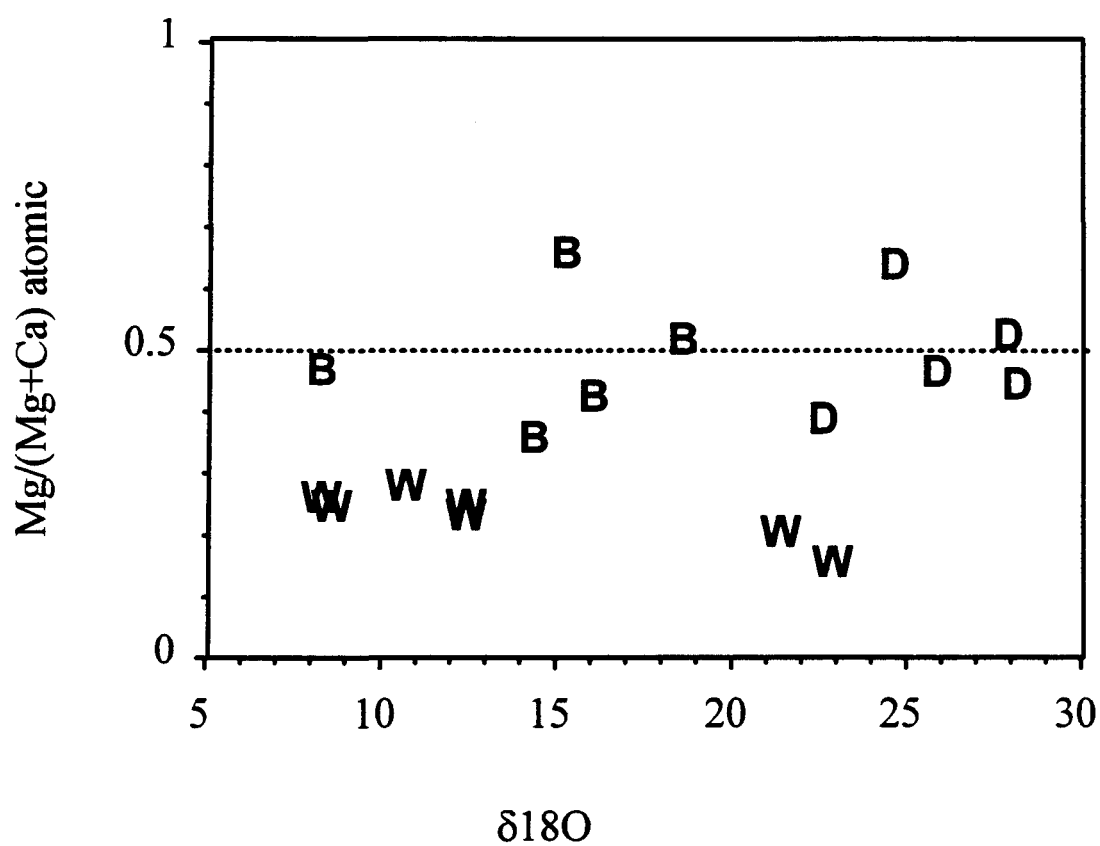
Figure 7.1. Cation ratio with respect to oxygen isotpie ratio for the metasedimentary lithological units. **D** represents dolomitic marbles; **B**, barren calc-silicate rocks; and **W**, wollastonite-bearing calc-silicate rocks.

present in the protolith with an isochemical reaction, the process termed skarnoid or

recrystalised skarn (Einaudi *et al.*, 1981), or introduced in a fluid emanating from a

crystallising pluton creating a metasomatic reaction termed skarn, or reaction skarn (Einaudi *et al.*, 1981).

The stable isotope work, presented in chapter 6, suggests that the silica is externally

derived, as in the skarn process since the $\delta^{18}O$ values of the calc-silicate rocks are lower than

those of the marbles (figure 6.5). The oxygen isotopic values of the calc-silicate rocks are

higher or equal to the values of the neighbouring intrusions, therefore, the silica is probably

derived from the intrusions, or it was in equilibrium with them. There is no evidence of

interaction of meteoric fluids since there are no isotopic values of the calc-silicate rocks near

zero or negative (the value of meteoric water), therefore if meteoric water was involved it

must have been already equilibrated with the intrusions before interacting with the

metasediments.

The source of the silica was most likely the Astra Pluton as judged by the isotopic

cross-sections. Figure 6.7 representing the $\delta^{18}O$ versus distance along a SW-NE cross-section

(A-A') shows a gradual increase in light oxygen of the calc-silicates towards the Astra Pluton.

Conversely the SE-NW cross section (B-B') represented in figure 6.8 shows an increase in

heavy oxygen isotope toward the Du Bras Pluton. This suggests that the possible light oxygen

fluids emanating from the Du Bras Pluton did not interact with the neighbouring rocks. The

fact that the source is not the Du Bras Pluton is supported by the fact that there are marbles in contact with the du Bras granite and not calc-silicate rocks. However, fluids, being less dense than rock, probably tend to flow upwards and, therefore, the source of the fluids would lie under the wollastonite bearing calc-silicate rocks. The limited drilling thus far by Ressources Orleans (K. Kobze, pers. comm) found marble under the calc-silicate rocks suggesting that the Du Bras Pluton does not continue under the latter.

Further proof of a skarn ore forming process could include endoskarning, or alteration of the pluton neighbouring the calc-silicate skarn rock. Examples of this include epidotisation of the syenite at the Valentine deposit (Gerdes and Valley, 1994) and the Willsboro deposit (Valley, 1982). At the Canton Saint-Onge deposit no endoscarning is seen in the Du Bras Pluton and there are no outcrops of the Astra Pluton near the contact with the metasediments (fig. 3.1)

7.2.3 Nature of the Fluid

Without the study of fluid inclusions nothing definite can be determined about the composition and nature of the fluids involved with the skarn process. However, based on the oxygen isotope analyses and the whole rock geochemistry and comparing the results of the

reactant (marble) with product (calc-silicate rocks) conclusions can be drawn as to what that fluid may have contained.

The stable isotope work suggests that the fluid concerned probably emanated from the Astra Pluton, or at least is a fluid in isotopic equilibrium with one of the plutons. The fluid must have been rich in H_2O to lower the partial pressure of the CO_2. It must have been rich in silica in order to provide it to complete the reaction from marble to calc-silicate rock.

Figure 5.4 characterises the mass transfer of several elements between the different sedimentary units. It suggests that the fluid also contained titanium, aluminium, iron, sodium, potassium, cobalt, barium, strontium, zirconium, lanthanum, and lutetium. These elements may have been introduced only in minor quantities, however, since the marble lacked nearly all these elements their possibly small quantity in the fluid affected the rocks. The only element that seems to have been removed from the marble is magnesium.

Very few studies have been made characterising metasomatic fluids using a comparison of whole rock geochemistry between lithological units alone. The few studies made, however, all show that the resulting rock was richer in the trace and rare elements examined. At the Traversella Fe, W, Cu skarn deposit at Ivrea, Italy the skarned rock is enriched in REE as compared to the protolith marble (Auwera and Andre, 1991). The skarned rocks at the Shizhyuan W, Sn, Bi, and Mo deposit in South China also show an increase in

REE (Chen *et al.*, 1992). At the Bergell and Adamello contact aureoles in Italy, Ti, Zr, U, Th, Y and REE were found to have migrated in a potassium-rich fluid (Gieré, 1989). These three studies are in

agreement with the results of the Canton Saint-Onge wollastonite deposit were there is an increase in REE in the calc-silicate rocks as compared to the marbles.

7.2.4 Fluid Path

The path most likely taken by the fluids would be along a zone of weakness: a lithological contact or a fault as in the skarn examples at Stephen Cross Quarry (Cartwright and Weaver, 1993) and at the Valentine wollastonite deposit (Gerdes and Valley, 1994). The Canton Saint-Onge wollastonite deposit area shows much evidence of brittle faulting at the outcrop scale. These brittle faults are relatively recent but could represent renewed movement along old zones of weakness that could have been active at many times. A major topographic low runs right through the deposit, trending in a NE-SW direction, and is regarded as evidence of a major fault defined by topography: a major valley, filled with lakes and glacial sediment. This fault is sub-parallel to the Lacs-Saint-Jean-Pipmuacan lineament. It is along this fault that the silica-bearing fluids were probably channelled. This can be seen by the form of the deposit where the wollastonite bearing calc-silicate rocks are NE-SW trending along the fault. Further evidence includes the oxygen isotope cross-sections which show a decrease in heavy

isotopes toward the Astra Pluton (figure 6.7) as well as some diffusion into the calc-silicate rocks away form the fault shown in the NW-SE cross-section (figure 6.8).

7.3 TIMING

Neither the metasediments nor the neighbouring granitoids have been dated, so no absolute timing of the ore forming processes can be determined. However, the dates of formation of the crust, the Elseverian Orogeny and the emplacement of the Lac Saint Jean Anorthositic Complex, and field relationships of the lithological units allow for some idea of the relative timing.
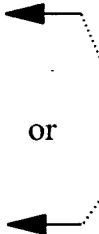
The basement rocks in the Saguenay-Lac-Saint-Jean area and therefore to the Canton-Saint-Onge wollastonite deposit consist of grey gneisses. These gneisses have a depleted mantle model age of 1.5 Ga and a solidification age of 1.4 Ga (Dickin and Higgins, 1992). These dates represent the oldest ages of the rocks of the region, and therefore the lower limit of ages for subsequent units and events.

The sedimentary protolith to the wollastonite bearing calc-silicate rocks must have been deposited before the neighbouring plutons. This is suggested by the fact that similar metasediments to the marbles are found outside of the Lac Saint Jean Anorthositic Complex at

Saint-Eugène (Laurin and Sharma, 1975) suggesting that the metasediments predate the anorthosite. The sediments were deposited as limestone and were later metamorphosed to form marbles. The recrystallisation overprinted all primary textures so little more can be said about their origin. The metamorphism of the limestones/dolostones to marble probably took place before or early in the Elseverian Orogeny, around 1.2 Ga (Easton, 1986).

The only other carbonate metasedimentary rocks with which to compare the Canton-Saint-Onge metasediments within the Grenville Province would be the carbonates of the Central Metasedimentary Belt (CMB). These carbonates were deposited in between 1.3 and 1.25 Ga (Easton, 1992) and later metamorphosed during the Elzeverian Orogeny around 1.2 Ga. Although there is no evidence linking these two metasedimentary units, the ages for the sediment deposition in the CMB and metamorphism possibly cover the same range as for the Canton-Saint-Onge metasediments which fall somewhere in-between 1.4 and 1.15 Ga (Table 7.1).

The Lac-Saint-Jean Anorthositic Complex, which presently underlies the metasediments, was emplaced as a multiple intrusion early in the Grenville Orogeny, ca. 1157 Ma (Higgins and Van Breeman, 1992). The Anorthosite complex was probably emplaced

Time (Ga)	Event	History of metasediments
	Emplacement of Astra Pluton	
1.0	Ottawan Orogeny	metasomatism or wollastonite formation
1.15	Emplacement of Du Bras Pluton	
	Emplacement of Lac-Saint-Jean Anorthosite	
1.2	Elzeverian Orogeny	metamorphism
		deposition of sediments
1.4	solidification of crust	
1.5	Formation of crust	

Table 7.1. Chronology of events at the Canton Saint-Onge wollastonite deposit.

through the Lacs Saint-Jean-Pipmuacan lineament, using the zone of weakness as a condiut

(Higgins, pers. comm.), stratigraphically below the metasediments.

Immediately following the emplacement of the LSJ Anorthosite Complex the Du Bras

Pluton was emplaced along the lineament as suggested by its NE-SW lenticular form, parallel

to the lineament. The Du Bras Pluton possibly the represents a partial melt of the

metasediments along the lineament as suggested by its situation parallel to the band of

metasediments (figure 2.6). However mantle oxygen isotopic values (ca. 8 ‰) of the Pluton

similar to that of the LSJ Anorthosite presented in Chapter 6, suggest a different origin: where

the Du Bras Pluton is a granophyre produced by fractional crystalisation of the same magma

forming the LSJ Anorthosite complex. The spatial distribution of the Du Bras Pluton is in

accordance with this theory, since it occurs along the lineament, along which the Anorthosite

was emplaced. The Du Bras Pluton was later deformed as seen by the mylonite textures in its

southern part. The deformation was probably the result of later movement along the

lineament, as seen by the fact that only part of the Pluton has been deformed, this possibly

took place during the Ottawan Orogeny, or later.

The Astra Pluton was emplaced following the Ottawan Orogeny, and the emplacement

of the LSJ Anorthosite complex. Again it was emplaced in, and probably channelled along,

the Lacs Saint-Jean-Pipmuacan Lineament. The Astra Pluton was probably emplaced

anorogenically as seen by the fact that the Pluton is undeformed, and circular in shape and

validated by the petrogenitic discrimination diagrams discussed in Chapter 5 (figures 5.13 and 5.14).

It is not easy to determine the timing of the metasomatism that transformed the marbles to calc-silicates. The relationship of the NE-SW trending calc-silicates to the parallel SW-NE fault in the middle, and the gradation of the stable isotopes increasing away from the Astra Pluton suggest that the metasomatism took place following the emplacement of the Astra Pluton as fluids emanated from the crystallising Pluton. However there is insufficient evidence to correlate the Astra with the metasomatism since hot fluids will generally tend flow upwards, therefore, it is probably the pluton situated underneath the calc-silicates and the parallel fault that is responsible for the metasomatism.

Only small lenses of metasediments are found within and around the Lac-Saint-Jean Anorthosite Complex, these sediments may have been more extensive. The remaining sediments are mainly associated with the LSJP lineament and other brittle associated faults. This association suggests that the sediments were preserved along the fault, they were probably dropped down by later movements along the fault and then preserved from subsequent erosion.

7.4.0 COMPARISON WITH OTHER DEPOSITS

Other wollastonite deposits are found with in the Grenville Province: in Quebec, Ontario and New York as well as in Finland, Mexico, and India. Few published studies have been made of these deposits.. The Canton Saint Onge wollastonite deposit shares many similarities with the deposits of the Grenville Province as well as many differences. It will be compared with the other wollastonite deposits, with a particular emphasis on those deposits in the Grenville Province, based of the existing literature.

7.4.1 New York State

The United States is the largest producer of wollastonite in the world with the bulk of the production coming from New York state (Andrews, 1970). The Deposits of Willsboro, Valentine and Lewis being the largest producers and the most studied. They are similar to the Canton Saint Onge deposit in that they are all within the Grenville Province and are spatially associated with a large anorthositic complex, the New York deposits with the Adirondack Massif, Canton Saint Onge with the Lac Saint Jean anorthosite, but that is where the similarities end.

The Willsboro wollastonite mine is located in a 0.25 km thick skarn belt at the contact of the Port Kent-Westport unit of the main Adirondack anorthosite massif (Valley and O'Neil,

1982). The anorthosite forms a structural trough in the region of this belt and shows evidence of extensive magmatic assimilation of metasediments, indicating that the originally overlying metasediments were engulfed in the roof zone of the anorthositic body (Valley, 1982). Therefore, at the Willsboro mine the calc-silicate rocks are roof pendants to the anorthosite like the Canton Saint Onge deposit, however, their mineralogy is different. At the Willsboro deposit the ore consists of parallel layers of three coarse grained minerals: wollastonite, clinopyroxene and grandite garnet. Although the Canton Saint Onge ore consists of parallel layers of clinopyroxene and wollastonite it has no garnet (i.e. the Canton Saint-Onge rocks were purer).

The Willsboro mine is believed also to be of metasomatic origin because of the ore's lack of calcite and quartz and few (three) phases. Oxygen isotopes were also studied at the deposit. They revealed at 400 ft wide zone of ^{18}O depletion of the ore rock at the contact with the anorthosite with values ranging from 2 to -1.3 ‰ $\delta^{18}O$. These extremely low values are explained by the interaction of meteoric waters at the time of the wollastonite formation. The Canton Saint-Onge deposit however shows no evidence of meteoric water interaction and is not directly associated with the anorthosite.

The Valentine wollastonite deposit is located in the north-west Adirondack Mountains New York. The ore is composed primarily of wollastonite (90 %) with minor quantities of calcite, diopside and secondary prehnite. The deposit is interpreted by Gerdes and Valley

(1994) to be of skarn origin formed by pure calcite with channelled infiltration of H_2O-rich silica-bearing fluids emanating from the syenitic Diana Complex. Oxygen isotopes were also studied at the deposit. The marbles at the contact revealed high $\delta^{18}O$ values of around 21 ‰ and the wollastonite had a wide range of values from -1 ‰ to 13 ‰, with steep gradients of increasing isotopic ratio towards the marble. The Canton Saint-Onge wollastonite deposit also has a similar gradient towards the Astra syenitic pluton but does not have the low and negative isotopic values.

7.4.2 Finland

Oy Partek operates the only producing wollastonite deposit in Finland at Ihalaenen located near Lappeenranta in Southeast Finland. Unfortunately little has been published on the deposit with the exception of small paragraphs in general texts. From the limited references it can be gathered that: The deposit consists of wollastonite beds of 1mm to 1 m thick within the limestone in association of with calcite, quartz, grossularite, diopside, and serpentine. The limestone is surrounded by a large massif of rapakivi granite and is cut by veins of rapakivi granite, pegmatite, and amphibolite. The wollastonite occurs in the central part of the limestone and at its contacts with the rapakivi pegmatites (Bowie *et al.*,1978). The genesis of the wollastonite is contact metamorphism of siliceous limestone by the rapakivi granite (Andrews, 1970).

The deposit is similar to that of the Canton -Saint-Onge Wollastonite deposit in that it consists is in contact with a rapakivi granite. Both the Du Bras and the Astra plutons have a rapakivi texture. However the Finnish deposit contains limestone(?) where the CSO deposit is in contact with a marble and the former is the results of contact metamorphism whereas the latter is the results of contact metasomatism.

7.4.3 Quebec

There is presently no operating wollastonite mine in the province of Quebec however there are over 100 showings in the Grenville Province (Simandl *et al.*, 1990). The showings have been classified based on their relationship to intrusive rocks , discordant or concordant contacts with the host rocks, morphology and structural controls. The deposits consist mainly of wollastonite, calcite and clinopyroxene.

The deposits are classified in nine categories (figure 7.2). Type A consists of wollastonite ore in calc-silicates at the contact between marbles and felsic or mafic intrusions. Type B are similar to A but are almost entirely surrounded by intrusive rocks and can be found far from the periphery of the intrusion, suggesting they are in fact xenoliths exposed by erosion. Type C surround certain pegmatite or granitic dykes. Type D consist of calc-silicate rocks out-cropping along escarpments and seem to be spatially related to mylonites or other structural discontinuities. Type E consist of layers or concordant lenses found at the contact
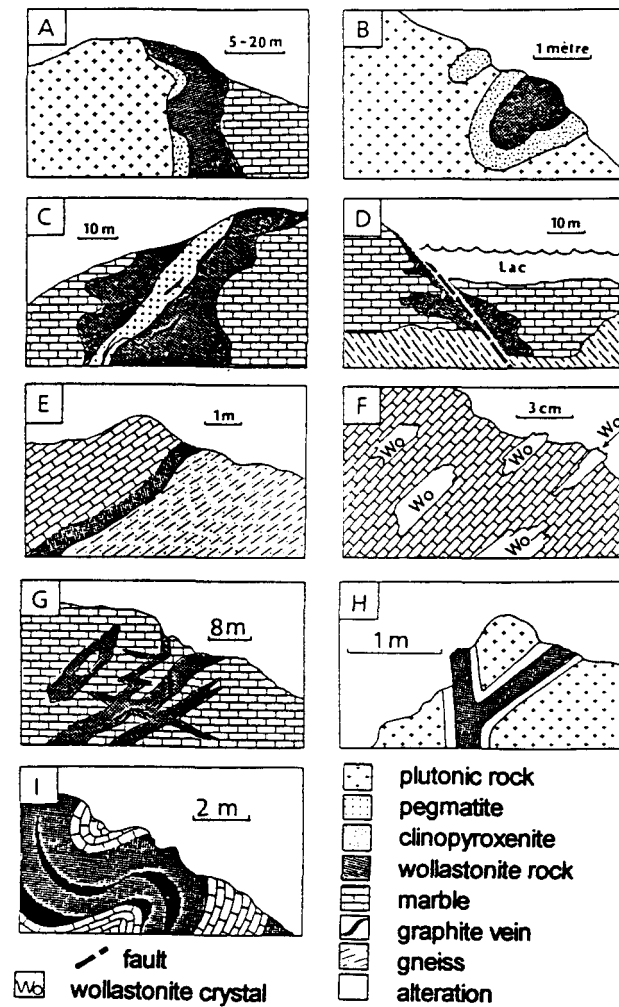
Figure 7.2. Lithostructural classification of wollastonite deposit in the Grenville Province of Quebec (after Simandl, et al., 1990).

between quartzofeldspathic gneisses and marbles. Type F are characterised by wollastonite crystals disseminated in calcitic marbles, they contain less than 3% wollastonite and are of no economic value. Type G consists of irregular or tabular bodies of calc-silicate rock entirely surrounded by marble. Type H are composed of veins of calc-silicate rock cross-cutting plutonic rocks, these veins fill joints near the contact with marbles and charnockitic rocks. Type I deposits form concordant layers of calc-silicate rocks in marbles.

Based on this classification by Simandl *et al.* (1990) the Canton Saint Onge wollastonite deposit falls in the category D where the deposit is located along an escarpment flanked by marble on both sides and associated with a structural discontinuity, the Lacs Saint-Jean- Pipmuacan lineament and associated with mylonitic rocks.

7.4.4 Ontario

Ontario has no operating wollastonite deposit but a deposit 55 km north of Kingston, owned by Ram Petroleum may go into production soon (Christie, 1994, Northern Miner). However, like Quebec it has several showings in the Grenville Province. McKinnon (1990) describes around 20 showings in south-eastern Ontario. Particular attention is given to the Marmora Township study area, where eight wollastonite occurrences are associated with altered calcitic marbles along the western margin of the Deloro granitic pluton. The other

wollastonite occurrences mentioned are in the Kingston- Gananoque area, and in the Frontenac

Axis of the Grenville-Province.

In his report McKinnon classified wollastonite deposits into three groups according to

their genesis, using a modified form of the classification of Kuzvart (1984), as follows:

Type I - contact metamorphic, metasomatic

(i) contact metasomatic (skarn, or reaction skarn)

(ii) contact metamorphic (reaction skarn or bimetasomatic diffusion skarn and calc-silicate

bands)

(iii) skarnoid - any skarn-like body of complex or uncertain origin.

deposits of type I include Partek deposit (Finland), NYCO deposit (Willsboro, United

States).

Type II: regional metamorphic, i.e. California (United States), and the former soviet

republic.

Type III: carbonatitic i.e. Japan, India, Kenya, Mexico, Australia, and the former soviet

republic.

Economically viable wollastonite deposits are rare and are generally restricted to impure

limestones which have undergone shallow contact metamorphism by intrusive bodies of

granite or other acidic rocks, i.e. type I (McKinnon, 1990). The Marmora occurrences are of

this type having formed in the thermal metamorphic aureole of the Deloro Pluton and its

satellites(McKinnon, 1990). By this classification the Canton Saint Onge deposit is of type

I(i) being the result of contact metasomatism. Table 7.2 shows the classification with

examples and how the Quebec deposit classification fits in.

Genetic Classification of Wollastonite deposits			Quebec deposits (see fig. 7.2)	Examples	
Type I	(i)	contact metasomatic	type A,B,Cand G	Willsboro mine, Valentine mine	Canton-Saint-Onge
	(ii)	contact metamorphic	type I	Finland	
	(iii	skarnoid	Type D		
Type II		regional metamorphic	type F		
Type III		carbonatitic	type H		

Table 7.2 Genetic Classification of Wollastonite deposits (after MacKinnon, 1990).

7.5 CONCLUSIONS AND EXPLORATION CRITERIA

The formation of wollastonite deposits depends on three basic requirements:

1) a source of calcite and silica to react to produce wollastonite

2) a source of heat for the reaction to proceed, bring the rocks into the wollastonite pressure-temperature stability field, and

3) a means of depleting the CO_2 during the reaction so that the reaction will proceed to the right.

In the case of the Canton Saint Onge wollastonite deposit the source of calcite was the neighbouring marbles, the source of silica and heat, the neighbouring Astra Pluton and the NE-SW fault allowed for the depletion of CO_2 during the reaction.

Therefore similar wollastonite deposits in the area would require

1) a young granitoid

2) marble, or calc-silicates near the contact

3) a major fault

A young granite is suggested since the large mafic masses in the area (the anorthosites) were emplaced at too great a depth to allow for the depletion of the CO_2 created during the reaction forming wollastonite. A younger acid intrusion is more favourable since it would more likely have been emplaced at a shallower depth, allowing for diffusion of CO_2, and fluids emanating during crystallisation would also contain the necessary silica for the reaction, such silica rich fluids can not be provided from a mafic intrusion. Marble near the contact is necessary for the

protolith containing sufficient calcite for the reaction, or calc-silicates which may be interbedded with wollastonite. A major fault or structure is needed as a means of a pathway of conduit to deplete the system of CO_2, otherwise the accumulation of CO_2 will inhibit the reaction forming wollastonite. Sufficient H_2O to dilute the CO_2 and reduce the activity of the CO_2 (a_{CO2}) is another possibility, this would require the metamorphism of pelites or other H_2O rich rock which would provide the necessary H_2O during contact metamorphism to dilute the CO_2.

REFERENCES

Al-AAsm,I.S., Taylor,B.E. and South,B. 1990. Stable isotope analysis of multiple carbonate samples using selective acid extraction. Chemical Geology (Isotope Geoscience Section), **80**: 119-125.

Andrews, R.W. 1970. Wollastonite. Institute of Geological Sciences, London, England. 114p.

Auwera, J.V. and Andre, L. 1991. Trace elements (REE) and isotopes (O,C,Sr) to characterize the metasomatic fluid sources: evidence from the skarn deposit Fe,W,Cu) of Traversella (Ivrea, Italy). Contributions to mineralogy and Petrology, **106**: 325-339.

Avramtchev, L. and Piché, G. 1981. Cartes des gîtes minéraux du Québec, Région de Laurentie-Saguenay. Ministère de l'Energie et des Ressources Naturelles, DPV-809.

Batchelor, R.A. and Bowden, P. 1985. Petrogenetic interpretation of granitoid rock series using multicatonic parameters. Chemical Geology, **48**: 43-55.

Bowie, S.H.U., Kvalheim, A. and Haslam, H.W. 1978. Ihalainen wollastonite deposit. Mineral Deposits of Europe, vol 1.: Northwest Europe, Institution of Mining and Metallurgy, London. p. 89.

Bowman, J.R., O'Neil, J.R. and Essene, E.J. 1985. Contact skarn formation at Elkhorn, Montana II: Origin and evolution of C-O-H skarn fluids. American Journal of Science, **285**: 621-660.

Cartwright, I. and Weaver, T.R. 1993. Fluid-rock interaction between syenites and marbles at Stephen Cross Quarry, Quebec, Canada: petrological and stable isotope data. Contributions to Mineralogy and Petrology, **113**: 533-544.

Chen, J., Halls, C. and Stanley, C.J. 1992. Rare earth element contents and patterns in major skarn minerals from the Shizhuyuan W, Sn, Bi and Mo deposit, South China. Geochemical Journal, **26**: 147-158.

Christie, B. 1994. Positive feasibility study for wollastonite project. Northern Miner, December 5, vol **80**, no.40.

Christie, B. 1993. Orleans seeks funds to develop Quebec wollastonite play. Northern Miner, June 29. pp.1-2.

Clayton, R.N., Mayeda, T.K. 1963. The use of bromine pentaflouride in the extraction of oxygen from oxides and silicates for isotopic analysis. Geochemica et Cosmochemica Acta, **29**: 43-52.

Daigneault, R. 1994. Rapport des travaux d'analyse structural sur l'horizon de skarn à wollastonite de la propriété St-Onge. Cahier du CERM 94-1.

Deer, W.A., Howie, R.A., and Zussman, J. 1966. An Introduction to the Rock forming minerals. Longman Scientific and Technical, John Wiley and Sons Inc., New York, USA. 528p.

Dimroth, E., Woussen, G., and Roy, D.W. 1981. Geological history of the Saguenay region, Quebec (Central Granulite Terrain of the Grenville Province): a working hypothesis. Canadian Journal of Earth Sciences, **81:** 1506-1521.

Easton, R.M. 1992. The Grenville Province and the Proterozoic history of Central and Southern Ontario. Geology of Ontario, OGS special Volume 4 part 2. pp. 715-907.

Einaudi, M.T., Meinert, L.D., and Newberry, R.J. 1981. Skarn deposits. Economic Geology, 75th Anniversary Volume. pp. 317-391.

Faure, G. 1986. Oxygen in hydrogen in the lithosphere. *In* Principles of Isotope Geology, Second Edition. John Wiley, Toronto. pp. 460-484.

Firth, R.A. and Doig, R. 1975. Pre-Kenoran tonalitic gneisses in the Grenville Province. Canadian Journal of Earth Sciences, **12**: 844-849.

Firth, R.A. and Doig, R. 1973. Rb-Sr Isotopic ages and petrologic studies of the rocks in the Lac St. Jean Area, Quebec. Canadian Journal of Earth Sciences, **44**: 881-899.

Fourniner, A. and St. Seymour, K. 1992. Geology and physical characteristics of wollastonite in Grenville supergroup marbles, Quebec. CIM Bulletin, **85**: 62-66.

Fowler, C.M.R. and Nisbet, E.G. 1982. The thermal background to metamorphism- II, simple two dimensional conductive models. Geoscience Canada, **9**: 208-214.

Gerdes, M.L. and Valley, J.W. 1994. Fluid flow and mass transport at the Valentine wollastonite deposit, Adirondack Mountains, New York State. Journal of Metamorphic Geology, **12**: 589-608.

Gervais, R. 1990. Géologie préliminaire du feuillet SNRC E/O4 avec détails de la zone de wollastonite du lac aux Grandes Pointes. Ministère de l'Énergie et des Ressources, Québec; MB 91-01.

Gervais, R. 1991. Géologie de la région du lac aux Grandes Pointes, feuillet 22E/04. *in* Rapport d'activité 1992. Ministère de l'Énergie et des Ressources, Québec; DV 91-25. pp. 22-23.

Gieré, R. 1989. Hydrothermal mobility of Ti, Zr and REE: examples from the Bergell and Adamello contact aureoles (Italy). Terra Nova, **2**: 60-67.

Greenwood, H.J. 1967. Wollastonite: Stability in H_2O-CO_2 mixtures and occurrence in contact metamorphic aureole near Salmo, British Columbia, Canada. The American Mineralogist, **52**: 1669-1680.

Harker, R.I. and Tuttle, O.F. 1956. Experimental data on the P_{CO2}-T curve for the reaction: calcite + quartz = wollastonite + carbon dioxide. American Journal of Science, **254**: 239-256.

Hébert, C. 1991. Linéament lacs Saint-Jean-Pipmuacan. Rapport d'activité 1991. Ministère de l'Énergie et des Ressources, Québec; DV 91-25. p. 19.

Higgins, M.D. and van Breeman,O. 1996 (in Press). The three generations of AMCG magmatism, contact metamorphism and tectonism in the Saguenay-Lac-Saint-Jean region Grenville Province, Canada. Journal of Precambrian Research.

Higgins, M.D. and van Breeman, O. 1992. The age of the Lac-Saint-Jean Anorthosite Complex and associated mafic rocks, Grenville Province, Canda. Candian Journal of Earth Sciences, **29**: 1412-1423.

Holland, T.J.B. and Powell, R. 1990. An enlarged and updated internally consistant thermodynamic dataset with uncertainties and correlations: the system $K_2O-Na_2O-C_aO-MgO-MnO-FeO-Fe_2O_3-Al_2O_3-TiO_2-SiO_2-C-H_2-O_2$. Journal of Geology, **80**: 89-124.

Kuzvart, M. 1984. Wollastonite, in Industrial Minerals and Rocks; Czechoslovakia, pp. 263- 265.

LaSalle, Y. 1988. La wollastonite: une substance minérale recherchée. Ministère de l'Énergie et des Ressources; MB88-12. 33 p.

Laurin, A.F. and Sharma, K.N.M. 1975. Mistassini, Péribonca and Saguenay Rivers Area (Grenville 1965-1967). Ministère des Richesses Naturelles, Québec; Geological Report 161. 89p.

MacKinnon, A. 1990. Wollastonite in South-eastern Ontario. Ontario Geological Survey Open File Report 5715. 289p.

Meinert, L.D. 1992. Skarns and skarn deposits. Geoscience Canada, **19**: 145-162.

Moore, J.M. 1986. The 'Grenville Province' then and now. The Grenville Province. GAC Special Paper 31. pp. 1-12.

O'Neil, J.R. 1986. Theoretical and experimental aspects of isotope fractionation. *In* Stable Isotopes in High Temperature Geological Processes. Mineralogical Society of America, Reviews in Mineralogy. pp. 1-37.

Pearce, J.A., Harris, N.B.W. and Tindle, A.G. 1984. Trace element discrimination diagrams for the tectonic interpretation of granitic rocks. Journal of Petrology, **25**: 956-983.

Rivers, T., Martingole, J., Gower, C.C., and Davidson, A. 1989. New tectonic divisions of the Grenville Province, Southeast Canadian Shield. Tectonics, **8**: 63-84.

Roy, D.W., Woussen, G., Dimroth, E., and Chown, E.H. 1986. The central Grenville Province: a zone of protracted overlap between crustal and mantle processes. The Grenville Province. Geological Association of Canada Special Paper **31**, pp.51-60.

Simandl, G.J., Valiquette, G., Jacob, H.-L., and Paradis, S. 1990. Gîtes de wollastonite, province tectonique de Grenville, Québec. CIM Bulletin, **83** no.934: 101-107.

Taylor, H.P. and Sheppard, S.M.F. 1986. Igneous rocks: I. Processes of isotopic fractionation and isotope systematics. *In* Stable Isotopes in High Temperature Geological processes. Mineralogical Society of America, Reviews in Mineralogy, vol.13. pp. 185-226.

Valley, J.W., Bohlen, S.R., Essene, E.J. and Lamb, W. 1990. Metamorphism in the Adirondacks: II. The role of fluids. Journal of Petrology, **31**: 555-596.

Valley, J.W. 1986. Stable isotope geochemistry of metamorphic rocks. *In* Stable Isotopes in High Temperature Geological processes. Mineralogical Society of America, Reviews in Mineralogy, vol. 13. pp. 445-486.

Valley, J.W. 1985. Polymetamorphism in the Adirondacks: Wollastonite at contacts of shallowly intruded anorthosite. *In* The Deep Proterozoic Crust in the North Atlantic Provinces. D. Reidel Publishing Company. pp. 217-236.

Valley, J.W. 1984. Fluid Heterogeneity during granulite facies metamorphism in the Adirondacks: stable isotope evidence. Contributions to Mineralogy and Petrology, **85**: 158-173.

Valley, J.W. and O'Neil, J.R. 1982. Oxygen isotope evidence for shallow emplacement of Adirondack anorthosite. Nature, **300**: 497-500.

Whalen, J.B., Currie, K.L. and Chappell, B.W. 1987. A-type granites: geochemical characteristics. Contributions to Mineralogy and Petrology, **95**: 407-419.

Winkler, H.G.F. 1974. Petrogenesis of Metamorphic Rocks; 4th edition. Springer Verlag, New York. 320p.

Woussen, G., Martignole, J. and Nantel, S. 1988. The Lac-St-Jean Anorthosite in the St-Henri-de-taillon area (Grenville Province): A relic of a layered complex. Canadian Mineralogy, **26**: 1013-1025.

Woussen, G., Dimroth, E Corriveau, L. and Archer, P. 1981. Crystallization and Emplacement of the Lac St-Jean Anorthosite Massif (Quebec, Canada). Contributions to Mineralogy and Petrology, **76**: 343-350.

Wynne-Edwards, H.R. 1972. The Grenville Province, in Price, R.A., and Douglas, R.J.W., eds, Variations in Tectonic Styles in Canada: Geological Association of Canada Special Paper 11, pp. 263-334.

Appendix

Structural Measurements

Structural measurements recorded in the field plotted on the steronet of figure 3
The location of the station numbers are shown on figure 3.1.

station #	measurement	degree of folding*	comment
1	030/65	2	compositional layering
	030/70		compositional layering
2	050/85	1	compositional layering
	228/90		compositional layering
3	036/?	1	compositional layering
	180/?		dyke
4	184/?	1	compositional layering
5	165/80	1	compositional layering
7	238/88	1	compositional layering
8	240/40	1	compositional layering
9	236/45	1	compositional layering
10	080/85	1	compositional layering
12		1	compositional layering
13		2.5	compositional layering
14	055/60	1	compositional layering
15	055/60	1	compositional layering
16		2	compositional layering
17	040/?	3	compositional layering
18	070/45		compositional layering
19	250/75	3	compositional layering
21		2.5	compositional layering
22		4	compositional layering
24	080/?	3.5	compositional layering
25	080/varies	2.5	compositional layering
28	140/?		veins

station #	measurement	degree of folding*	comment
	140/?		compositional layering
32		4	compositional layering
33	170/?		compositional layering
34		2.5	compositional layering
35	040/?		compositional layering
36	040/?		compositional layering
39	210/85	2	compositional layering
40	250/80		compositional layering
41	030/?		compositional layering
	030/?		fold axis
	030/?		pegmatite dyke
42	050/85		compositional layering
43	084/70		compositional layering
44	200/85		compositional layering
	50→020		fold axis
45	224/80		compositional layering
47	257/73		compositional layering
49	192/82		compositional layering
50	120/90	3	compositional layering
52	050/90		compositional layering
53	105/?	4	compositional layering
54	070/85	2	compositional layering
55	055/90	1	compositional layering
56	massive		compositional layering
58		4	compositional layering
59	052/90	2	compositional layering
60	040/90		compositional layering
61	044/?		isoclinal folds
62	040/90		compositional layering
	90→040		fold axis
63	044/90		compositional layering
	90→044		compositional layering
64	065/90	3	compositional layering
65	062/?	2	compositional layering
66	052/varies		compositional layering

station #	measurement	degree of folding*	comment
67	046/?	1	compositional layering
68	052/?	1	compositional layering
70	010/?	2	compositional layering
71	030/90	3	compositional layering
72	038/90	1	compositional layering
75	084/?		compositional layering
78	230/80	1	compositional layering
79	046/90		compositional layering
80	220/85	1	compositional layering
81	240/85	1	compositional layering
	270/80		compositional layering
83	052/?		compositional layering
84	030/?		compositional layering
85	030/90		compositional layering
86	032/90	2	compositional layering
87	026/90	2	compositional layering
88	055/90		compositional layering
89	022/90		compositional layering
90	010/90		compositional layering
92	225/80		compositional layering
95	015/90		compositional layering
96	200/80		compositional layering
97	030/90		compositional layering
99	022/90		compositional layering
101	216/80		compositional layering
102	222/80		compositional layering
104	040/90		compositional layering
	028/90		compositional layering
107	040/?		compositional layering
108	000/?		compositional layering
109	42→030		fold axis
110	055/?	2	compositional layering
111	060/?		compositional layering
115	040/?		compositional layering
118	040/90		compositional layering

143

station #	measurement	degree of folding*	comment
119	050/90		compositional layering
121	130/?		foliation
122	040/?		compositional layering
123	055/85		compositional layering
124	035/90		foliation
126	040/90		foliation

* degree of folding: 1 = parallel, 5 = chaotic